Aus der Abteilung für Experimentelle Pharmakologie, European Center for Angioscience der Medizinischen Fakultät Mannheim
(Direktor: Prof. Dr. rer. nat. Thomas Wieland)

Implication of Platelet-derived Growth Factor (PDGFB) in arterial-venous malformations

Inauguraldissertation
zur Erlangung des medizinischen Doktorgrades
der
Medizinischen Fakultät Mannheim
der Ruprecht-Karls-Universität
zu
Heidelberg

vorgelegt von
Yanzhu Lin

aus
Guangdong, China
2023

Dekan: Prof. Dr. Sergij Goerdt

Referentin: Jun.-Prof. Dr. Roxana Ola

CONTENTS

Abbreviations

HHT	Hereditary Hemorrhagic Telangiectasia
AVMs	Arteriovenous malformations
LOF	Loss-of-function
TGF-β	Transforming growth factor beta
ACVRL1 or ALK1	Activin receptor-like kinase 1
SMAD4	SMAD family member 4
GDF2	Differentiation factors 2
BMP	Bone morphogenetic proteins
ECs	Endothelial cells
ENG	Endoglin
vSMCs	Vascular smooth muscle cells
bAVMs	Brain arteriovenous malformations
VEGFA	Vascular endothelial growth factor-A
Tx	Tamoxifen
AV	Arterial-venous
HOHF	High-output heart failure
CNS	Central nervous system
BRB	Blood-retina barrier
VEGFR2	Vascular endothelial growth factor receptor 2
ANGPT2	Angiopoietin-2
KLF4	Krüppel-like factor 4
CK2	Casein Kinase 2
PTEN	Phosphatase and Tensin homolog
CX37	Connexin-37
NRP1	Neuropilin-1
COUP-TFII	Chicken ovalbumin upstream promoter transcription factor II
APJ	Apelin receptor
EphB4	EPH receptor B4
LSS	Laminar shear stress
FSS	Fluid shear stress

MCs	Mural cells
PCs	Pericytes
α-SMA	α-smooth muscle actin
BBB	Blood-brain barrier
PDGFRβ	Platelet-derived growth factor receptor beta
NG2	Nerve-glial antigen-2
MYH11	Myosin heavy chain 11
PDGFB	Platelet Derived Growth Factor B
i.p	Intraperitoneal
HUVECs	Human umbilical cord vein endothelial cells
HBMVPs	Human brain microvascular pericytes
PFA	Paraformaldehyde
WB	Western blot
PCR	Polymerase chain reaction
P21	Cyclin-dependent kinase inhibitor 1
BSA	Bovine serum albumin
DLL4	Delta like canonical Notch ligand 4
SOX17	SRY-box transcription factor 17
CD13	Cluster of differentiation 13
P/S	Penicillin/Streptomycin
PBS	Phosphate buffered saline
TBS	Tris-buffered saline
FBS	Fetal bovine serum
JAG1	Jagged1
UNC5B	Unc-5 Netrin Receptor B
PI3K	Phosphoinositide 3-kinase
IB4	Isolectin B4
NOTCH	Neurogenic locus notch homolog protein
GI	Gastrointestinal
EphrinB2	EphB ligand ephrinB2

Units

%	Percentage
°C	Degree Celsius
l	Liter
ml	Milliliter
µl	Microliter
g	Gram
mg	Milligram
µg	Microgram
ng	Nanogram
M	Molar
mM	Millimolar
µM	Micromolar
nM	Nanomolar
cm	Centimeter
µm	Micrometer
cm^2	Centimeter Square
mm^2	Millimeter Square
h	Hour
min	Minute
U	Unit
V	Volt
rpm	Rounds Per Minute

1. INTRODUCTION

1.1 Hereditary Hemorrhagic Telangiectasia vascular disorder

Hereditary Hemorrhagic Telangiectasia (HHT) is a genetically inherited autosomal dominant vascular disorder with a prevalence of 1 in 5000 individuals [1, 2] and it is considered a rare disease. HHT is characterized by torturous dilations of blood vessels involving small caliber vessels in the mucous membranes (nose, lips, tongue) called telangiectasias, or large caliber vessels called arteriovenous malformations (AVMs) occurring in internal organs such as the lungs, liver, or brain. Rupture of these focal vascular lesions results in repeated episodes of epistaxis causing anemia or visceral hemorrhage, a life-threatening condition [3].

HHT is caused by heterozygous loss-of-function (LOF) mutations in genes involved in the transforming growth factor beta (TGF-β) signaling pathway, which plays a well-defined role in vasculogenesis and angiogenesis and in maintaining vascular homeostasis in mature vessels [4-6]. Approximately 90% of HHT cases are associated with heterozygous mutations in activin receptor-like kinase 1 (*ACVRL1* or *ALK1*) causing type 2 HHT (HHT2) [7] or *ENG* coding for Endoglin (causing type 1 HHT (HHT1)) [8]. Less frequent mutations (1-2 %) of patients are found in SMAD family member 4 (*SMAD4*) gene (causing the juvenile polyposis (JP-HHT)), and coding for SMAD4, the transcriptional effector downstream of all TGF-β family ligands [9]. A rare group of patients (less than 1 %) with an HHT-like phenotype display mutations in growth and differentiation factors 2 (*GDF2*), coding for the bone morphogenetic proteins (BMP9) ligand) [10]. **Figure 1** summarizes the percentages of the different gene mutations found in HHT patients and highlights the BMP9/BMP10 pathway as a common genetic determinant for HHT.

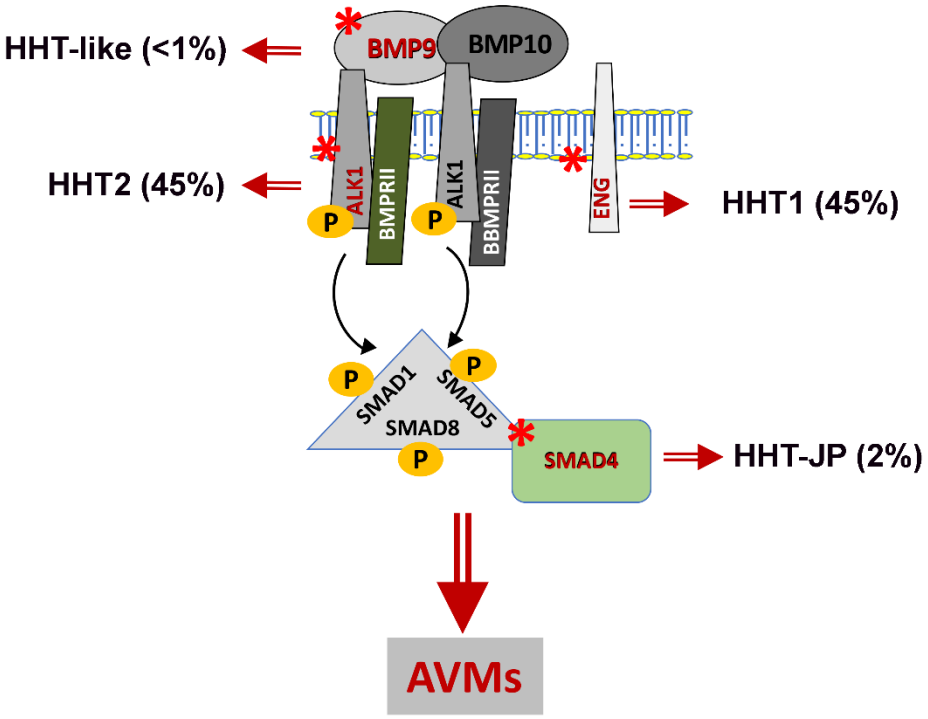

Figure 1. Mutated genes in HHT encode members of BMP9/BMP10 signaling pathway.
The cartoon illustrates the percentage of the mutated genes found in individuals with HHT. Patients with HHT can be classified into four distinct groups, HHT1, HHT2, JP-HHT and HHT-like as a result of heterozygous mutations in *ENG*, *ALK1*, *SMAD4* and *BMP9* genes. Mutations in any of these genes encoding for the components of BMP9/10 pathway lead to formation of AVMs.

Currently, the therapeutic treatments for HHT are intended to reduce symptoms and complications. These include measures to control bleeding, such as local therapies for epistaxis, or interventions to address AVMs in critical organs [11]. However, no mechanism-based targeted therapy is available so far. Therefore, early diagnosis, appropriate management, and supportive care play crucial roles in improving the quality of life for individuals living with HHT.

1.1.1 AVMs

Regardless of which gene within the BMP9/10 pathway is mutated, the pathological outcome of HHT patients is the age-related propensity to develop AVMs (**Figure 1**). AVMs are vascular abnormalities characterized by direct connections between arteries and veins, lacking a capillary bed in between the two large caliber vessels [12, 13]. These abnormal connections lack capillary regulation and proper exchange of nutrients. Unlike high resistance capillary beds, veins are unable to maintain blood flow, resulting in structural remodeling and dilation of the draining veins. This pathologic change can result in tissue destruction and structural deformity, ischemia, and in severe cases can lead to heart failure.

Most frequently, patients with HHT display localized AVMs in the lungs, liver, spine, or brain.

The anatomic location and stage of development of these direct arterio-venous connections determine the severity of complications, including stroke, brain abscess, hypoxemia, or local rupture with hemorrhage, all of which can be life-threatening [13, 14]. AVMs are often congenital and may develop progressively as the patient grows and develops. While a few individuals may maintain some state of vascular quiescence and stability during early life, most AVMs develop symptoms and complications with age. In addition, external stimuli such as injury, infection, incomplete surgical excision, and hormones can accelerate the expansion of the AVM and exacerbate symptoms.

Currently, the predominant therapeutic modalities for the AVMs' treatment consist of surgical, catheter-guided procedures or stereotactic radiosurgery aimed at resecting, embolizing, or irradiating AVMs to manage the associated risks [13, 15, 16]. However, the high rate of resistance after surgical treatment contributes to the poor prognosis of AVMs. It is estimated that 25% of patients experience recurrence of AVM within the first year after surgery due to reperfusion from recanalization, previously unrecognized inflow, or adjacent arteries [17, 18]. This emphasizes the great need for medical treatment of multiple or diffuse AVMs for which surgical intervention is not considered safe, technically feasible or effective. Treatment of AVMs remains a major challenge, and it is imperative to uncover the underlying mechanisms to find a promising cure.

1.1.2 BMP9/10 signaling

Despite numerous studies aimed at unraveling the importance of TGF-β family signaling, its precise role in endothelial cells (ECs) falls short of being elucidated. The contrasting outcomes of TGF-β signaling could be explained by the existence of a multitude of ligand-receptor pairing in a spatial and temporal context, by interactions with non-vascular cells, but also by different downstream activated SMAD complexes and crosstalk with other signaling pathways that influences the final signaling outcome [19, 20].

This ancient and highly conserved pathway is activated by a large number of homologous ligands that have been grouped into: TGF-βs, BMPs, Activins, Nodal, Inhibins, and the GDF subgroups of proteins. These proteins regulate a wide variety of cellular responses in many different settings by binding to one of five possible transmembrane type II receptors (TGF-β receptor type II (TGF-βRII), BMP receptor type II (BMPRII), Activin receptor type II a and b

(ActRIIa, ActRIIb) and then the recruitment of one of seven type I receptors (ALK1-7) that contain cytoplasmic serine/threonine kinases, that upon activation phosphorylate regulatory downstream SMAD proteins. Additionally, there are also accessory receptors, the non-kinase type III receptors, which include ENG for BMP ligands and Betaglycan/TGF-βRIII for TGF-β, that may interfere with receptor-ligand interaction affinities (**Figure 2**).

Whereas TGF-β ligands binding to TGF-βRII/ALK5 receptor complex mainly promotes subsequent activation of SMADs 2 and 3, the BMP ligands binding to the other ALKs-1,2,3,4,6,7 specifically activate the canonical SMADs 1, 5, and 8. Activated SMAD2/3 and SMAD1/5/8 will further complex with the unique cytoplasmic transcriptional effector- SMAD4 and this complex of SMADs, either SMAD2/3-SMAD4 or SMAD1/5/8-SMAD4 is shuffled in and out of the nucleus to regulate transcription of distinct sets of genes with a plethora of biological functions.

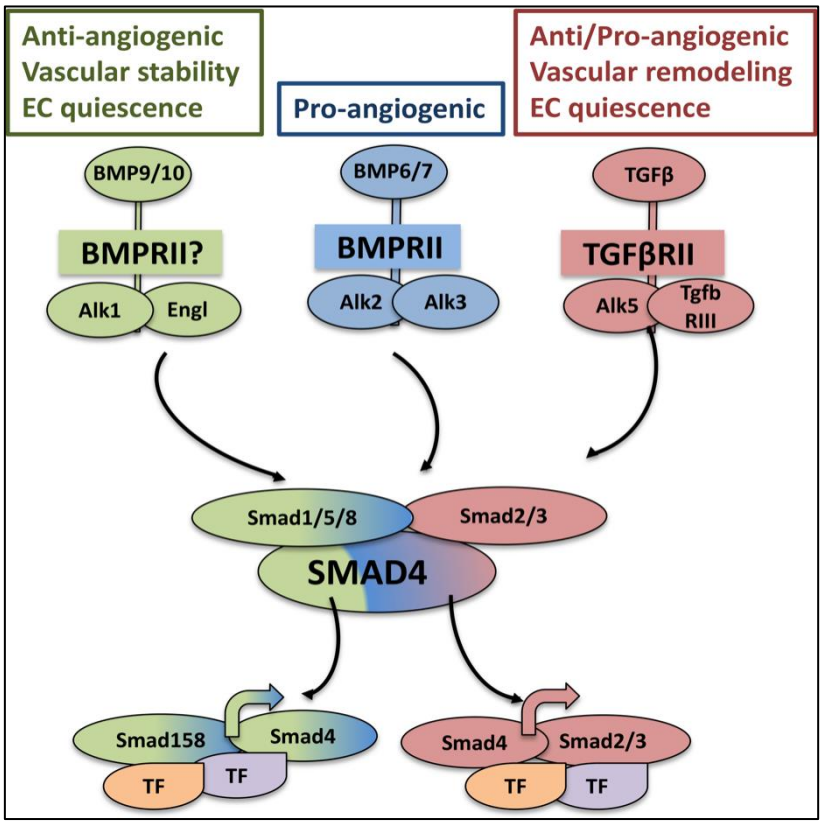

Figure 2. TGF-β/BMP signaling in ECs.
TGF-β signaling through TGF-βRIII/TGF-βRII/Alk5 receptors activates the Smad2/3-Smad4 complex to promote or inhibit angiogenesis, vascular remodeling or EC quiescence (red); BMP9/10 signaling through an unknown BMP type II/Eng/Alk1 receptor complex activate the Smad1/5/8-Smad4 complex to exert anti-angiogenic effects promoting EC quiescence and vascular stability (green); BMP6/7 signaling through BMPRII/Alk2/3 receptors activate Smad1/5/8-Smad4 to regulate downstream pro-angiogenic genes (blue).

While the BMP6 and BMP7 signaling through engagement of BMPRII-ALK2/3 receptor complex

activates downstream pro-angiogenic genes [21], BMP9 and BMP10 bind with a high affinity to an unknown BMPRII and to ALK1/ENG receptor complex present at the surface of ECs and promote ECs quiescence and vessel stability. BMP9 and BMP10 are circulatory growth factors produced by the stellate cells in the liver (BMP9) and right cardiac atrium (BMP10) and subsequently released into the bloodstream [22, 23] (depicted in **Figure 2**). Phosphorylation of ALK1 leads to phosphorylation and activation of the canonical SMAD1/5/8 which will complex with the unique transcriptional effector SMAD4, and together translocate from the cytoplasm into the nucleus. Circulating levels of these ligands are high during embryogenesis and neonatal development and thereafter drop, consistent with active angiogenesis during development and decreased sprouting with age [24]. However even the low levels found in adults are still above threshold levels required for receptor activation. Despite the vast evidence for BMP9 and BMP10 activity as promoters of vasculature stability, there are studies showing also a pro-angiogenic role of these ligands in tumors [25] and age-related macular degeneration [26].

Dysfunctional BMP9/10 signaling pathway due to mutations in genes encoding for any of the components of BMP9/10 pathway such as the ligand- *GDF2*, the receptors- *ALK1* and- *ENG*, and transcriptional effector *SMAD4*, all lead to AVM formation. Interestingly, no mutation in the canonical SMAD1/5 have been yet reported. Also, little is known with regards to downstream target genes that contribute to HHT.

1.1.3 Genetic mouse models of HHT

The development of animal models that accurately mimic the pathophysiology of HHT is essential for a better understanding of the cellular and molecular mechanisms that trigger AVM formation and for the identification of novel therapeutic approaches. Global depletion of *Eng* or *Acvrl1* result in embryonic lethality. The yolk sacs of $Eng^{-/-}$ or $Acvrl1^{-/-}$ mice embryos exhibit abnormalities in the primitive cardiac cushion, leading to delayed maturation of large blood vessels and reduced coverage of peripheral vascular smooth muscle cells (vSMCs) [27-31]. The embryonic lethality of mutant mice has highlighted the crucial function of ALK1/ENG signaling pathway in vascular development and morphogenesis.

For a closer modeling of HHT pathophysiology caused by heterozygous LOF mutations, further studies were conducted on global *Eng* and *Alk1* heterozygous ($Eng^{+/-}$ and $Alk1^{+/-}$) adult mice,

which mimic the patient genotype at these genetic loci. Both genotypes developed vascular lesions between 7 and 20 months resembling HHT-like lesions, including capillary dilatation in different organs and hemorrhage [31, 32]. However, these lesions occur at incomplete penetrance and in an unpredictable manner. Unlike human patients, these mice did not show any spontaneous brain AVMs (bAVMs). Yet, upon an external stimulus, e.g vascular endothelial growth factor-A (VEGFA) stimulation, brains of *Eng*$^{+/-}$ or *Alk1*$^{+/-}$ adult mice developed cerebral microvascular dysplasia [33]. Interestingly, the HHT-like lesions were more frequent in the 129/Ola genetic background than C57BL/6, suggesting that genetic modifiers may play a role in susceptibility to HHT disease [27, 32] .

Recent preclinical mouse models utilizing the Cre/Lox recombination system to delete the *Eng* or *Alk1* genes specifically in ECs in a temporal manner using the Tamoxifen (Tx) inducible VE-Cadherin (*Cdh5*) Cre mouse line, robustly mimicked the HHT-like phenotype, including AVM formation. Depletion of *Eng* in vSMCs did not facilitate the development of AVMs [34], thus emphasizing the crucial role for the canonical BMP9/10 signaling exclusively in ECs. The deletion of *Alk1* or *Eng* specifically in ECs results in dilation of blood vessels and AVM formation in the brain, lungs, and intestine causing severe hemorrhage [35, 36]. Yet, similar to heterozygous mice with global deletion, AVM development in adults with homozygous depletion in ECs, also require a 'second hit' such as angiogenic or inflammatory stimuli. Skin AVMs form only post-dermal wounding [34] while the bAVMs require exogenous stimulation with VEGFA [37]. Nevertheless, loss of EC *Eng* in adult mice results in the development of peripheral AVMs in the vasculature that supplies the pubic symphysis, however this specific region is characterized by elevated levels of endogenous VEGFA [38]. These pubic AVMs lead to an increase in venous return to the heart, causing cardiac enlargement and ultimately resulting in high-output heart failure (HOHF). HOHF is also encountered in some HHT patients [39-41]. Thus, EC ENG and ALK1 are required to maintain EC quiescence of mature blood vessels in response to external stimuli, and AVM development in stable vessels requires a 'second hit' mechanism.

Global loss of *Smad4* mice results in embryonic lethality at E10.5 [42]. Furthermore, constitutive *Smad4* deletion in ECs leads to loss of vessel integrity and cerebral bleeding during embryonic development, underlying the crucial function for Smad4 in embryonic vascular development [43].

1.1.4 Mouse retina AVM models

HHT-related AVM pathogenesis can also be mimicked by postnatal homozygous EC gene depletion in neonates, using retina as a model for angiogenesis. The developing retina is a component of the central nervous system (CNS) and serves as a widely accepted model to study various angiogenic properties, including EC sprouting, tip-stalk versus arterial-venous specification, and vascular remodeling and blood-retina barrier (BRB). In mice, retinal vascularization starts at birth, with blood vessels extending from the optic nerve towards the periphery until postnatal day 7 (P7) to form the superficial vascular plexus. The superficial retinal plexus is a stereotypical vascular network that can be visualized by whole mount imaging, enabling the examination of intricate vascular structures such as AVMs. Subsequently, blood vessels penetrate the neuroretina to establish the deep vascular plexus by P12, and by P15 the intermediate plexus forms. The vascular network reaches full maturation by P21 [44].

Using retina vasculature to model AVM pathogenesis, on one side it uncovered that formation of HHT-like AVMs in neonates are exclusively a pathogenic feature of canonical BMP9/10 signaling through ALK1/ENG - SMAD1/5 and SMAD4 transcriptional effector in ECs. On the other side, it had significantly enhanced our comprehension of the underlying cellular and molecular mechanisms responsible for AVM formation. Blockade of BMP9/10 ligands in neonates or by delivery of the blocking antibodies through the trans-mammary administration, or EC depletion of both ligands lead to AVMs formation [45-47]. Intriguingly, BMP10 was found to be the relevant physiological ligand of the ENG-ALK1 signaling pathway pertinent to HHT pathogenesis, as single EC knockout of *Bmp10* is sufficient to drive AVMs formation [48]. Similarly, specific EC depletion of any of the genes downstream of BMP9/10 ligands: *Alk1* [46], *Eng* [49], *Smad1,5* [50] or of *Smad4* [47], all lead to formation of retinal AVM and visceral organs within few days.

Most recently, novel genetic tools have been developed to selectively induce gene depletion in distinct EC subtypes, e.g capillaries or veins, arteries, and tip cells to investigate the initiation and further development of AVMs. These murine models have significantly enhanced our comprehension of the underlying cellular and molecular mechanisms responsible for AVM formation. Depletion of *Eng* [51], *Smad4* [52], and *Alk1* [53] specifically in capillary and venous ECs, using a Tx inducible *Msfd2a*-Cre line [54] trigger AVM formation, suggesting a non-arterial but rather a capillary-venous contribution to AVM formation [44].

1.1.5 BMP9/10 signaling crosstalk regulation

HHT lesions appear later in life and are focally distributed. Although the signaling components are expressed by all ECs, genetic variants in *ALK1* or *ENG* genes lead to the development of AVMs mainly in the liver or lungs, respectively [55]. The reasoning for the organotypic development of AVMs remains unknown. Perhaps, this could be a result of a paracrine-autocrine or endocrine modulation of BMP9/10 signaling, the availability of different receptors and effectors, or crosstalk with context-dependent signaling pathways in different vascular beds.

Indeed, multiple interactions of BMP9/10 with other signaling pathways have emerged in the last years (**Figure 3**). Identifying and further targeting the relevant pathways is likely to restore a normal vasculature. Together with Neurogenic locus notch homolog protein (NOTCH), ALK1 signaling antagonizes VEGFA to limit excessive EC sprouting and tip cell formation [24]. In HHT patients, high levels of circulating VEGFA have been detected, hence providing the rationale for the use of anti-VEGFA therapy in AVM pathology [56]. Yet, bevacizumab treatment is not beneficial in all HHT patients, or patients develop drug resistance [57-59], emphasizing the need for identifying novel therapeutical approaches. Also, *Alk1* depletion resulted in an increased integrin signaling interaction with the VEGFA main receptor, the vascular endothelial growth factor receptor 2 (VEGFR2). Specific inhibitors for integrins administered in these mice restored the lesions [53].

SMAD4 was also shown to be a direct repressor of Angiopoietin-2 (ANGPT2) in ECs [60]. ANGPT2 is a pro-angiogenic growth factor that functions through the tyrosine kinase receptor, TIE2. Interestingly, the blockade of excessive ANGPT2 by using LC10 rescues AVM formation in *Smad4*, *Alk1* and *Eng* mutant HHT mouse models [60, 61]. Very recently, it has been shown that TIE2 expression within the AVMs is regulated upon excessive Krüppel-like factor 4 (KLF4) [62], thus providing novel evidence for the ANGPT2 blockade as a targeted therapy for AVM pathogenesis. BMP9 signaling also acts upstream of chemokine response/chemotaxis secreted factors SDF1-CXCR4 signaling cascade to limit EC migration [63], yet the in vivo relevance for this crosstalk has not been established.

Interestingly, in HHT mouse models an increase in phosphoinositide 3-kinase (PI3K) activation, downstream of VEGFA and ANGPT2/TIE2 was found to be the responsible mechanisms for

AVM pathogenesis. Mechanistically it has been shown that SMAD4 activation represses the transcription of Casein Kinase 2 (CK2) to limit phosphorylation of Phosphatase and Tensin homolog (PTEN). Subsequently, unphosphorylated active PTEN restricts excessive EC PI3K/AKT1 signaling to maintain vascular homeostasis. Inhibitors for CK2 or PI3K/AKT1 (Wortmannin, Pictilisib) or specific deletion of *Akt1* in EC, all rescued AVM formation in *BMP9/10-Alk1-Smad4*- deficient mice [46, 47] and also improved vascular lesions in *Eng* LOF neonates [49]. Following these studies, increased PI3K signaling has been validated in HHT patients [64]. Downstream of PI3K, mTOR signaling was found to be activated. Ruiz et al. [65] found that sirolimus and nintedanib effectively restored the functionality of endothelial Smad1/5/8, VEGFR2, and mTOR signaling pathways, improving AVM pathology. Furthermore, an enhanced YAP/TAZ nuclear translocation was identified upon *Alk1* depletion, and pharmacologic inhibition of YAP/TAZ signaling (Verteporfin) also prevented vascular malformations in *Alk1*-deficient neonates [53].

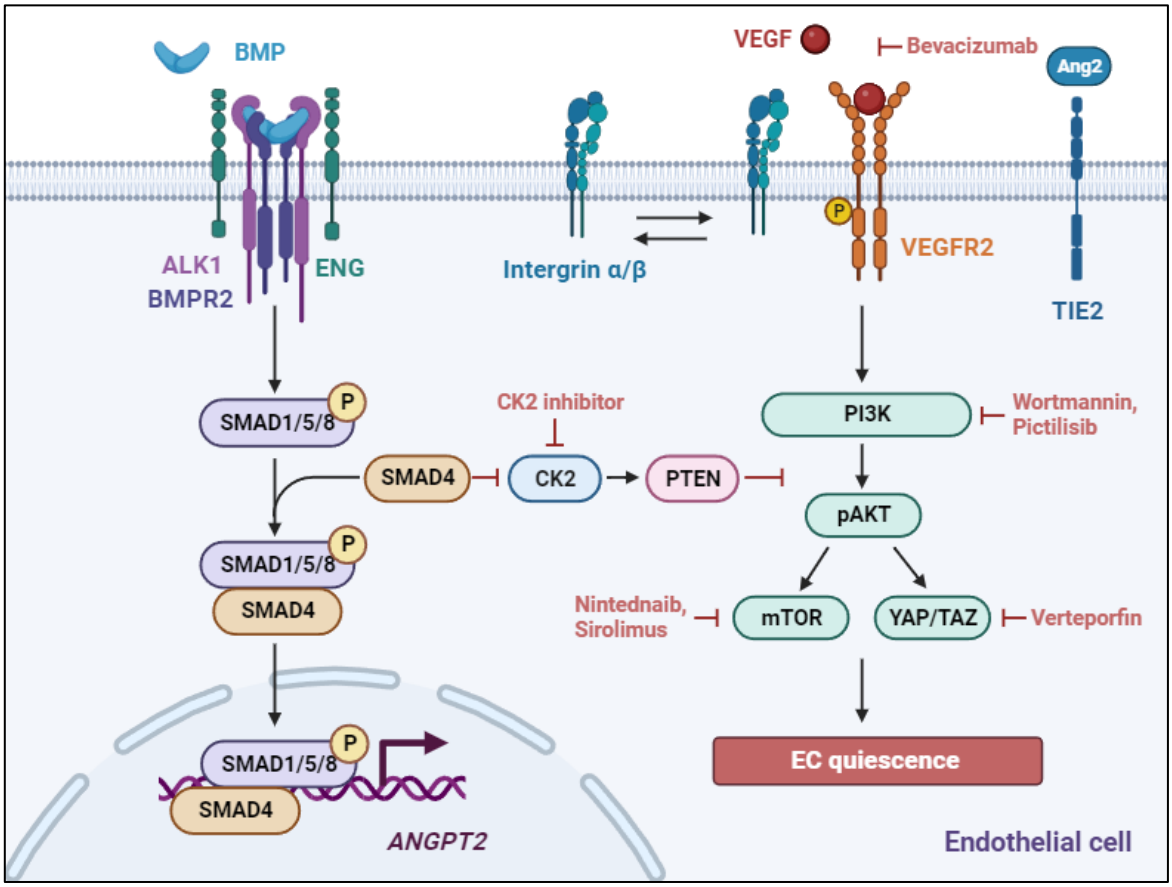

Figure 3. Crosstalk between BMP9 and VEGF signaling in ECs.
BMP9 induced activation of SMAD1/5, which then interacts with SMAD4 to translocate to the nucleus to inhibit ANGPT2 expression. In parallel, SMAD4 inhibits CK2 expression, which allows inhibition of PTEN through de-phosphorylation, thereby inhibiting the activity of PI3K, a downstream effector of VEGF2 pathway. Integrins interact with VEGFR2 at EC membrane to regulate the activation of the PI3K/AKT and YAP/TAZ signaling pathways. Several drugs (Bevacizumab, CK2 inhibitor,

Wortmannin, Pictilisib and Verteporfin) aim at restoring the balance between the BMP9 pathway and the VEGF pathways to re-establish vascular quiescence. Adapted from [66].

1.1.6 Arterial-venous (AV) differentiation in AVMs

The differentiation of the vascular system into arteries and veins is a complex process influenced by various developmental signaling pathways. Genetic factors, such as VEGFA, NOTCH, and Ephrins, play a crucial role in establishing AV identity before circulation begins. Hemodynamic forces, such as blood pressure and blood flow, also shape vascular development by maintaining the AV specification. Several arterial- and venous-specific signaling molecules have been identified in ECs (**Figure 4**). Markers of arterial identity include gap junction proteins Connexin-37 (CX37), CX40 [67-69], EphrinB2, Neuropilin-1 (NRP1) [70], and members of the NOTCH signaling pathway: the receptors: NOTCH1, NOTCH3, NOTCH4 [71], the ligands: delta-like ligand 4 (DLL4) or Jagged1 (JAG1) [72], and the NOTCH downstream effectors HES1/2 and HEY1/2. Markers of venous identity include chicken ovalbumin upstream promoter transcription factor II (COUP-TFII) [73], EPH receptor B4 (EphB4), apelin receptor (APJ) [74] and NRP2. Several of these markers have been shown to be direct targets of BMP9 signaling [24].

Arteries and veins are typically distinguished based on their unique structural and functional features. Arteries are characterized by having thick walls, smooth muscle layers, and a pulsatile flow and are responsible for carrying oxygenated blood away from the heart. On the other hand, veins have thinner walls and a lower pressure, allowing the return of deoxygenated blood into the heart in a continuous flow. In HHT-like AVMs, the conventional distinction between arteries and veins becomes blurred. This occurs because the arteries and veins become interconnected, resulting in an abnormal loss of arterial vessel characteristics and gain of venous vessels characteristics. Moreover, these abnormal AV connections result in turbulent and high-velocity blood flow, which further complicates the maintenance of AV identity due to altered flow patterns. Thus, AVMs are characterized by loss of arterial markers, e.g sex-determining region Y box 17 (SOX17), JAG1, EphB ligand ephrinB2 (EphrinB2), Unc-5 Netrin Receptor B (UNC5B) at the same time with gain of venous markers (EphB4) [46, 47]. If changes in AV identity is primary due to disruption of BMP signaling pathway in ECs or it is secondary due to altered hemodynamic forces remains to be established.

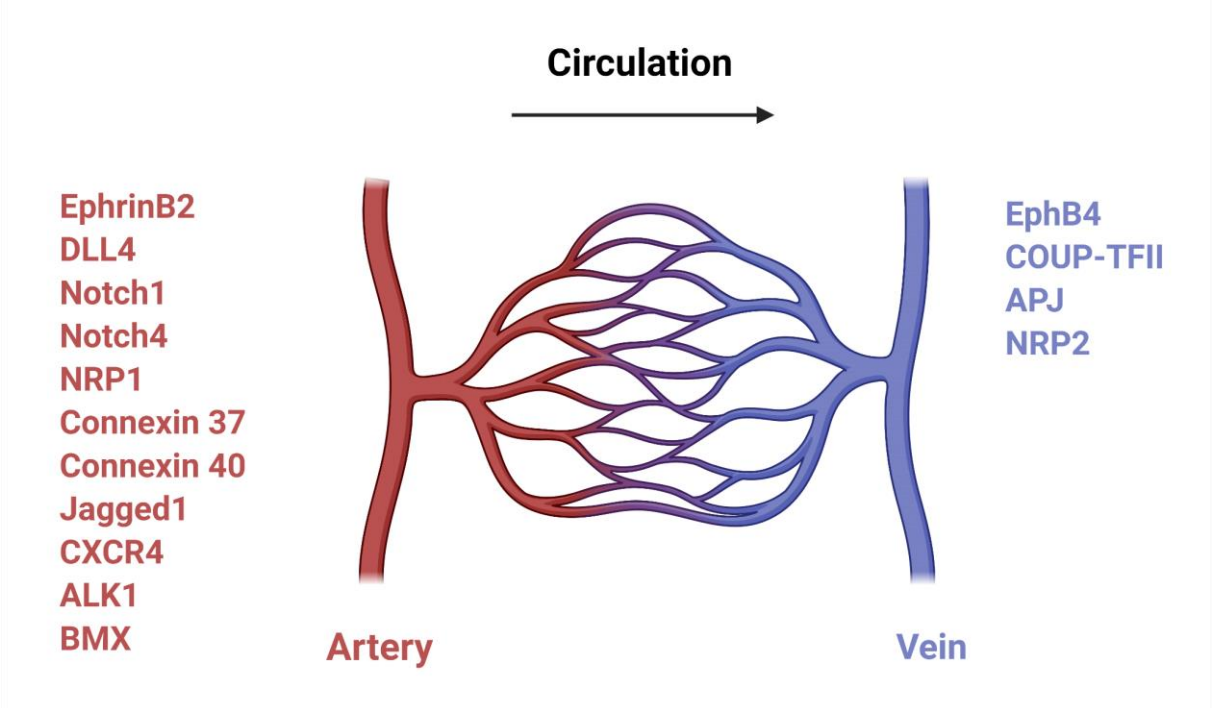

Figure 4. Arterial-venous specification markers in vascular formation.
Arterial ECs are known to express various molecular markers, including ephrinB2, Notch pathway molecules (DLL4, Notch1, Notch4 and Jagged1), NRP1, CXCR4, the gap junction proteins CX37 and CX40, ALK1, and BMX. Venous ECs express EPHB4, NRP2, COUP-TFII, and the APJ receptor. Adapted from [75].

1.1.7 Cellular mechanisms in AVM Pathogenesis

A comprehensive understanding of the pathogenesis of AVM development is crucial for designing effective AVM therapeutic strategies. Despite the identification of genetic contributors several decades ago, the cellular and molecular mechanisms responsible for AVM pathogenesis started to be elucidated in the past recent years. Yet, it remains unclear which cell and molecular event is triggering AVM formation and thereafter the lesion progression.

The ECs in blood vessels are exposed to blood flow which induces mechanical forces, such as shear stress and cyclic stretch. These physical stimuli are then sensed by cells and converted into intracellular biochemical signals, contributing to gene expression and adaptation processes. Laminar shear stress (LSS) within the physiological range maintains EC quiescence by inducing various EC responses. These responses include both, morphological: EC size and shape, position and EC number, and molecular: activation or inhibition of signaling pathways [76, 77]. Several fluid shear stress (FSS) responses are altered in ECs within the AVM suggesting contribution of FSS to AVM pathogenesis. Furthermore, in neonatal retinas the AVMs are positioned close to the optic nerve where the blood flow is the highest [45, 47, 49].

In zebrafish embryos with *Acvrl1* LOF mutation, AVMs also form in regions of high flow due to a diminished migratory capacity of ECs against the blood stream, and the blockade of the heart rate reversed the lesions [78]. An altered EC migration phenotype was also identified in EC knockouts of *Alk1* and *Eng* developing retinas [49, 53] and it has been proposed that impaired EC migration against the flow direction is the triggering cell event in AVM formation. Yet, in EC *Smad4* LOF retinas, loss of FSS-induced cell cycle arrest and loss of arterial identity was proposed to be the triggering event for AVM formation [62].

However, it is important to consider that there might be other indirect mechanisms that contribute to focal AVM formation. Loss of the capillary bed might lead localized hypoxia, that may be responsible for increased VEGFA among other pro-angiogenic factors to further exacerbate the expansion of AVMs. Disruption of mural cells (MCs)-ECs crosstalk might also contribute to AVM formation and development. Loss of *Eng* leads to a decrease in the contact between pericytes (PCs) and ECs, which can potentially impact the blood vessel diameter and vascular stability. The AVMs upon *Alk1* and *Smad4* LOF are also characterized by loss of PCs and gain of vSMC [46, 47]. Thus, the development of AVMs is influenced by various factors, including the genetic disruption of BMP9 signaling pathway, as well as over-activation of angiogenesis, blood flow, and local environmental triggers like hypoxia, infection or inflammation. These factors play a crucial role in driving the formation of AVMs in HHT. Additional research is required to enhance our comprehension of AVM formation and to facilitate the translation of these findings from animal models to humans.

1.2 Pericytes (PCs)

PCs together with vSMC comprise the MCs that surround and protect the blood vessels [79]. Charles-Marie Benjamin Rouget was the first to propose the concept of PCs in the 19th century, and thus PCs were also known as Rouget cells [80]. Later, K. W Zimmermann called these cells “pericytes” based on their perivascular location and the term has been used as such [81]. The majority of PCs develop from the mesoderm, like those found around the veins in the body's trunk, whereas others have a neural crest origin, like those found in the brain [82]. Initially it was thought that PCs play a role in vasoconstriction and the regulation of localized microvascular flow. More recent studies found additional roles for PCs in angiogenesis and permeability, vessel stabilization, immunomodulation and cell differentiation [83, 84].

1.2.1 PC biology

PCs communicate directly with ECs via a common basement membrane, whereas vSMC are physically separated from the ECs by an intimal layer of extracellular matrix (**Figure 5**). This interaction promotes PC proliferation, migration, and their attachment to the endothelium, resulting in the formation of PC-EC cross-interactions termed "pericyte coverage".

The localization and the content of α-smooth muscle actin (α-SMA) is a key determinant in providing the morphology of PCs [85]. Pre- and post- capillary PCs are shorter and stellate-shaped with varied quantities of α-SMA, whereas PCs in the middle of capillaries, which that lack α-SMA, are elongated and more spindle-shaped. The typical mature PCs extend along the outer wall of several microvascular ECs along the axis of the microvasculature. The nucleus exhibits an oval shape, and the cytoplasm surrounds the nucleus, releasing finger-like synapses that gradually thin, with their ends enclosing and supporting the endothelial lumen [86, 87]. This specialized morphology facilitates the identification of the various PC subtypes within the microvessels.

PCs are embedded in the basement membrane of small blood vessels including precapillary arterioles, capillaries, postcapillary venules and small refluxing veins. There are substantial differences in the density of PCs in various tissues and organs, and these variations are closely related to PC physiological organotypic functions [88]. For example, the PC density in the retinal and CNS microvasculature is relatively high (between 1:1 to 1:4 relative to ECs) [84, 89].

During angiogenesis, PCs are recruited to the immature vasculature to promote tip-stalk differentiation. PCs stabilize blood vessels by inhibiting EC proliferation and regulation of capillary size and AV differentiation [90, 91]. Failure to recruit PCs to ECs results in multiple vascular defects, including microaneurysms, hemorrhage, edema, BRB and blood-brain barrier (BBB) breakdown [92].

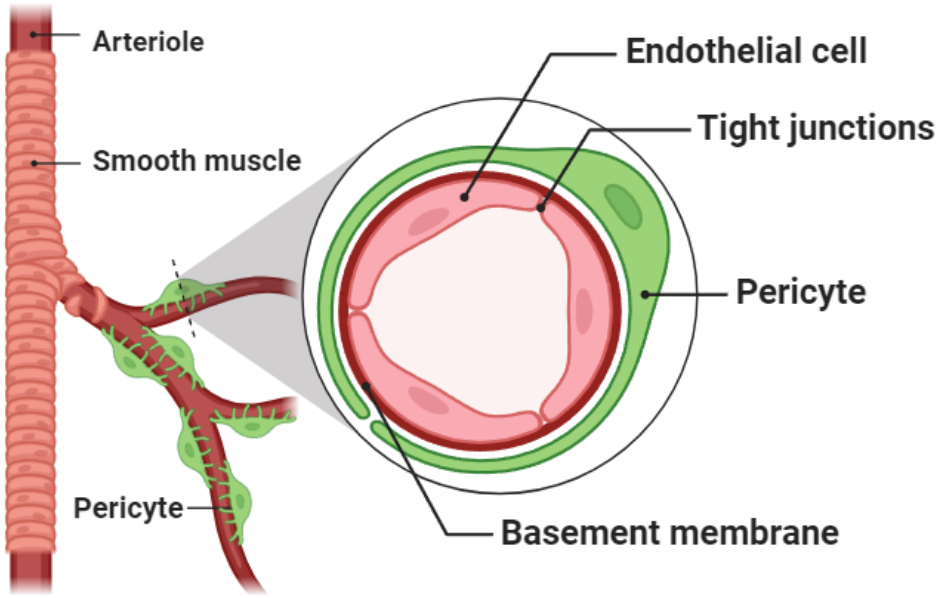

Figure 5. PC-EC interactions in microvessels.
Illustrative representation showing typical PC-EC interconnection. PCs surrounding the ECs share a common basement membrane with ECs. A direct PC-EC contact is established via tight junction. Adapted from [93].

1.2.2 Identification of PCs

The identification of specific markers to distinguish different subtypes of PCs within an organ or between different organs has been a challenge in recent decades. Yet, recent development in molecular profiling by single-cell (scRNA) sequencing technique is shedding light on tissue-specific PC molecular profiles and functions [90]. Yet, there is no single marker to distinguish just the PC population, as all perivascular cell types express very similar and overlapping expression patterns. PCs are positive for MC markers, such as platelet-derived growth factor receptor beta (PDGFRβ), nerve-glial antigen-2 (NG2), cluster of differentiation 13 (CD13) and desmin. While these markers are particularly powerful to distinguish MCs from other cell types, such as ECs or neurons, none of them is specific to a single subgroup of MCs. To overcome this hurdle, it is conducive that certain markers specifically identify SMCs, α-SMA and myosin heavy chain 11 (MYH11). Thus, PCs are defined by exclusion, and it is appropriate to use a combination of different markers for a sharp tissue-specific MC and PC identification. At this point, experts in the field adopted the view, that PCs are best described by being PDGFRβ positive and α-SMA negative.

1.2.3 Models to study PC-EC interactions

Several in vitro co-culture systems and animal models have been developed to study the EC-

PC cellular and molecular interactions and have significantly provided insights into the role of specific molecular pathways in PC-EC communication during various physiological and pathological processes.

Co-culture systems employ incorporation of three-dimensional scaffolds or microfluidic devices to better mimic the *in vivo* microenvironment. D'Amore et al. used primary ECs and PCs from the bovine retinas to elucidate their roles in vessel development and function, as well as the angiocrine-paracrine regulatory mechanisms [94, 95].

Animal models have also been instrumental in studying PC-EC interactions. Genetically modified mice with PC-specific gene deletion or fluorescent protein labeling for PC tracking in a specific spatial-temporal manner have been recently developed [96].

Zebrafish embryos have also emerged as a powerful model for studying PC-EC interactions. Zebrafish embryos allow direct visualization of vascular development and dynamic cell interactions using live imaging techniques [97]. Manipulations of gene expression either genetically or chemically can be easily performed in zebrafish, providing a valuable system for studying the functional consequences of disrupting PC-EC interactions.

1.2.4 Signaling pathways involved in PC-EC interactions

Along the years, various autocrine-paracrine signaling pathways that regulate EC-PC crosstalk have been identified to be essential for angiogenesis and stabilizing the already existing micro-vasculature (**Figure 6**).

PDGFRβ signaling pathway

The Platelet Derived Growth Factor B (PDGFB) produced and secreted by the ECs is very abundant in angiogenic sprouts and remodeling arteries during angiogenesis. PDGFB signals through binding to its receptor, PDGFRβ, expressed exclusively by the PCs, to trigger the PC recruitment, migration and proliferation [84]. Currently, it is generally established that PDGFB is a key molecule in MC biology [98]. Mice lacking the ligand, *Pdgfb* in ECs or the receptor, *Pdgfrβ* in PCs display similar phenotypes including loss of PCs and exhibit a plethora of vascular anomalies and fractured microaneurysms [99, 100].

TGF-β/TGFβR signaling

TGF-β signaling has been shown to be implicated in PC and EC proliferation and differentiation. The exact role of TGF-β in ECs and PCs is further complicated by the fact that both, the TGF-β ligands and receptors are expressed on both ECs and PCs. The resulting cellular outcome of TGFβ/TGFβR signaling axis is dependent on the composition of the receptor-ligand pairing, making it difficult to discern the precise angiocrine versus paracrine signaling in EC and PCs function. Yet, a definitive role for TGF-β secreted from the PCs is to mediate PC-vSMC transition.

VEGFA/VEGFR signaling

VEGFA is required for differentiation of PCs and the proliferation, migration and survival of ECs. VEGF ligands include VEGF A-E and receptors mainly include VEGFR1, VEGFR2 and VEGFR3. VEGFR1 typically binds to VEGF-A and B, whereas VEGFR2 normally binds to VEGF-A, C, D, and E. PC-derived VEGF-A upon binding to VEGFR2 on ECs promotes cell survival through Bcl-2 and survivin. Disturbance of VEGF-A signaling prevents the recruitment and migration of PCs to ECs [101].

ANGPT/TIE1-TIE2 signaling

ANGPT1 that is released mostly from PCs bind the TIE2 receptor on ECs to promote cell survival through PI3K-Akt activation, whereas ANGPT2 offers antagonistic properties on TIE2 [102]. The role of ANGPT1/TIE2 signaling in PCs still remains controversial, as a small fraction of TIE2 has also been identified in the PCs. Still, loss of TIE2 in PCs leads to a pro-migratory phenotype[103]. Alterations in ANG-1/TIE-2 leads to reduced PC recruitment and inhibition of angiogenesis. Thus, the role ANGPT/TIE signaling axis in PC and EC remains controversial.

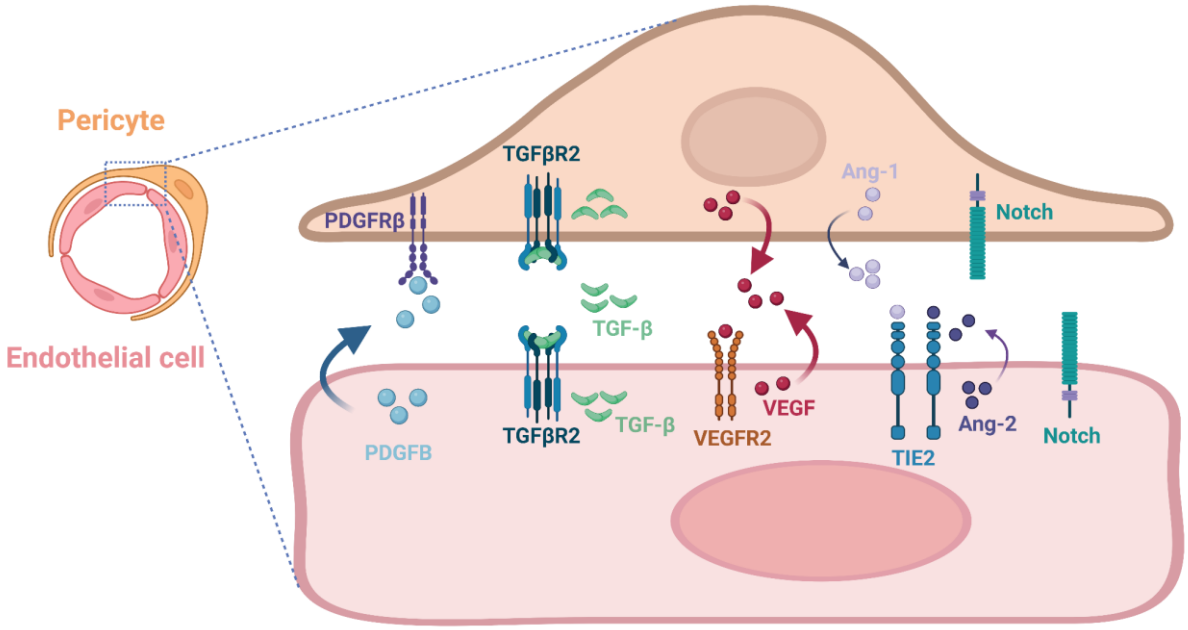

Figure 6. Signaling pathways mediating ECs-PCs communication.
The recruitment of PCs to the endothelium and their communication with ECs is facilitated by multiple pathways, including PDGFB/PDGFRβ, VEGF/VEGFR2, Ang/Tie-2, TGF-β signaling pathway and the Notch pathway. Adapted from [84].

1.2.5 The role of PDGFB in PC recruitment and maintenance

PDGFB-PDGFRβ is essential for PC recruitment during angiogenesis. Embryonic deletion of either of the *Pdgfb* or *Pdgfrb* genes are perinatally lethal due to widespread hemorrhage and generalized edema [104, 105]. The complete loss of PDGFB or PDGFRβ proteins results in failure of MC recruitment and proliferation to the developing vasculature, which has secondary consequences to ECs leading to blood vessel dilation and dysfunction [99, 106]. Similarly, early postnatal deletion of EC-specific *Pdgfb* also revealed that PDGFB plays an important function in attracting and therefore recruiting PCs to developing retinal capillaries [107]. Furthermore, LOF mutations in the *PDGFB* and *PDGFRβ* genes cause formation of microvascular calcification in both mice and humans [108]. The adult quiescent microvasculature maintains the expression of PDGFB in ECs. The *Pdgfb* retention motif knockout mouse (*Pdgfb*$^{ret/ret}$) is a hypomorphic *Pdgfb* mouse model used to investigate the postnatal effects of PCs loss [109]. Adult constitutive *Pdgfb* LOF mutants are also characterized by reduced PC coverage in the brain resulting in substantially increased capillary diameter with skewed endothelial AV zonation and disrupted EC junctions. Furthermore, in these mice decreased *Pdgfb* expression promoted a neuroinflammatory disorder, that was further confirmed by depletion of PCs upon inhibition of *Pdgfrβ* [110-112]. Yet induced depletion of *Pdgfb* in the ECs at adult stages did not result in any

observable phenotype [111]. Overall, all these findings suggest that PDGFB is indispensable during development to ensure vascular stabilization, yet once the vasculature matures, PDGFB become dispensable.

1.2.6 PCs in AVM pathogenesis

Impaired PC coverage has been reported in human sporadic bAVMs but also in animal models of HHT. In the patient bAVMs, the decrease in PC coverage was correlated with increased lesion rupture and the degree of hemorrhage [113].

In animal models of HHT, irrespective of the depleted gene, the retinal AVMs are characterized specifically and exclusively by loss of PCs [46, 47, 114], whereas the sprouting front retains the PC coverage [45, 47]. This emphasizes that an altered flow within the AVMs is a contributing factor to loss of PCs. Whether the localized reduction in PC coverage is a consequence of pathological flow, a contributor factor, or a causally determinant for the high flow-AVMs is still not clear. Much less is known about the angiocrine-paracrine signaling pathways whose disruption contributes to PC loss and AVM formation. In addition, the bAVMs upon *Alk1* depletion display a deficit in PC coverage associated with vascular leakage and hemorrhage [114]. Yet, the cause and consequence of this abnormal cell event is still not understood. ALK1 signaling is required for FSS-induced expression of *PDGFB*, *TGF-β1 and JAG1* in ECs that signal paracrine to mediate PC migration [45].

Several studies have highlighted implication of PDGFB signaling in AVM pathogenesis. Treatment of *Eng*-heterozygous deficient mice with thalidomide, a PDGFB expression stimulator ameliorated AVM severity, in part, by increasing PDGFB expression mediated PC coverage [115]. Overexpression of PDGFB by lentiviruses or the administration of thalidomide or lenalidomide can effectively restore PC and vSMCs coverage with an improvement in bAVM vascular lesions in adult *Alk1*-deficient mouse model [116]. Yet, the requirement and the molecular regulation of PDGFB signaling have not been addressed.

2. AIMS OF THE STUDY

Either inherited or sporadically occurring, the high flow AVMs among other cellular abnormal features are characterized by a specific loss of PCs. Recent studies have shed light on the crucial role of PCs in angiogenesis and maintenance of vascular integrity. Disruption of angiocrine-paracrine PDGFB-PDGFRβ has been linked to AVM pathogenesis, yet the precise cellular and molecular mechanisms are far from being understood. It is still unclear whether impaired PC coverage triggers AVMs or whether it is a secondary event due to increased blood flow within AVMs. Understanding the mechanisms involved in PC-mediated vascular quiescence and homeostasis and their role in protecting the endothelium against AVMs would provide valuable insights into developing novel therapeutic interventions.

In the present study, the major aims were **i)** to investigate the impact of the BMP9/10 - blood flow signaling pathway crosstalk on PDGFB-mediated PCs biology and function and **ii)** to elucidate the role of EC derived PDGFB-mediated PC recruitment and maintenance in protecting the endothelium against AVM formation.

3. MATERIALS AND METHODS

3.1 Materials

3.1.1 Animals

Depletion of *Smad4* and *Pdgfb* genes specifically in the ECs were achieved by crossing *Smad4 fl/fl* or *Pdgfb fl/fl* with Tamoxifen (Tx) inducible Cdh5-CreERT2 mice to obtain $Smad4^{i\Delta EC}$ and $Pdgfb^{i\Delta EC}$. Gene deletion was achieved by intraperitoneal (i.p) injection of 100µg Tx (2 mg/ml, dissolved in corn oil (Sigma, T5648) up to 50 µl final volume) at postnatal days (P1-P3) or (P5-P7). Tx-injected Cre-negative littermates ($Smad4^{fl/fl}$ or $Pdgfb^{fl/fl}$) were used as controls in all experiments. All animal procedures used in this study were approved by the animal welfare commission of the Regierungspräsidium Karlsruhe (Karlsruhe, Germany).

3.1.2 Cells

Human umbilical cord vein endothelial cells (HUVECs) were obtained from the umbilical cords of pregnant women who provided informed consent and were in good health. HUVECs were cultured in EC medium (Promocell) with 5% fetal bovine serum (FBS). The human brain microvascular pericytes (HBMVPs) were purchased from ScienCell and cultured in PC specific growth medium (Promocell).

3.1.3 Cell culture medium and reagents

Table 1. Medium and buffers for cell culture

Components	Company	Catalog Number
Endothelial Cell Growth Medium 2 (EGM2)	Promocell	C-22022
Pericyte Growth Medium 2	Promocell	C-28041
Penicillin/Streptomycin (P/S)	Sigma-Aldrich	P4333
FBS	Sigma-Aldrich	F-7524
Trypsin-EDTA	Sigma-Aldrich	T3924
Phosphate buffered saline (PBS)	Sigma-Aldrich	D-5652
Opti-MEM™ Reduced Serum Medium	Thermo Fisher	31985070

3.1.4 Retina digestion buffers

Table 2. Retina digestion buffers

Buffer	Contents
Fixation solution	4% Paraformaldehyde (PFA)
Blocking buffer	1% FBS, 3% bovine serum albumin (BSA), 0.5% Triton X-100, 0.01% sodium deoxycholate, 0.02% sodium azide in PBS at pH 7.4
Wash buffer	1x PBS
PBLEC buffer	1 mM $CaCl_2$, 1 mM $MgCl_2$, 1 mM $MnCl_2$ and 0.25% Triton X-100 in PBS
Antibody dilution buffer	Dilute in Blocking buffer

3.1.5 Primary antibodies

Table. 3 Primary antibodies for Immunofluorescence

Antibody	Company	Catalog Number	Dilution
NG2	Millipore	AB5320	1:200
Isolectin B4 (IB4)	Life Technologies	121412	10 µg/ml
GOLPH4	Abcam	ab28049	1:200
ERG	Abcam	ab196149	1:200
GM130	BD Biosciences	610823	1:600
KLF4	R&D systems	AF3158	1:200
SOX17	R&D systems	AF1924	1:200
VE-Cadherin	BD Biosciences	555289	1:400
JAG1	R&D systems	AF599	1:200
Endomucin	Santa Cruz	sc-65495	1:200
DLL4	R&D systems	AF1389	1:200
phospho-SMAD3	Abcam	ab52903	1:100
phospho-SMAD1/5	Cell Signaling	13820S	1:100
ID1	R&D systems	AF4377	1:100
Endoglin	R&D systems	AF1320	1:100

BMP6	Abcam	ab15640	1:100
TGF-β1	R&D systems	MAB7666	1:100
PDGFRβ	R&D systems	AF1042	1:100
Phalloidin	Thermo Fisher	R415	1:500
αSMA	Abcam	ab184675	1:600
ICAM2	BD Biosciences	553326	1:200
Collagen IV	Abcam	ab6586	1:400
DAPI	Thermo Fisher	62248	1:1000
VE-Cadherin	Cell signaling	2500S	1:400

Table 4. Primary antibodies for Western blot (WB)

Antibody	Company	Catalog Number	Dilution
PDGFB	Abcam	ab23914	1:1000
Smad1	Cell Signaling	6944S	1:1000
Smad2/3	Cell Signaling	8685S	1:1000
phospho-Smad1/5/8	Cell Signaling	13820S	1:1000
phospho-Smad3	Abcam	ab52903	1:1000
TGF-β1	Santa Cruz	sc-52893	1:500
BMP6	Abcam	ab15640	1:1000

3.1.6 Secondary antibodies

Table 5. Secondary antibodies for Immunofluorescence and WB

Antibody	Company	Catalog Number	Dilution
Alexa Fluor donkey anti-goat	Thermo Fisher	A-21432	1:500
Alexa Fluor donkey anti-rabbit	Thermo Fisher	R37118	1:500
Alexa Fluor donkey anti-rat	Thermo Fisher	A-21209	1:500
Alexa Fluor donkey anti-mouse	Thermo Fisher	A-21202	1:500
Goat anti-rabbit peroxidase	Sigma-Aldrich	A9169	1:10000
Rabbit anti-mouse peroxidase	Sigma-Aldrich	A9044	1:10000

3.1.7 Human small interfering RNA (siRNA)

Table 6. Human siRNA

siRNA	Company	Catalog Number
ON-TARGETplus Non-targeting Control siRNA	Dharmocon	D-001810-01-05
ON-TARGETplus Human *SMAD4* siRNA	Dharmocon	L-003902-00-0005
ON-TARGETplus Human *PDGFB* siRNA	Dharmocon	L-011749-00-0005

3.1.8 Polymerase chain reaction (PCR) Primers

Table 7. Mouse and human primer sequence for quantitative PCR (qPCR)

Primer	Forward Sequence (5' to 3')	Reverse Sequence (5' to 3')
Mouse *Dll4*	TTCCAGGCAACCTTCTCCGA	ACTGCCGCTATTCTTGTCCC
Mouse *Notch1*	GATGGCCTCAATGGGTACAAG	TCGTTGTTGTTGATGTCACAGT
Mouse *Notch4*	GAACGCGACATCAACGAGTG	GGAACCCAAGGTGTTATGGCA
Mouse *Hey1*	CCGACGAGACCGAATCAATAAC	TCAGGTGATCCACAGTCATCTG
Mouse *Hey2*	CGCCCTTGTGAGGAAACGA	CCCAGGGTAATTGTTCTCGCT
Mouse *Hes1*	TCAACACGACACCGGACAAAC	ATGCCGGGAGCTATCTTTCTT
Mouse *Klf4*	GGCGAGTCTGACATGGCTG	GCTGGACGCAGTGTCTTCTC
Mouse *Bmp6*	GCGGGAGATGCAAAAGGAGAT	ATTGGACAGGGCGTTGTAGAG
Mouse *Tgf-β1*	CCACCTGCAAGACCATCGAC	CTGGCGAGCCTTAGTTTGGAC
Mouse *Pdgfb*	CATCCGCTCCTTTGATGATCTT	GTGCTCGGGTCATGTTCAAGT
Mouse *Ephb4*	GGAAACGGCGGATCTGAAATG	TGGACGCTTCATGTCGCAC
Mouse *Nrp2*	GCTGGCTACATCACTTCCCC	GGGCGTAGACAATCCACTCA

Mouse *Nr2f2*	CATCGAGAACATTTGCGAACTG	GTCGGCTGACATGGGTGAAG
Mouse *Aplnr*	CCAGTCTGAATGCGACTACG	CTCCCGGTAGGTATAAGTGGC
Mouse *Sox17*	GATGCGGGATACGCCAGTG	CCACCTCGCCTTTCACCTTTA
Mouse *Nrp1*	ACCTCACATCTCCCGGTTACC	AAGGTGCAATCTTCCCACAGA
Mouse *Unc5b*	CGGGACGCTACTTGACTCC	GGTGGCTTTTAGGGTCGTTTAG
Mouse *Efnb2*	TTGCCCCAAAGTGGACTCTAA	GCAGCGGGGTATTCTCCTTC
Human *PDGFB*	CTCGATCCGCTCCTTTGATGA	CGTTGGTGCGGTCTATGAG

3.1.9 Protein analysis buffers

Table 8. Recipe for preparing solutions and buffers

Buffer	Contents
Ponceau S (100 ml)	0.2 g Ponceau; 5 ml acetic acid; 95 ml H_2O
Tris-buffered saline (TBS) (10x)	100 mM Tris; 1.5 M NaCl; pH: 7.4
TBST (1000 ml)	100 ml 10X TBS; 10 ml 10% Tween-20; 890 ml H_2O
Western Blot buffer (10x) (1000 ml)	32.5 g Tris, 144 g Glycine, 1000 ml H_2O
SDS-PAGE electrophoresis buffer (5X)	0.125 M Tris; 1.25 M Glycine; 0.5% SDS; in H_2O
Tris buffer for stacking gel	1 M Tris; pH 6.8
Tris buffer for resolving gel	1.5 M Tris; pH 8.8

3.1.10 Reagents

Table 9. Reagents

Reagent	Company	Catalog Number
Lipofectamine™ RNAiMAX	Thermo Fisher	13778150
Dispase II	Roche	04942078001
Collagenase I	Worthington	LS004194

Clarity Western ECL Substrate	Bio-Rad	1705061
Roti-Mount FluorCare	Roth	HP19.1
PowerUp™ SYBR™ Green Master Mix	Thermo Fisher	A25777
CD31 Microbeads Mouse	Miltenyi Biotec	130-097-418
CD45 Microbeads Mouse	Miltenyi Biotec	130-052-301
Tamoxifen	Sigma-Aldrich	T5648
Corn oil	Sigma-Aldrich	C8267
Red Blood Cell Lysis Buffer	Sigma-Aldrich	11814389001
Recombinant Human PDGF-BB	PeproTech	100-14B
Laemmli buffer	Bio-Rad	1610747
Latex	Connecticut Valley Biological	868703
Recombinant Human BMP9	R&D systems	3209-BP-010

3.1.11 Kits

Table 10. Kits

Kits	Company	Catalog Number
RNeasy Plus Universal Mini Kit	Qiagen	73404
Click-iT™ EdU Cell Proliferation Kit	Thermo Fisher	C10337
High-Capacity cDNA Reverse Transcription Kit	Thermo Fisher	4368813

3.1.12 Chemicals

Table 11. List of chemicals

Chemicals	Company	Catalog Number
Ammonium Persulfate	Roth	9592.3
BSA	Sigma-Aldrich	A9647
Dimethyl sulfoxide	Sigma-Aldrich	D8418
PFA	Merck	1.04005.100
Ponceau S	Roth	5938.1

Precision Plus Protein	Bio-Rad	1610395
Roti-Block	Roth	A151.1
TEMED	Sigma-Aldrich	T9281
Tris	Roth	4855.2
Triton-X-100	Sigma-Aldrich	X100
Tween 20	Roth	9127
Gelatin	Fluka	48720

3.1.13 Consumable materials

Table 12. Consumables

Material	Type	Company
Cell culture dishes	6 cm, 10 cm	Sarstedt
Cell culture flasks	T75 cm^2, T25 cm^2	Sarstedt
Cell culture multi-well plates	6-well, 12-well, 24-well	Sarstedt
Falcon tubes	50 ml, 15 ml	Sarstedt
MicroAmp® Fast Optical Reaction Plate	96-well, 0.2 ml	Applied Biosystems
MicroAmp® Optical Adhesive Film		Applied Biosystems
Microscope object slides	76×26 mm	R. Langenbrinck
Microscope square coverslips	24×24 mm, 24×60 mm	Carl Roth
PCR tubes	Multiply® µStrip Pro 8-strip	Sarstedt
Pipette tips	1000 µl, 100 µl, 10 µl	Sarstedt
Nitrocellulose membrane	0.2 µm	Amersham
Serological pipettes	5 ml, 10 ml, 25 ml	Sarstedt
Insulin syringes	1ml/40 I.U., 0.5ml/ 50 I.U.	NeoLab
µ-Slide VI 0.4 ibiTreat		Ibidi
Culture-Insert 2 Well in µ-Dish	35 mm, high	Ibidi
Cell Strainer 70 µm Nylon	70 µm	Corning
MS columns		Miltenyi Biotec

3.1.14 Equipment

Table 13. List of equipment

Equipment	Company
BioRad gel casting system	Bio-Rad
BioRad gel running system	Bio-Rad
BioRad Western Blotting equipment	Bio-Rad
Cell culture hood	Thermo Fisher
Cell culture incubator	Thermo Fisher
Centrifuge	Thermo Fisher
Freezing box	Thermo Fisher
Pipettes	Eppendorf
Surgery and dissection tools	Fine Science Tools
Vortex	Neolab
Water bath	Julabo
Dissecting microscope	Leica
Confocal	Zeiss
Pump system	Ibidi
Gel Imaging Systems	Vilber

3.1.15 Software

Table 14. Software

Software	Company
Graph Pad Prism (8.0)	Graph Pad
ZEN blue	Zeiss
Fiji	Image J

3.2 Methods

3.2.1 Maintenance of the animals

This study was approved by the local ethics committee (Medical Faculty Mannheim, Heidelberg University, Germany) for the use of mice in this study. Animal care and experimental use were performed according to institutional guidelines and in accordance with the Association for Research in Vision and Ophthalmology (ARVO) statement. Mice were maintained under artificial lighting that mimicked a light and dark cycle of 12 h during the day and 12 h at night in the animal house building. The room temperature was kept constant at 21 °C. The mice were provided with water and food free of charge.

3.2.2 Tx application

Tx (Sigma, T5648) was dissolved in corn oil (Sigma, C8267) at 2 mg/ml overnight at 37°C. I.p injections with 100 µg Tx in pups at P0-P2 or P5-P7 (50 µl) were used to induce gene deletion. Mice were sacrificed on day P6, P7 or P12, depending on the experiment. The corresponding protocol is indicated in the figures. Cre-negative littermates were also treated with Tx and subsequently used as control mice.

3.2.3 Latex dye injection

The P7 or P12 pups were anaesthetized and then perfused with 2 ml PBS. The left ventricle was slowly injected with latex dye using a 1-ml insulin syringe. For the pulmonary arteries, latex was injected into the right ventricle. The stained whole animals were fixed in 4 % PFA at 4 °C overnight and washed in PBS following day. The organs were dissected and imaged using a dissecting microscope (Leica).

3.2.4 Retina isolation and antibody staining

The eyes from P6, P7 or P12 pups were fixed in 4 % PFA for 17 min at room temperature (rt). The eyes were dissected under a microscope, and the retinas were isolated. After dissection, the retinas were washed 3 times with PBS and incubated with blocking buffer for 15 min at rt. They were then incubated with specific primary antibodies diluted in blocking buffer at 4 °C overnight. The next day, the retinas were washed and incubated with IB4 together with the corresponding secondary antibody in PBLEC buffer for 1 h at rt, then post-fixed with 4 % PFA for 40 min at rt. The retinas were flattened by four radial incisions and the spherical structure

in the shape of a four-leaf clover was opened. The retinas were then covered with a thin glass with mounting medium (RotiMount FluorCare #HP19.1, CarlRoth). Images of the entire retina were acquired using a Zeiss LSM800 confocal microscope and Zeiss software. Quantification of retinal vasculature was analyzed using Image J.

3.2.5 Proliferation assay

To analyze cell proliferation in the retinas, I injected pups with 5-ethynyl-2-deoxyuridine (EdU, 100 mg/Kg; Thermo Fischer) by i.p injection 4 h prior to dissection. The retinas were harvested and EdU labeling was detected using the Click-it EdU Alexa Fluor-488 Imaging Kit (C10337, Life Technologies) following the manufacturer's instructions.

3.2.6 Isolation of mouse lung endothelial cells (mLECs)

Isolation of mLECs was performed using MACS (Miltenyi Biotec). Mice were sacrificed and lungs were harvested immediately. The lungs were dissected into small pieces and then digested with collagenase I at 37 °C for 45 min. The tissue suspension was filtered with a 70 µm cell strainer and incubated with red blood cell lysis Buffer (11814389001, Sigma) for 5 min and washed several times with PEB buffer (0.5% BSA, 2 mM EDTA in PBS). The cell suspension was incubated with CD45 MicroBeads (130-052-301, Miltenyi Biotec) at a ratio of 1:10 for 15 min at 4 °C. After incubation, the mixture was passed through the MS columns (130-042-201, Miltenyi Biotec). Cells without labels were collected and then centrifuged at a speed of 1000 rpm for 10 min at 4 °C. The cell pellets were resuspended in PEB buffer and then incubated with CD31 MicroBeads (diluted 1:10, 130-097-418, Miltenyi Biotec) for 15 min at 4 °C. After incubation, the mixture was applied to MS columns and washed 3 times with PEB. The columns were then eluted with PEB buffer, and the eluate was used directly for RNA or protein extraction.

3.2.7 Isolation of HUVECs

HUVECs were isolated from the umbilical cords of newborns with the informed consent of the mothers. The umbilical cords were wiped with ethanol-soaked wipes. The umbilical cord was further examined for the presence of the vein, a 3-way valve was inserted into the vein to allow bidirectional flow of fluid through the vein. The vein was then washed with pre-warmed DMEM supplemented with 1% (P/S) until no blood was present. A solution of 1X DMEM-Dispase II was then filled into the vein via the valve. The cord was then placed in a 15 cm dish

and placed in a humidified incubator at 37 °C for 30-40 min. The contents of the vein, including the detached cells, were then collected in a falcon tube containing 4 ml FBS to halt the enzymatic reaction. The collected suspension was centrifuged at 1000 rpm for 5 min to obtain a cell pellet, which was then resuspended in EGM medium. Cells were plated on a 1% gelatin-coated T25 flask and maintained in a humidified incubator at 37 °C and 5 % CO_2, changing the medium after 2 h.

3.2.8 Cell culture

The freshly isolated HUVECs in passage 0 were cultured in EGM2 containing 5 % FBS supplemented with 1X P/S solutions. Experiments were performed with HUVECs from passages 2 to 4. HBMVPs were cultured in PC growth medium on gelatin-coated flasks with 5% FBS supplemented with 1X P/S solutions. All cells were cultured under humid conditions at 37 °C and 5% CO_2.

3.2.9 Gene silencing with siRNA transfection

siRNA transfection was performed to silence the *SMAD4* or *PDGFB* gene in HUVECs. *SMAD4* or *PDGFB* siRNA (2 µl) were added to 200 µl of serum-free medium (Opti-MEM, Life Technologies). Lipofectamine RNAiMAX reagent (2 µl, Life Technologies) was added to another 200 µl of Opti-MEM. The reagents were mixed and incubated at rt for 20 min. The mixture was then added to HUVECs (≈70% confluent) in 1.5 ml medium without P/S in a well of a 6-well plate. After 48 h of culture, the cells were ready for experiments.

3.2.10 Exposure of ECs to shear stress

HUVECs transfected with siRNAs were carefully placed on a µ-Slide VI0.4 (Ibidi) and subjected to laminar FSS levels of 1 and 12 DYNES/cm^2 for 24 h. This was accomplished by employing a pump system (Ibidi, #10902). For stimulation studies, 20 ng/ml recombinant human PDGFB was added to the culture medium for 24 h.

3.2.11 HUVECs-PCs co-culture

Ibidi culture-insert 2 well in µ-dish 35 mm high (Ibidi product #81176) were used to produce a gap between two different cell types (HUVECS and HBMVPs). HUVECs were transfected with *CTRL* siRNA or *SMAD4* siRNA and *PDGFB* siRNA, followed by changing of fresh complete endothelial cell medium 24 h after transfection. After 48 h of transfection, cells were plated at

a density of 20-30,000 cells/well. Before gap-filling, cells were serum starved in 0.2% FBS medium for 12-16 h. The “wound” was created according to the manufacturer's protocols by removing the insert and carefully adding 2% FBS medium to the dish. Immediately after removal of the insert, images of the “wound” were taken to identify the initial locations of the cells. The culture dish was then incubated for 10 h. Cells were then fixed, stained and imaged as described above.

3.2.12 qPCR

Total cellular RNA was extracted using the RNeasy Mini Kit (Qiagen) according to the manufacturer’s protocol. RNA concentration was measured using a NanoDrop ND-1000 spectrophotometer and stored at -80 °C. An aliquot of 500 ng-1 µg RNA was used for reverse transcription using the High-Capacity cDNA Reverse Transcription Kit (4368813, Thermo Fisher) according to the manufacturer’s protocol. GAPDH was used for normalization. All RT-PCR experiments were performed in triplicate. The differences in mRNA expression were determined by ΔCT against an internal control. The primer sequences can be found in Table 7.

3.2.13 WB

Total proteins from mLECS were lysed with Laemmli buffer (1610747, Bio-Rad). Equal amounts of proteins were separated using polyacrylamide separation and electrophoresis with SDS running buffer. The proteins were transferred to a nitrocellulose membrane by semi-dry transfer for 30 min. After-transfer, the membranes were washed 3 times with TBST and stained with 0.2 % Ponceau S solution to confirm successful protein transfer. The membranes were then washed with TBST to remove the Ponceau stain, and blocked with Roti Block for 1 h at rt. After blocking, the membranes were incubated with the primary antibodies overnight at 4 °C. The next day, the blots were washed 3 times with TBST for 10 min, and incubated with the respective secondary antibodies (diluted in TBST) for 1 h at rt. The secondary antibodies used were HRP-conjugated. After-incubation, the membranes were washed 3 times with TBST. The immunoblotted proteins were visualized with an enhanced chemiluminescent substrate in an imager (Vilber). The images obtained were analyzed and quantified using Image J.

3.2.14 Immunofluorescence staining

For Ibidi slides and co-cultured HUVECs and PCs, immunostaining was performed according to the following protocol: Cells were washed three times with 1x PBS and then fixed with 4% PFA

for 10-15 min at rt. After fixation, cells were washed and blocked with blocking buffer for 1 h at rt. The primary antibodies were then incubated overnight at 4 °C. The next day, cells were washed again three times with 1x PBS and incubated with secondary antibodies for 1 h at rt. Slides or co-culture dishes were mounted with mounting medium and imaged with the LSM800 Confocal.

3.2.15 Statistical analysis

The data are presented as mean ± standard error of the mean (S.E.M.). The experiments were performed in triplicate and repeated independently at least three times. Student's t-test was conducted to determine the statistical significance between the experimental groups. To compare multiple groups, one-way analysis of variance and conducted Tukey's posthoc test were used. A P value <0.05 was considered statistically significant. Statistical analyses were performed for all quantitative data using Prism 8.0 (Graph Pad).

4. RESULTS

4.1 SMAD4 regulates BMP9 and FSS-induced *PDGFB* expression

4.1.1 EC *Smad4* deletion results in a decrease of PC coverage in AVMs

To investigate the impact of Smad4 signaling on PC recruitment, I labelled Tx induced postnatal day 6 (P6) *Smad4*$^{fl/fl}$ (control) and *Smad4*$^{i\Delta EC}$ retinas with IB4 to visualize the ECs, and with NG2 and PDGFRβ to identify MCs (**Figure 7B**). *Smad4* depletion was achieved by administration of Tx at P1-P3 (**Figure 7A**). While the control retinas displayed regular PC abundance in all vessels, *Smad4* depleted retinas displayed a significant loss of PC coverage specifically in AVM regions, as depicted in **Figure 7B** and quantified in **Figure 7C**, consistent with previous findings [47]. Yet, as quantified by PDGFRβ labeling intensity per NG2 positive area within the AVMs regions, the remaining PCs within the AVMs showed decreased PDGFRβ expression (**Figure 7D**). These findings suggest that *Smad4* loss results in a diminished capacity of PCs to associate with the endothelium in AVM-affected regions.

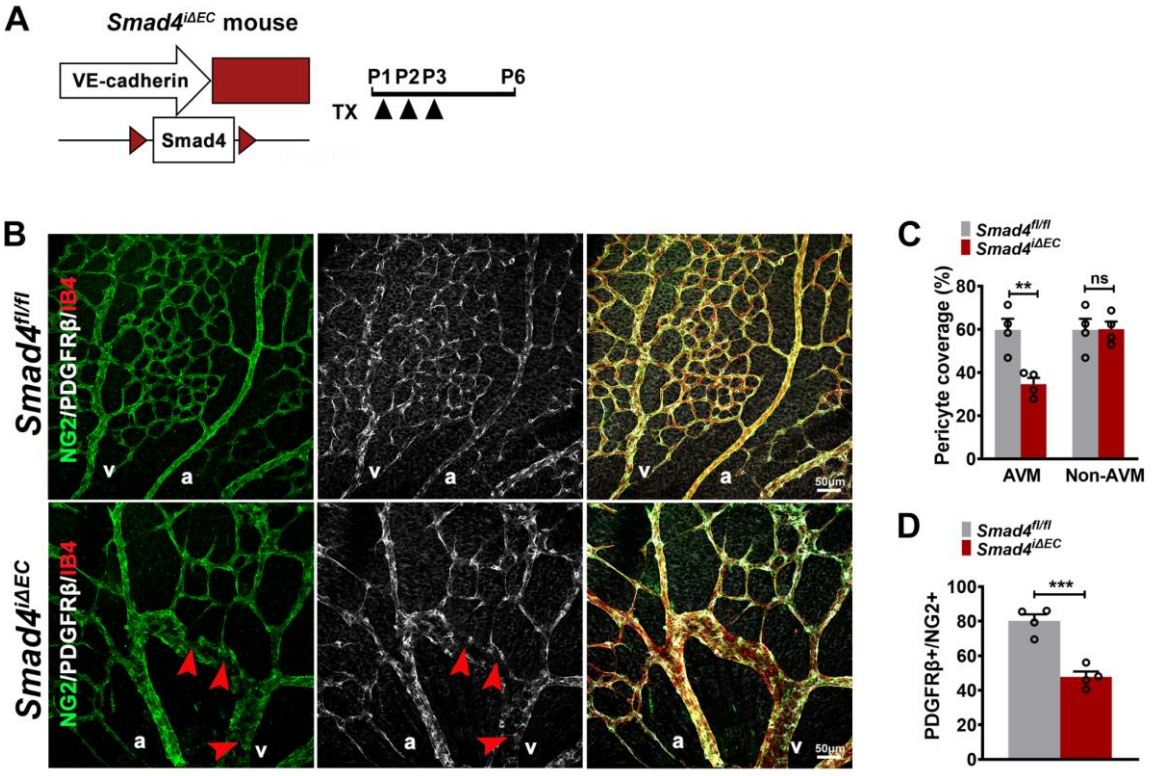

Figure 7. Deletion of *Smad4* in ECs reduces PC recruitment in AVM regions
(A) Schematic representation of gene deletion strategy in *Smad4*$^{i\Delta EC}$ mouse model. EC-specific deletion of *Smad4* was accomplished by Tx administration at P1-P3 and retina vasculature was analyzed at P6. (B) Immunofluorescence co-labeling for NG2 (green), PDGFRβ (white) and IB4 (red) in the vascular plexus of *Smad4*$^{fl/fl}$ and *Smad4*$^{i\Delta EC}$ retinas. Red arrowheads indicate loss of PCs in AVMs. (C) Quantification of PC coverage in the AVM and non-AVM regions. (D) Quantification of PDGFRβ

labeling intensity in the NG2+ PCs in AVMs and non-AVM regions. ns- non-significant, **P<0.01, ***P<0.001. a: artery, v: vein.

4.1.2 PCs exhibit decreased migration and polarization in response to *SMAD4*-deficient ECs

To investigate the effects of EC SMAD4 deficiency on PC recruitment in vitro, I depleted *SMAD4* in HUVECs using a siRNA strategy and cultured them with PCs in a dual chamber using an Ibidi culture-insert. This culture-insert contains a cell-free gap between EC and PC layers that allows us to assess the migration of PC towards the EC layer, with PCs in the right chamber and ECs in the left chamber. After 10 h incubation, PCs showed significantly reduced migration towards *SMAD4* siRNA HUVECs compared with HUVECs treated with CTRL siRNA (**Figure 8A**, quantified in **Figure 8B**). As migration requires cell orientation (cell polarization), I next determined the impact of EC *SMAD4* deficiency on PC polarization by measuring the orientation of Golgi apparatus. The co-cultured cells were stained with GM130, a specific marker for Golgi apparatus, with DAPI to distinguish the nucleus and with Phalloidin to visualize actin fibers. Cells at the wound edge were then divided into polarized (with the Golgi apparatus localized ahead of the nucleus in the wound direction) and non-polarized (when the Golgi apparatus was localized elsewhere in relation to the nucleus) (**Figure 8D**). Quantification showed that PCs co-cultured with *SMAD4*-deficient HUVECs exhibited a significant decrease in polarization towards the wound compared to PCs co-cultured with *CTRL* siRNA HUVECs (**Figure 8C**, quantified in **Figure 8D**). These findings indicate that SMAD4 in ECs is required for PC polarization and subsequent migration towards the EC layer.

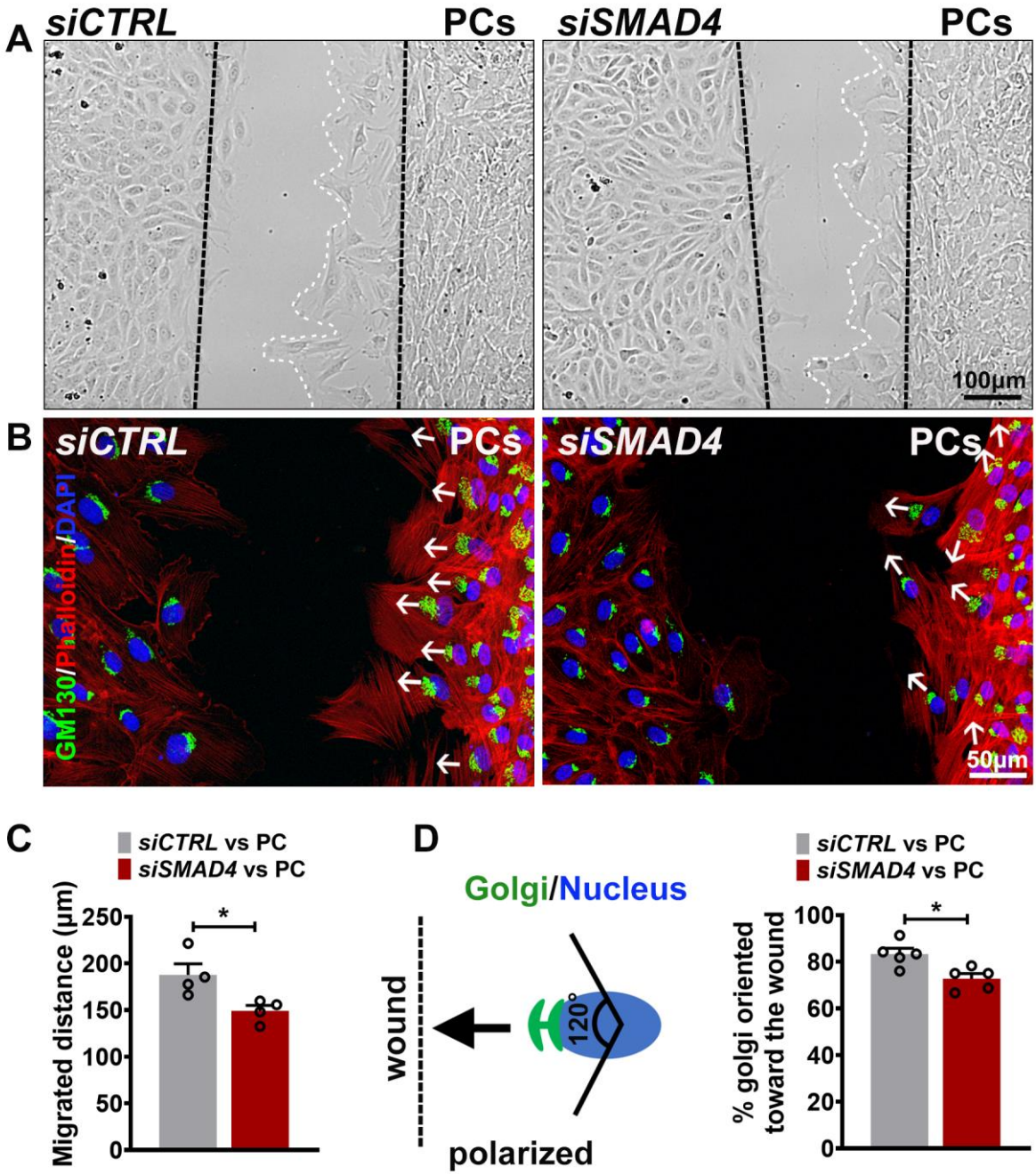

Figure 8. PCs exhibit decreased polarization and migration towards *SMAD4*-deleted HUVECs.
(A) Wound healing assay was performed to examine the migration of PCs cultured with *CTRL* or *SMAD4* siRNA HUVECs. *CTRL* or *SMAD4* siRNA HUVECs were positioned on left side, wherea PCs were placed on the right side. The white dashed lines represent the migration front after 10 h post-wounding. (B) Immunofluorescence staining for GM130 (green), Phalloidin (red) and DAPI (blue). (C) Quantification of PC migration distance following a 10 h co-culture with *CTRL* or *SMAD4* siRNA HUVECs. (D) Quantification of percentage of PCs exhibiting polarized Golgi towards the wound area following their co-culture with *CTRL* or *SMAD4* siRNA HUVECs. *P<0.05. PCs: pericytes.

4.1.3 BMP9-SMAD4 regulates FSS-induced *PDGFB* expression

Numerous studies have demonstrated that PC recruitment to developing blood vessels is due to factors produced and released by ECs that provide paracrine signals to PCs. One such factor

is PDGFB. To investigate if impaired polarization and migration of PCs towards the *SMAD4* depleted ECs is due to impaired PDGFB expression, *PDGFB* expression was analyzed by qPCR in *SMAD4* depleted versus *CTRL* siRNA treated HUVECs. Cells were subject to laminar FSS (12 DYNES/cm^2) in the presence or absence of BMP9, mimicking the physiological conditions. BMP9 or FSS alone induced expression of *PDGFB* in ECs and BMP9 further augmented the FSS induced *PDGFB* mRNA expression. However, the upregulation of *PDGFB* in response to FSS and BMP9 was blocked upon *SMAD4* depletion (**Figure 9**), emphasizing the cooperation between BMP9 and FSS to induce *PDGFB* expression in a SMAD4 dependent manner.

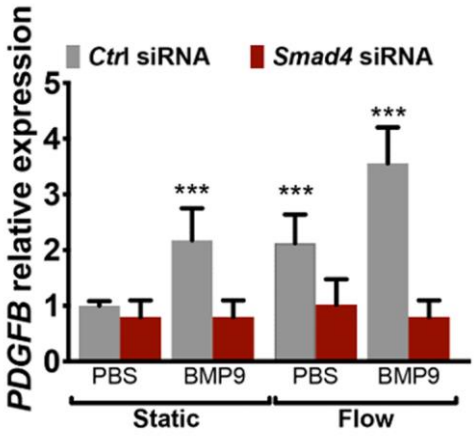

Figure 9. SMAD4 regulates FSS and BMP9-induced expression of *PDGFB*.
HUVECs were transfected with *CTRL* and *SMAD4* siRNA and subject to stimulation with 1 ng/ml BMP9 and/or 12 DYNES/cm² for 24 h. The mRNA expression of *PDGFB* was determined by qPCR technique. *** P<0.001.

4.1.4 Loss of PDGFB in ECs reduces PC migration and polarization

To further understand if PDGFB downregulation upon *SMAD4* depletion in HUVECs is responsible for impaired orientation and migration of PCs towards the ECs, *PDGFB* gene was depleted by siRNA in HUVECs and these cells were co-cultured with normal PCs. Similar to *SMAD4* siRNA HUVECs, loss of *PDGFB* in ECs led to a decreased polarity and migration of PCs towards HUVECs (**Figure 10A and C**, quantified in **Figure 10B and D**).

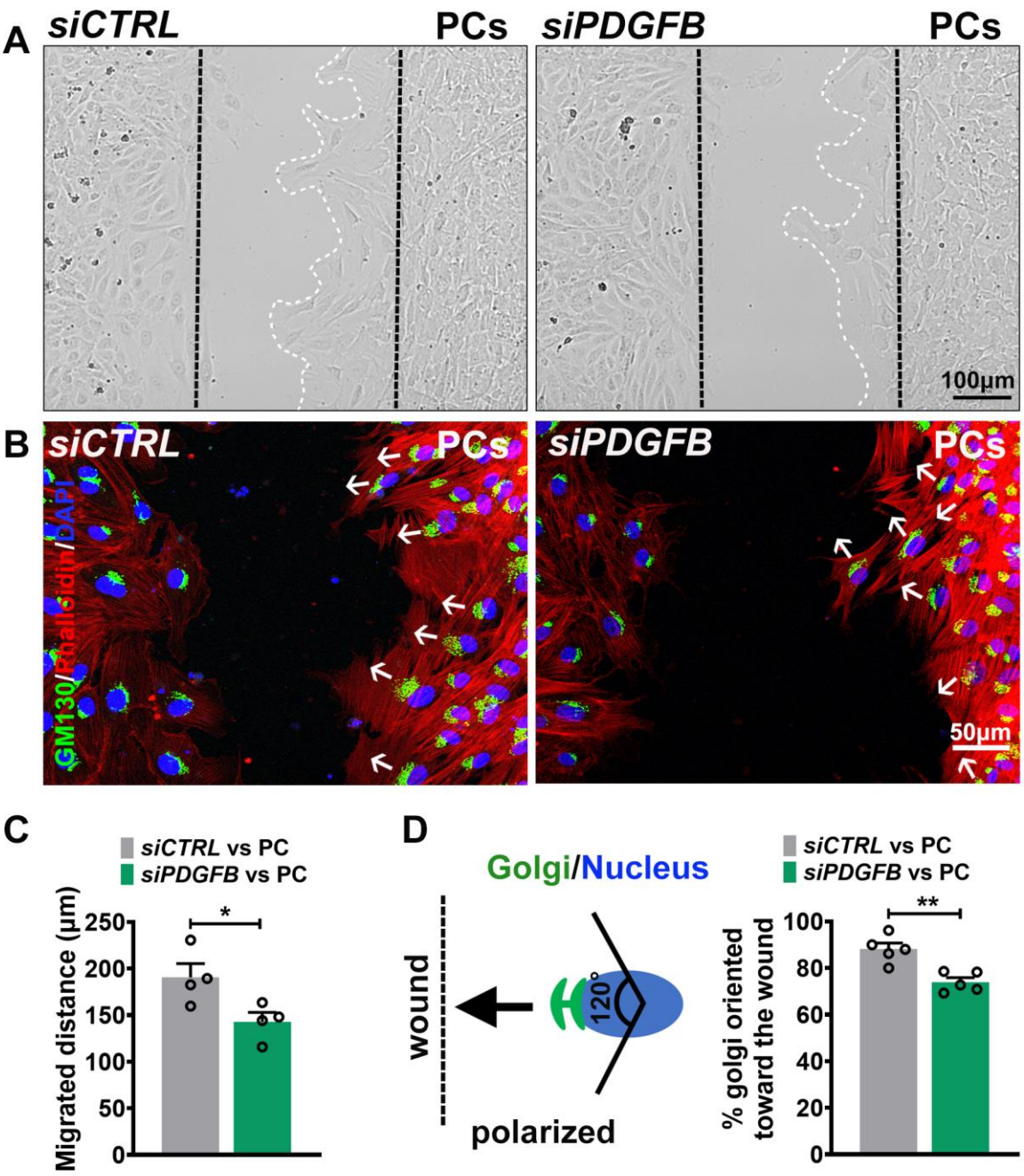

Figure 10. PCs exhibit reduced migration and polarization towards *PDGFB*-deleted HUVECs.
(A) Wound healing assay to evaluate migration of PCs towards *CTRL* or *PDGFB* siRNA HUVECs. *CTRL* or *PDGFB* siRNA HUVECs were positioned on the left side, whereas PCs were placed on the right side. The white dashed lines represent the migration front 10 h post-wounding. (B) Co-staining for GM130 (green), Phalloidin (red) and DAPI (blue). (C) Quantification of the migrating distance of PCs after a 10 h co-culture with *CTRL* or *PDGFB* siRNA HUVECS. (D) Quantification of percentage of PCs exhibiting polarized Golgi towards the wound following co-culture with *CTRL* or *PDGFB* siRNA HUVECs. *P<0.05, **P<0.01, PC: pericytes.

4.1.5 Depletion of *PDGFB* in ECs leads to increased sensitivity to FSS

Among the physiological FSS-induced cell responses, ECs increase in size and elongate and parallel to the direction of flow. To elucidate if PDGFB affects these cellular responses to flow,

I depleted *PDGFB* in ECs and evaluated its loss on FSS-mediated cell responses. HUVECs treated with *PDGFB* or *CTRL* siRNA were subject to low FSS (L-FSS) at a magnitude of 1 DYNE/cm^2 and physiological (P-FSS) at a magnitude of 12 DYNES/cm^2 for 24 h. *PDGFB* depleted HUVECs were already elongated in static condition as determined by quantifying the length/width ratio of individual ECs (**Figure 11A**, quantified in **Figure 11B**). Surprisingly, *PDGFB* siRNA HUVECs exposed to 1 DYNE/cm^2 exhibited a greater increase in size and elongation, whereas no changes were observed in *CTRL* siRNA HUVECs. When subjected to 12 DYNES/cm^2, *PDGFB* depleted HUVECs exhibited further elongation in comparison to the *CTRL* cells. These results demonstrate that loss of *PDGFB* increases the sensitivity of ECs to FSS-induced cellular responses, such as EC size and elongation.

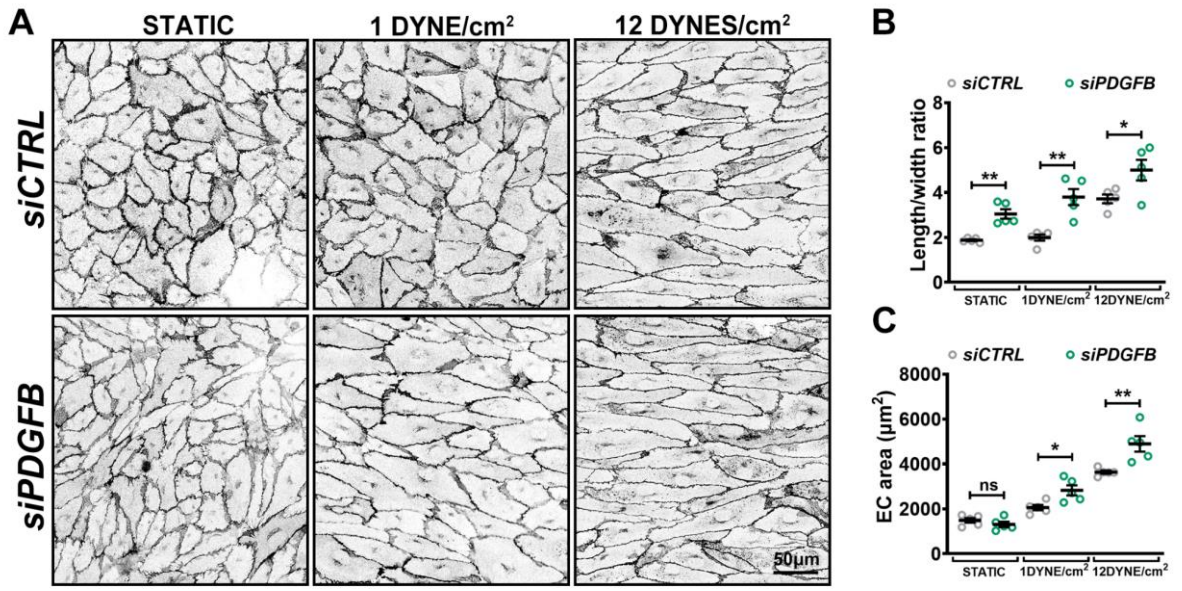

Figure 11. **Depletion of *PDGFB* in ECs enhances sensitivity to FSS.**
(A) VE-Cadherin staining (negative images) of *CTRL* and *PDGFB* siRNA HUVECs under static conditions, 1 DYNE/cm^2 and 12 DYNES/cm^2 for 24 h. Flow direction: right to left. (B,C) Quantification of length/width ratio and EC area in *CTRL* and *PDGFB* siRNAs HUVECs in static, 1 and 12 DYNES/cm^2 . ns- non-significant, *P<0.05, **P<0.01.

As shown in **Figure 9**, SMAD4 regulates the expression of *PDGFB* in response to FSS and *SMAD4* depleted HUVECs exhibit a more elongated shape under low FSS [62]. To determine if this effect is due to loss of *PDGFB* upon *SMAD4* depletion, *SMAD4* depleted HUVECs were subjected to 12 DYNES/cm^2 with 20 ng/ml recombinant human PDGF-BB for 24 h. Interestingly, exogenous PDGFB treatment significantly rescued the increased elongation in *SMAD4* siRNA HUVECs (**Figure 12A**, quantified in **Figure 12B**). Thus, the loss of *PDGFB* in *SMAD4* depleted HUVECs might be responsible for the increased sensitivity of ECs to FSS.

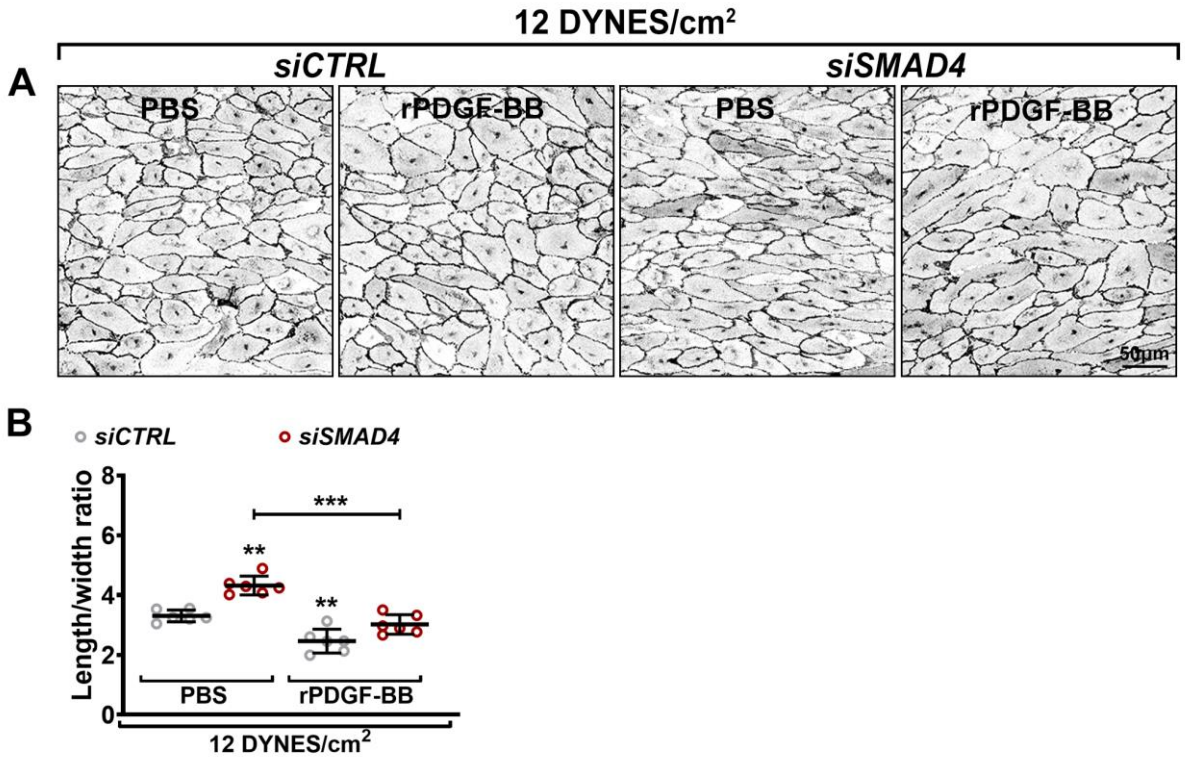

Figure 12. Exogenous PDGFB reversed the excessive EC elongation of *SMAD4* depleted HUVECs.
(A) VE-Cadherin staining (negative images) of HUVECs transfected with *CTRL* and *SMAD4* siRNAs subject to 12 DYNES/cm^2 and treated with or without 20 ng/mL recombinant PDGF-BB for 24 h. (B) Quantification of the length/width ratio of *CTRL* and *SMAD4* siRNA PBS versus PDGF-BB treated HUVECs. **P<0.01, ***P<0.001. rPDGF-BB: recombinant human PDGF-BB.

4.2 Loss of EC derived *Pdgfb* contributes to AVM pathology

4.2.1 PDGFB-mediated PC recruitment is critical for the regulation of retinal angiogenesis

To further investigate the impact of PDGFB-mediated PC recruitment on AVM pathogenesis, *Pdgfb* was depleted in ECs in *Pdgfb*$^{i\Delta EC}$ mice by crossing *Pdgfb*$^{fl/fl}$ mice with the Tx inducible Cdh5-CreERT2 mouse line (**Figure 13A**). Depletion of *Pdgfb* gene was achieved by administration of Tx by i.p. injection at P0-P2. Subsequently, pups were sacrificed and the retinal vasculature was analyzed at P7. Loss of *Pdgfb* did not cause any significant changes in body weight when compared to control neonates (*Pdgfb*$^{fl/fl}$) (**Figure 13B**). Efficient deletion of the gene was confirmed by qPCR and WB in mLECs isolated from Tx induced P7 pups (**Figure 13C** and **13D**).

As previously identified [107, 117], P7 *Pdgfb*$^{i\Delta EC}$ retinas exhibited significant vascular abnormalities, including a reduction in vascular area and outgrowth, as well as loss of side branches in both arteries and veins (**Figure 13E-H**). Yet, it is worth noting that the most notable defect was

observed in the capillaries, where a marked increase in capillary enlargement was observed (**Figure 13I**).

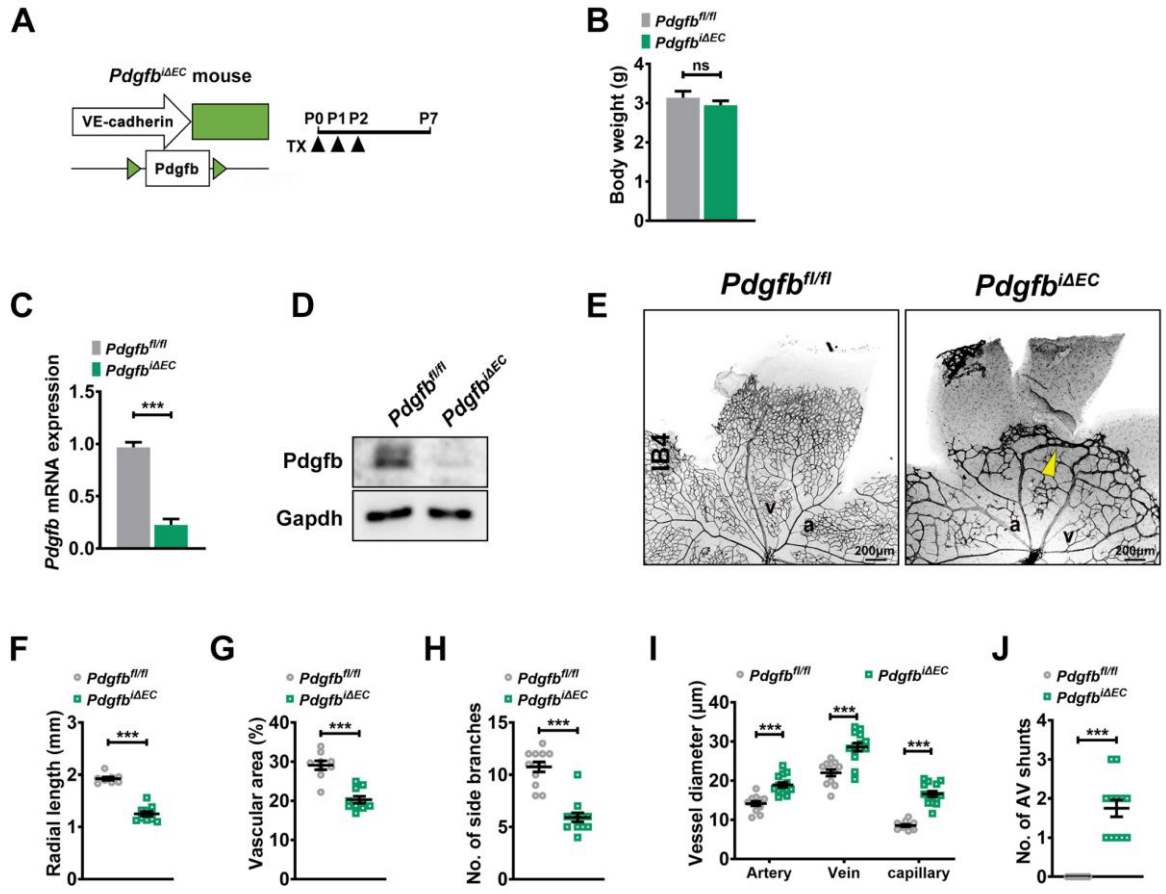

Figure 13. Loss of *Pdgfb* in ECs impairs retinal vascular development
(A) Schematic representation of the experimental strategy used to delete *Pdgfb* in ECs (P0–P7). Arrowheads indicate i.p injection of 100 μg Tx at P0-P2 in *Pdgfb*$^{fl/fl}$ and *Pdgfb*$^{i\Delta EC}$. (B) Body weight was measured in P7 in *Pdgfb*$^{fl/fl}$ and *Pdgfb*$^{i\Delta EC}$ mice. (C,D) *Pdgfb* mRNA and protein expression was assessed by qPCR (C) and WB (D), respectively, in purified mLECs from P7 *Pdgfb*$^{fl/fl}$ and *Pdgfb*$^{i\Delta EC}$ mice. (E) Labeling with IB4 (negative images) of *Pdgfb*$^{fl/fl}$ and *Pdgfb*$^{i\Delta EC}$ P7 retinas. Yellow arrow indicates AV shunt. (F-J) Quantification of radial length (F), retinal vascular area (G) and the number of side branches (H), vessel diameter (I) and number of AV shunts (J) in *Pdgfb*$^{fl/fl}$ and *Pdgfb*$^{i\Delta EC}$ retinas. ns- non-significant, **P<0.01, ***P<0.001. a: artery, v: vein.

Furthermore, the number of tip cells as well as the number and length of filopodia were dramatically reduced in *Pdgfb* depleted retinas (**Figure 14A-D**). In addition to the previously described phenotypes, loss of *Pdgfb* resulted in the formation of direct connections between arteries and veins at the vascular front, on average 1.7 direct connections (arrowhead in **Figure 13E**, quantified in **13J**).

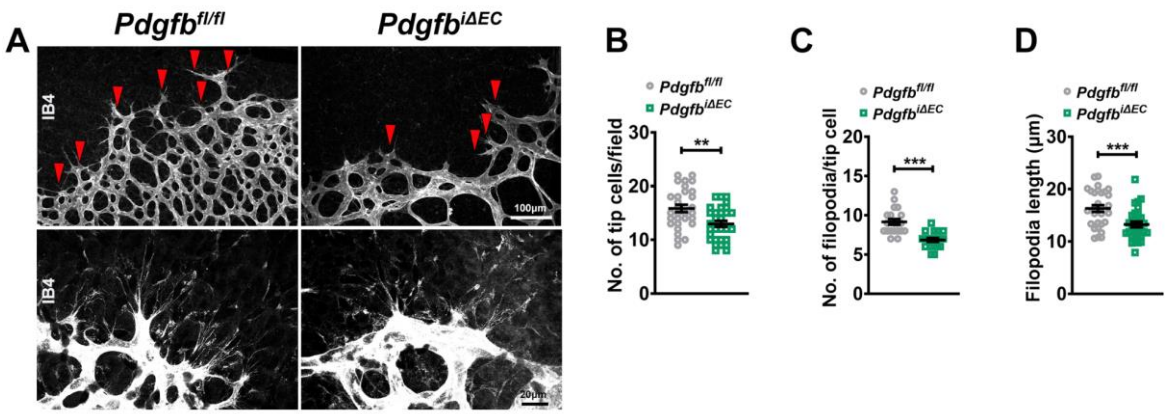

Figure14. Loss of *Pdgfb* in EC impairs vascular sprouting.
(A) High-magnification images of the angiogenic growth front in *Pdgfb*$^{fl/fl}$ and *Pdgfb*$^{i\Delta EC}$ retinas. Red arrowheads indicate tip ECs. (B, C, D) Quantification of the number of tip cells (B), number of filopodia per tip cell (C) and the filopodia length (D). **P<0.01, ***P<0.001.

To validate if these vascular abnormalities observed upon *Pdgfb* loss were linked to changes in the distribution of MCs, I labelled retinas for NG2 and α-SMA. *Pdgfb*$^{i\Delta EC}$ retinas showed a significant reduction of NG2+ PCs at the front and in the vascular plexus compared with the *Pdgfb*$^{fl/fl}$ retinas (**Figure 15A,** quantified in **15B**). Labeling for α-SMA showed a decreased in SMC coverage in arteries simultaneously with ectopic expression of α-SMA in capillaries and veins in *Pdgfb* LOF retinas (**Figure 15C,** quantified in **15D**). These results suggest that *Pdgfb*$^{i\Delta EC}$ mice exhibited loss of PC coverage and abnormal distribution of vSMCs.

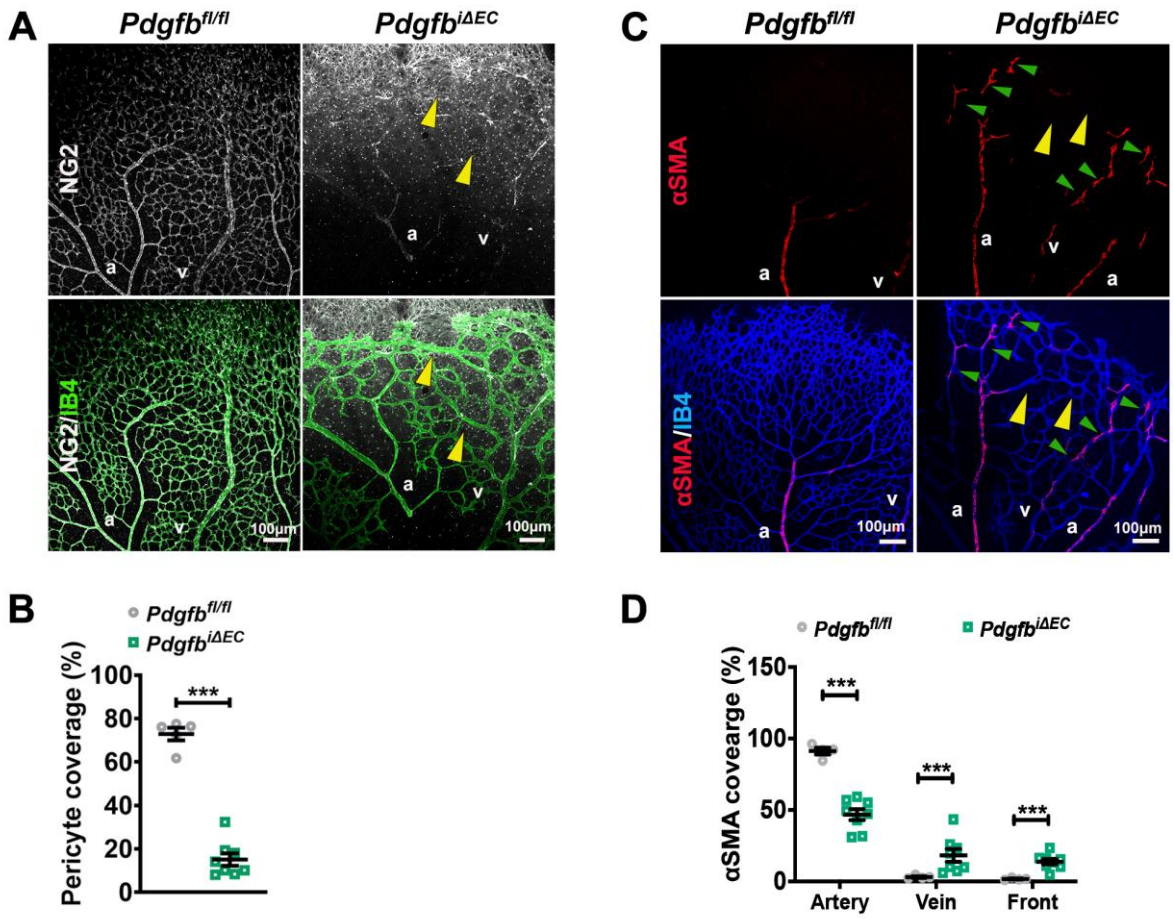

Figure 15. Depletion of *Pdgfb* in ECs results in altered PC and α-SMA coverage.
(A) Labeling for NG2 (white) and IB4 (green) of P7 *Pdgfb*$^{fl/fl}$ and *Pdgfb*^{iΔEC} retinas. Yellow arrowheads point towards dilated capillaries. (B) Quantification of the PC coverage of P7 *Pdgfb*$^{fl/fl}$ and *Pdgfb*^{iΔEC} retinas. (C) Labeling for α-SMA (red) and IB4 (blue) of P7 *Pdgfb*$^{fl/fl}$ and *Pdgfb*^{iΔEC} retinas. Green arrowheads in point towards αSMA+ cells in capillaries and veins and yellow arrowheads in point towards αSMA- capillaries. (D) Quantification of percentage of α-SMA coverage in *Pdgfb*$^{fl/fl}$ and *Pdgfb*^{iΔEC} retinas. ***P<0.001. a: artery, v: vein.

The most striking phenotypes in the *Pdgfb*^{iΔEC} retinas were enlargement of capillaries (**Figure 13I**) and a significant decrease in vascular area (**Figure 13G**). To confirm these data, P7 retinas were labelled for IB4 and ICAM2, a cell adhesion molecule found at the apical EC surface, and for Collagen IV, respectively. Immunostaining confirmed an increase in the ICAM2+ capillary lumen (**Figure 16A**, quantified in **16B**). At the same time, *Pdgfb*^{iΔEC} retinas displayed a higher number of empty collagen sleeves compared to controls, indicating increased vascular regression (**Figure 16C**, quantified in **16D**). These results emphasize that PDGFB plays a critical role in maintaining the capillary lumen size and structural integrity of retinal vasculature.

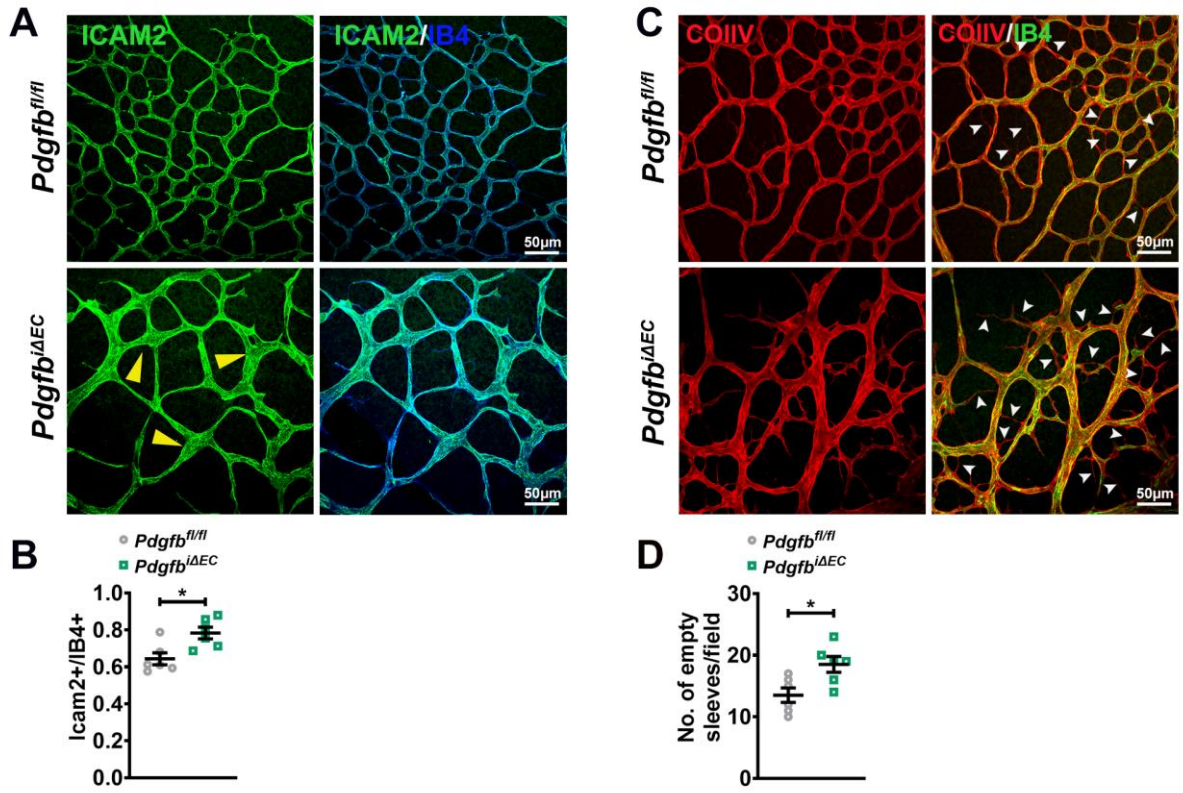

Figure 16. *Pdgfb*$^{i\Delta EC}$ mice exhibit enhanced vessel regression.
(A) Co-immunostaining with ICAM2 (green) and IB4 (blue) of P7 *Pdgfb*$^{fl/fl}$ and *Pdgfb*$^{i\Delta EC}$ mouse retinas. Yellow arrowheads indicate dilated capillaries. (B) Quantification of Icam2+/IB4+ (%) area. (C) Co-immunostaining with ColIV (red) and IB4 (green) of P7 *Pdgfb*$^{fl/fl}$ and *Pdgfb*$^{i\Delta EC}$ mouse retinas. White arrowheads indicate ColIV+/IB4- capillaries. (D) Quantification of the number of empty sleeves in P7 *Pdgfb*$^{fl/fl}$ and *Pdgfb*$^{i\Delta EC}$ mouse retinas. *P<0.05.

4.2.2 Depletion of *Pdgfb* in ECs leads to formation of AV shunting

To further identify if the observed connections between arteries and veins are indeed AV shunts, I injected latex-red dye into the left side of the neonatal P7 heart in control versus *Pdgfb* deficient mice. The latex protrudes from the arteries and cannot bypass the capillary bed due to its molecular size. However, in *Pdgfb*$^{i\Delta EC}$ retinas the latex was detected in the dilated capillaries and some retinal veins, indicating that these connections are indeed direct AV connections or AV shunts (**Figure 17A**).

To determine whether loss of *Pdgfb* leads to AV shunting in other organs, I analyzed other vascular beds after intracardial latex injection. Interestingly, I also found AV shunting in the pial vessels on the top of the brain (**Figure 17B**) and veins perfused latex in the skin of the scalp, gastrointestinal (GI) tract (small intestine) and lungs of mutant neonates, whereas no perfused veins were seen in control neonates (**Figure 17C-E**). Thus, loss of *Pdgfb* leads to AV shunting in visceral organs, emphasizing a crucial role for PDGFB-mediated PC recruitment in regulating

capillary size in different vascular beds.

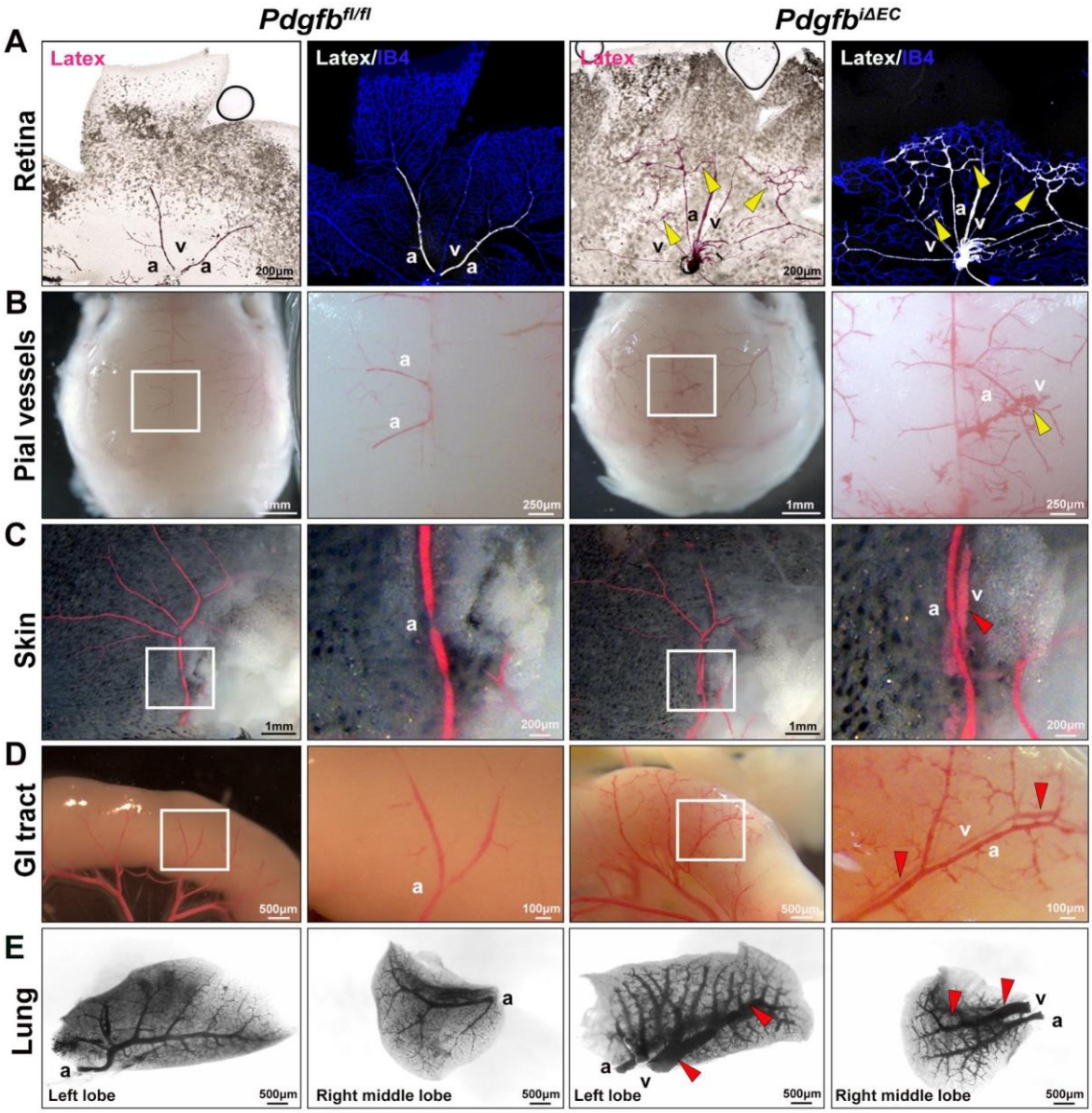

Figure 17. Loss of *Pdgfb* in ECs results in organotypic AV shunting.
(A-E) Images of P7 retinas (A), pial vessels (B), skin (C), GI tracts- small intestine (D) and lungs (negative images) (E) in *Pdgfb*$^{fl/fl}$ and *Pdgfb*$^{i\Delta EC}$ mice perfused with latex dye (red). Perfused retinas were subsequently stained with IB4 (blue). Yellow arrowheads in A,B indicate AV shunts. Red arrowheads in images C, D, and E indicate latex-perfused veins in the skin, GI tracts and lungs. a: artery, v: vein.

4.2.3 Endothelial PDGFB is required for PC maintenance to control the capillary size

To gain a better understanding of whether PDGFB-mediated maintenance of PCs on developing endothelium is required for preservation of capillary EC size, I depleted *Pdgfb* at P5-P7 and subsequently examined the retinas at P12 (as depicted in **Figure 18A**). Loss of *Pdgfb* in ECs at this particular developmental stage resulted in an increase in retinal hemorrhages, as shown

in **Figure 18B**. In P12 control retinas, PCs are covering the already stabilized vasculature. Surprisingly, *Pdgfb* loss led to a substantial decrease in PC coverage of blood vessels as measured by the ratio of NG2+/IB4+ cells within the vasculature (**Figure 18C**, quantified in **18D**). Furthermore, when measuring the vessel diameter, only the capillaries were enlarged at this stage with no significant changes in the diameter of veins or arteries (**Figure 18E**). These results suggest that PDGFB-mediated PC maintenance on developing vessels is required to support capillary size.

Interestingly, *Pdgfb* LOF retinas also exhibited AV shunting on average of 1.7 AVMs per retina, as indicated by IB4+ capillaries and veins filled with latex (**Figure 18F**, quantified in **18G**). Notably, at this particular stage, the AVM-like structures formed closer to the optic nerve in regions with higher blood flow, as indicated by the arrows in **Figure 18F**. This observation suggests that blood flow may also potentially play a role in the AV shunting upon EC *Pdgfb* loss. In addition, latex dye-positive veins were also identified in the GI system, as depicted in **Figure 18H**. Taken together, these findings suggest that PDGFB is crucial for maintaining PCs on developing endothelium to maintain capillary size and thus prevent AV shunting.

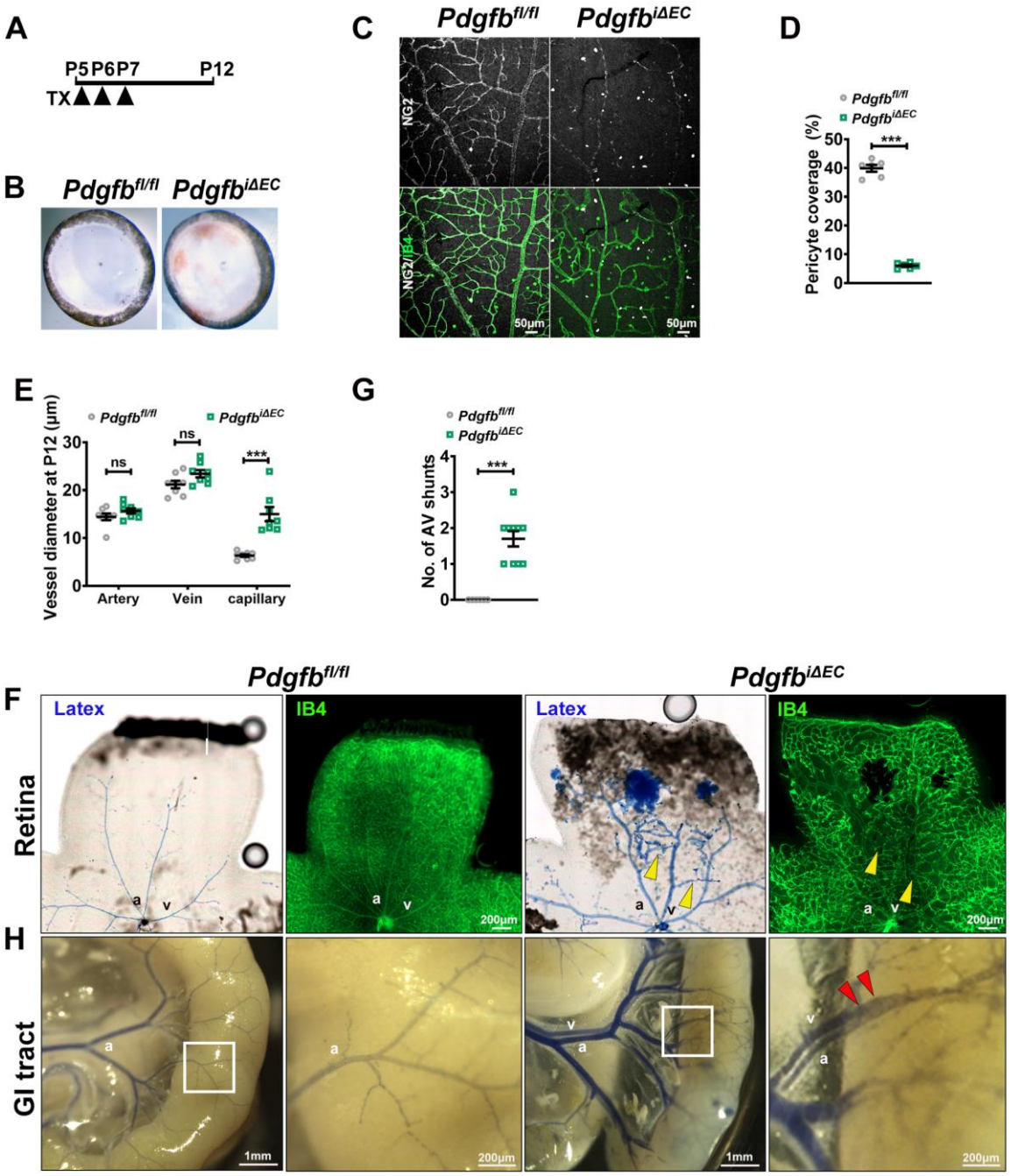

Figure 18. Endothelial *PDGFB* is required for PC maintenance to restrict the capillary size.
(A) Schematic representation of Tx administration in *Pdgfb*$^{fl/fl}$ and *Pdgfb*^{iΔEC} mice from P5-P7 and analysis of retinas at P12. (B) Representative images of hemorrhagic whole retinas in *Pdgfb*$^{fl/fl}$ and *Pdgfb*^{iΔEC} P12 neonates. (C) Labeling for NG2 (white) and IB4 (green) of P12 *Pdgfb*$^{fl/fl}$ and *Pdgfb*^{iΔEC} retinas. (D) Quantification of PC coverage in P12 retinas. (E) Quantification of retinal vessel diameter in P12 *Pdgfb*$^{fl/fl}$ and *Pdgfb*^{iΔEC} retinas. (F) Images of *Pdgfb*$^{fl/fl}$ and *Pdgfb*^{iΔEC} P12 retinas stained for IB4 (green) and latex perfusion (blue). (G) Quantification of the number of AV shunts in Pdgfb^{iΔEC} P12 retinas. (H) Images of latex-perfused P12 GI tracts in *Pdgfb*^{iΔEC} mice. Yellow arrowheads in F mark latex perfused retinal AV shunts. Red arrowheads in H mark the presence of latex-perfused veins in the GI tract. ns- non-significant, ***P<0.001. a: artery, v: vein.

4.2.4 Endothelial PDGFB regulates capillary EC size and number

The phenotype of the retina upon *Pdgfb* loss has been described previously [107, 117]. Yet the impacts of *Pdgfb* depletion on other vascular beds and the formation of AV shunting have not

been documented so far. Therefore, the AVM-like structures in P7 *Pdgfb*$^{i\Delta EC}$ retinas were further characterized. As capillary enlargement was identified as a common alteration in both P7 and P12 retinas, it is conceivable to reason that an increase in capillary diameter is the determining cause for AV shunting.

To determine whether the increase in capillaries was due to an increase in the size of individual EC and/or an increase in the number of proliferating capillaries EC, retinas were labelled with VE-cadherin, ERG, and EdU incorporation was performed. Staining with VE-cadherin revealed larger capillary single ECs and disruption of VE-cadherin at cell-cell junctions (yellow arrow) (**Figure 19A**, quantified in **19B**), thus explaining the increased hemorrhage observed in P12 mutant retinas (**Figure 18B**). Co-staining of the retinas for IB4 and ERG transcription factor [118] identified an increase in the number of capillary EC nuclei per capillary width. Whereas in control retinas, capillaries contained a single EC, capillaries in *Pdgfb*$^{i\Delta EC}$ retinas contained two to three EC nuclei (**Figure 19C**, quantified in **19D**).

To determine if EC proliferation drives capillary expansion, I quantified the S-phase ratio (EdU+ERG+/ERG+) in capillary ECs at the vascular retinal front in *Pdgfb*$^{fl/fl}$ and *Pdgfb*$^{i\Delta EC}$ neonates. Interestingly, the total percentage of S-phase (EdU+ERG+/ERG+) in P7 *Pdgfb*$^{i\Delta EC}$ retinas was decreased within the AVMs-like structures (**Figure 19E**, quantified in **19F**). In addition, retinas were labelled for P21, which is encoded by *Cdkn1a* (cyclin dependent kinase inhibitor 1A) and is used as an indicator of cell cycle arrest in ECs [119]. Quantification of the number of (P21+ERG+/ERG+) cells identified an increase in the number of arrested ECs within the dilated capillaries (**Figure 19G**, quantified in **19H**). Taken together, these data suggest that capillary enlargement in *Pdgfb*$^{i\Delta EC}$ retinas is not accompanied by proliferation but by an increase in the size of individual ECs.

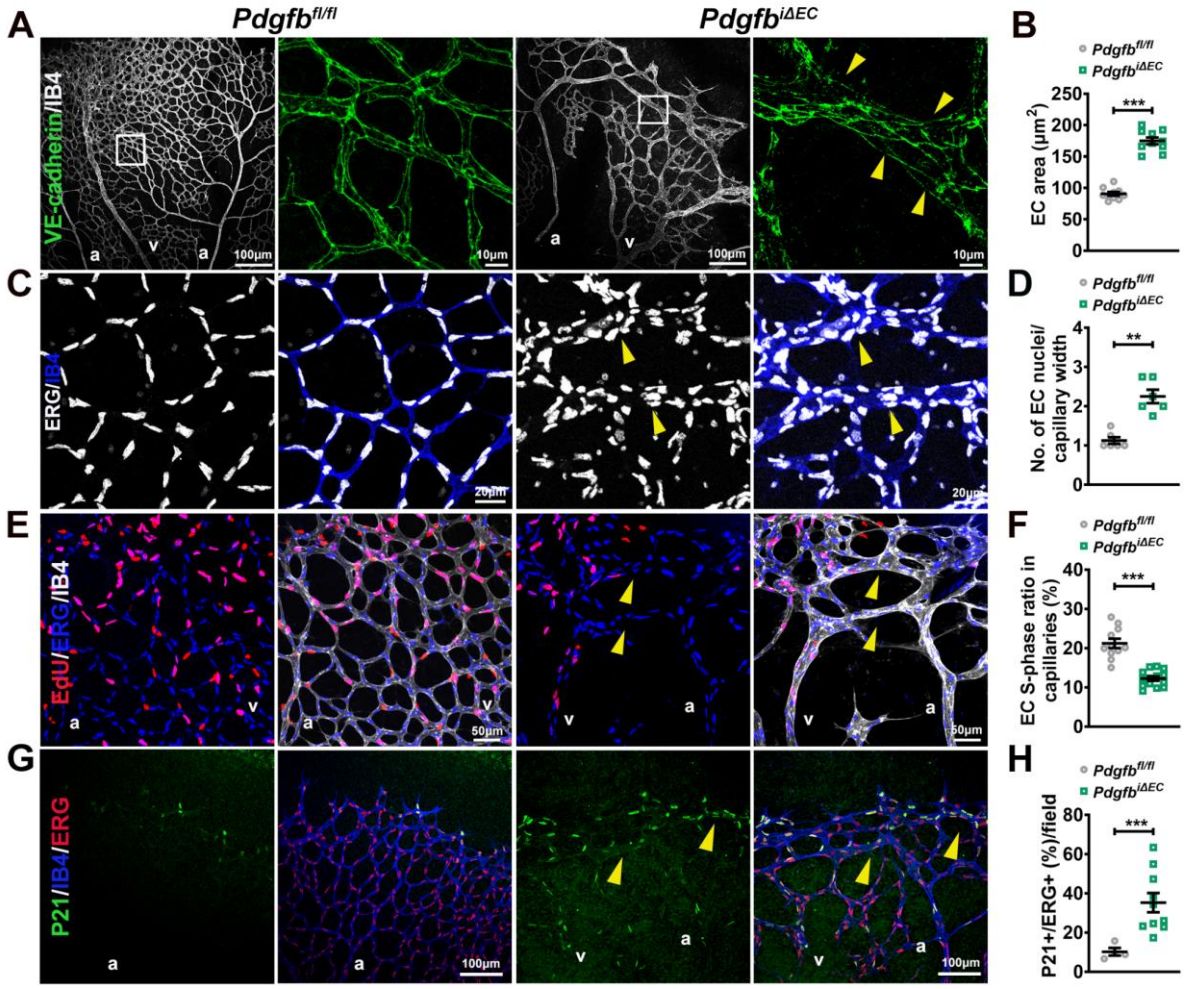

Figure 19. PDGFB maintains EC size independent of EC proliferation.
(A) Co-immunolabeling of VE-cadherin (green) and IB4 (white) of P7 *Pdgfb*$^{fl/fl}$ and *Pdgfb*$^{i\Delta EC}$ retinas. Yellow arrows in A point towards ECs with loss of VE-cadherin at the cell-cell junctions. (B) Quantification of the single EC area of P7 *Pdgfb*$^{fl/fl}$ and *Pdgfb*$^{i\Delta EC}$ retinas. (C) Co-immunolabeling of ERG (white) and IB4 (blue) of P7 *Pdgfb*$^{fl/fl}$ and *Pdgfb*$^{i\Delta EC}$ retinas. Yellow arrows in C towards the dilated capillaries containing more than one EC. (D) Quantification of the number of EC nuclei per capillary width. (E) Co-immunolabeling for EdU (red), ERG (blue) and IB4 (white) in P7 *Pdgfb*$^{fl/fl}$ and *Pdgfb*$^{i\Delta EC}$ retinas 4 h after EdU incorporation. The yellow arrowheads indicate the EdU- ECs in the AV shunt. (F) Quantification of the S-phase ratio (EdU+ ERG+/ERG+) in the capillaries of P7 *Pdgfb*$^{fl/fl}$ and *Pdgfb*$^{i\Delta EC}$ retinas. (G) Co-immunolabeling of P21 (green), IB4 (blue) and ERG (red) in P7 *Pdgfb*$^{fl/fl}$ and *Pdgfb*$^{i\Delta EC}$ retinas. Yellow arrowheads indicate AV shunts. (H) Quantification of the percentage of P21+ERG+ ECs in P7 *Pdgfb*$^{fl/fl}$ and *Pdgfb*$^{i\Delta EC}$ retinas. **P<0.01, ***P<0.001. a: artery, v: vein.

4.2.5 Endothelial PDGFB regulates capillary EC polarity

Pdgfb LOF retinas were characterized by fewer ECs accompanied by decreased EC proliferation, yet the dilated capillaries contained larger individual ECs but also more ECs. These results emphasize that a different cellular mechanism is responsible for the increased number of ECs per capillary width. Migration of ECs against the direction of flow, from low to higher flow regions is essential for both vessel regression-mediated vascular remodeling and artery formation [52, 120]. Also, maladapted migration against the bloodstream was proposed to be the

triggering event for AVMs upon *Alk1* or *Eng* EC depletion [49, 53]. As vascular regression was significantly increased in *Pdgfb* LOF retinas, it was plausible to further test if abnormal EC orientation (polarization), a prerequisite for EC migration was responsible for capillary dilation and AV shunting. To determine whether defective flow-mediated EC migration plays a role in capillary enlargement and AV shunting, $Pdgfb^{fl/fl}$ and $Pdgfb^{i\Delta EC}$ retinas were labelled for GM130, ERG and IB4. Quantification of the orientation of Golgi apparatus toward the flow direction in retinal vessels (in an angle ≤ 45° in relation to predicted flow direction-EC orientation) showed that in $Pdgfb^{i\Delta EC}$ retinas, more ECs were oriented towards the direction of blood flow in arteries, veins and capillary ECs involved in AV shunts, whereas ECs in $Pdgfb^{fl/fl}$ retinas were strongly polarized against the direction of flow (**Figure 20A** and quantified in **20B**).

To confirm these data *in vitro*, I depleted *PDGFB* in HUVECs and measured EC orientation under P-FSS. After 24 h, HUVECs were labelled with GM130, DAPI and VE-cadherin to visualize the Golgi apparatus, nucleus and EC junctions. Under P-FSS, approximately 50% of *CTRL* siRNA cells polarized in the opposite direction to against the flow, whereas *PDGFB*-depleted HUVECs polarized more in the direction of flow (**Figure 20C** and quantified in **20D**). Collectively, these findings imply that capillary enlargement is a result of the accumulation of ECs within the capillaries due to a failure of ECs to migrate against the bloodstream together with an increased in individual EC size.

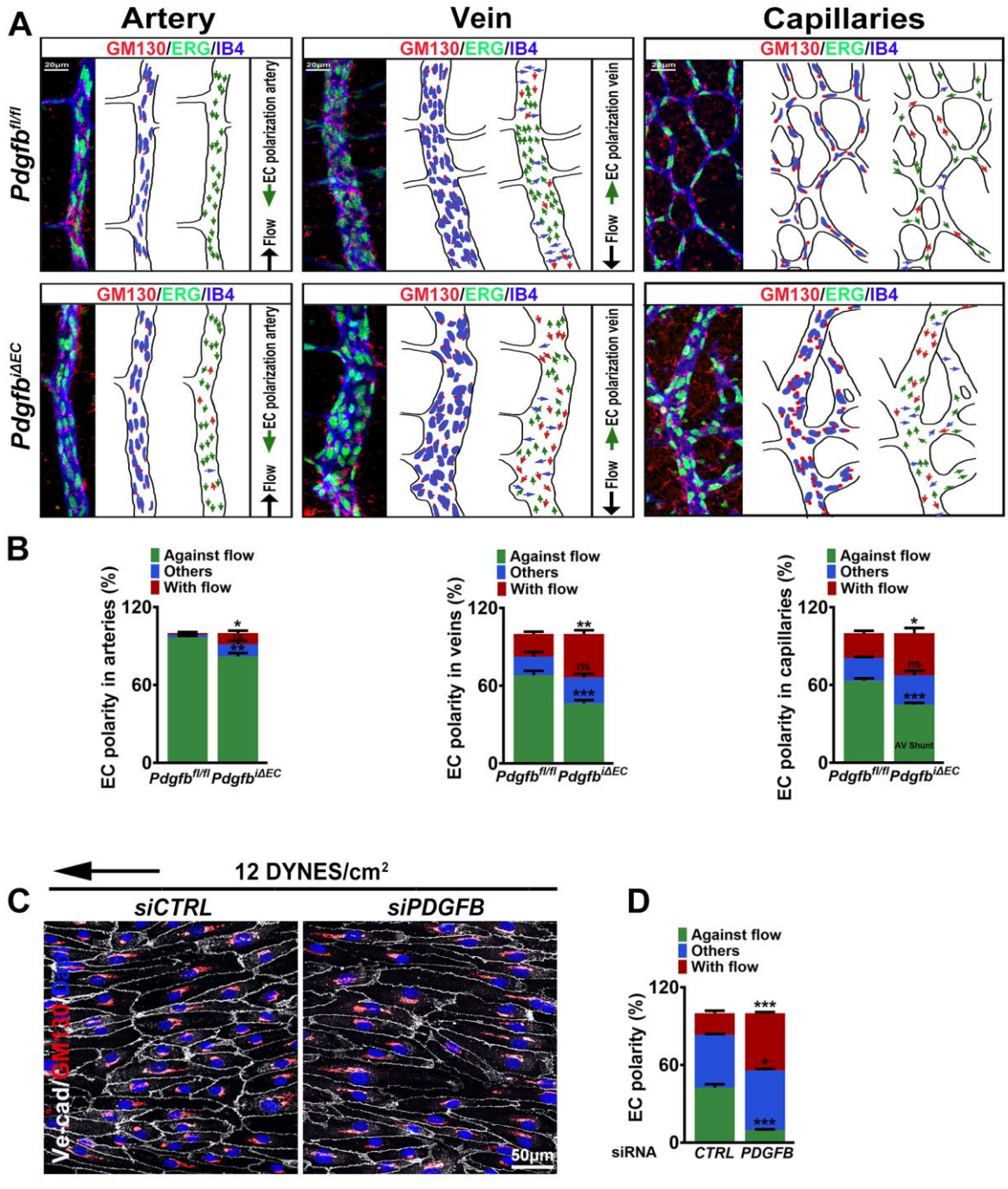

Figure 20. PDGFB regulates EC polarity in vivo and in vitro.
(A) Co-immunolabeling with ERG (green), IB4 (blue) and GM130 (red) in the arteries, veins and capillaries of P7 *Pdgfb*$^{fl/fl}$ and *Pdgfb*^{iΔEC} retinas. The right panels illustrate EC polarization, determined by the position of Golgi apparatus ahead of nucleus in the direction of migration (indicated by green arrows). (B) Quantification of EC polarization: against the direction of flow (indicated by green arrows), towards the direction of flow (indicated by red arrows) and non-oriented (indicated by blue arrows) in arteries, veins and capillaries from P7 *Pdgfb*$^{fl/fl}$ and *Pdgfb*^{iΔEC} retinas. (C) HUVECs labelled with GM130 (red), VE-cadherin (white) and DAPI (blue) for nuclei. (D) Quantification of EC orientation against the direction of flow, with the flow and others (non-oriented). ns- non-significant, *P<0.05, **P<0.01, ***P<0.001.

4.2.6 Loss of *Pdgfb* in ECs results in an altered capillary AV zonation

scRNA sequencing of brain ECs isolated from *Pdgfb* hypomorphs (*Pdgfb*$^{ret/ret}$) revealed

defective capillary zonation with venous skewing, supporting the role of PCs in maintaining capillary AV differentiation [90]. To determine whether loss of *Pdgfb* leads to a similar phenotype in retinal capillaries, retinas from *Pdgfb*$^{i\Delta EC}$ and control groups were immunolabelled for arterial and venous markers. While JAG1 was expressed in the arteries and arterioles in control retinas, in *Pdgfb* LOF retinas, JAG1 expression decreased in the arterioles but was maintained in the main arteries (red arrowheads in **Figure 21A**, quantified in **21B**). In contrast, expression of endomucin [121], a transmembrane mucin found exclusively on the surface of capillary and venous endothelium in control retinas, showed a contrasting pattern with extended labeling in all capillary ECs and arterioles in *Pdgfb*$^{i\Delta EC}$ retinas (blue arrowheads in **Figure 21C**, quantified in **21D**). These findings reveal that loss of *Pdgfb* in ECs leads to loss of arterial identity with a concomitant increase in venous identity.

To further confirm the occurrence of venous skewing in *Pdgfb*$^{i\Delta EC}$ retinas, qPCR analysis was performed on isolated mLECs. The results showed an increase in venous markers, such as *Ephb4, Nrp2*, *Nr2f2* and *Aplnr*, as shown in Figure **21E**. Nevertheless, qPCR analysis also identified upregulation of arterial markers, e.g *Sox17*, *Nrp1*, *Unc5b* and *Efnb2* upon *Pdgfb* loss (**Figure 21F)**.

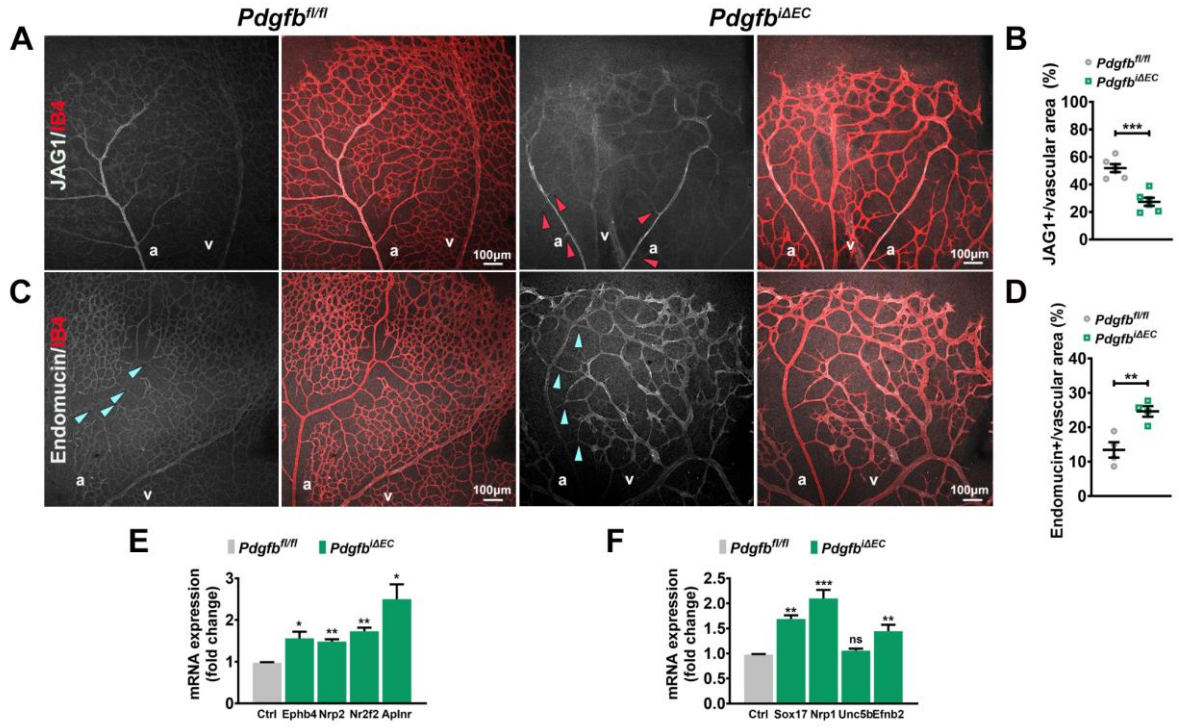

Figure 21. Endothelial PDGFB is essential for maintaining capillary AV zonation.
(A,C) P7 *Pdgfb*$^{fl/fl}$ and *Pdgfb*$^{i\Delta EC}$ retinas immunostained with IB4 (red) and JAG1 (white) (A), IB4 (red) and Endomucin (white) (C). (B,D) The labelling intensity for JAG1 (B) and Endomucin (D) in P7 *Pdgfb*$^{fl/fl}$ and *Pdgfb*$^{i\Delta EC}$ retinas was quantified. (E, F) qPCR

analysis was performed to compare the expression of venous markers (E) and arterial markers (F) in mLECs isolated from *Pdgfb*$^{fl/fl}$ and *Pdgfb*$^{i\Delta EC}$ mice. Red arrowheads in A indicate loss of JAG1 expression in arterioles. Blue arrowheads in C indicate endomucin expression in arterioles. ns: non-significant, *P<0.05, **P<0.01, ***P<0.001. a: artery, v: vein.

To perform a more comprehensive study of arterial identity acquisition, retinas were subsequently labelled for SOX17, an important regulator of arterial identity [122]. Remarkably, SOX17 expression was maintained in the artery after loss of *Pdgfb* and spread towards the vein via the AV shunt (**Figure 22A**, quantified in **22C**). Moreover, SOX17+ ECs were observed in the veins (indicated by yellow arrowheads in **Figure 22B**). Thus, these results suggest that the AV shunt upon *Pdgfb* loss is associated with the acquisition of arterial properties.

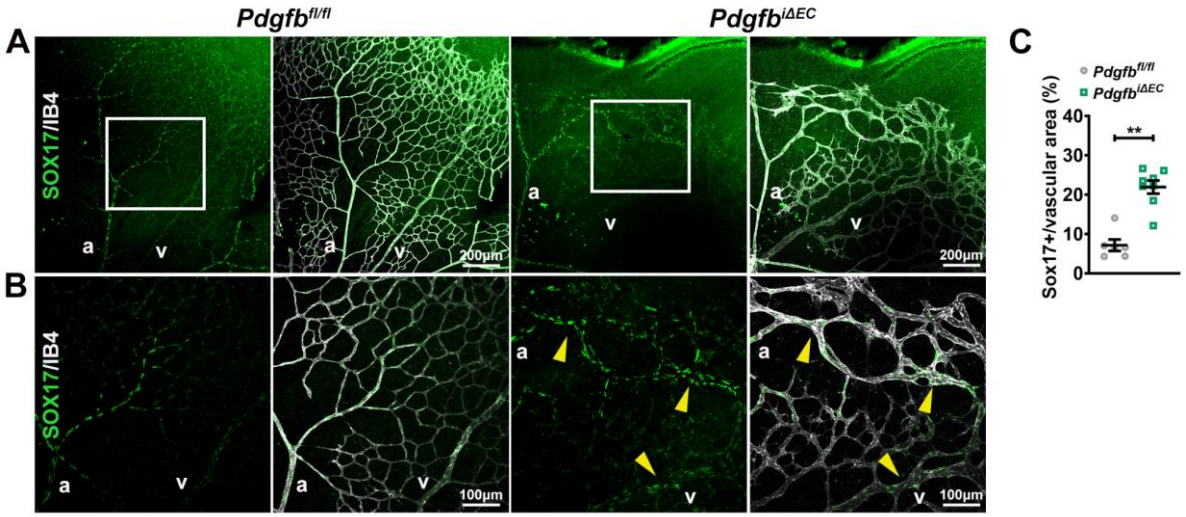

Figure 22. Depletion of *Pdgfb* in ECs results in SOX17+ cells in the vein.
(A) Immunostaining for SOX17 (green) and IB4 (white) on P7 *Pdgfb*$^{fl/fl}$ and *Pdgfb*$^{i\Delta EC}$ retinas. (B) Higher magnification from A (the white squares in A). (C) Quantification of the labelling intensity of SOX17 per vascular area in P7 *Pdgfb*$^{fl/fl}$ and *Pdgfb*$^{i\Delta EC}$ retinas. Yellow arrowheads indicate SOX17+ ECs. **P<0.01, a: artery, v: vein.

4.2.7 PDGFB-mediated PC recruitment is associated with activation of TGF-β/BMP and NOTCH signaling pathways

As loss of *Pdgfb* leads to a defective capillary AV zonation, I next investigated the signaling pathways that regulate AV identity. In addition to the well-described role of NOTCH signaling in maintaining arterial identity [71, 123], a recent study identified TGF-β and BMP signaling pathways in regulating arterial and venous identity, respectively [124]. To assess activation of TGF-β and BMP pathways, *Pdgfb*$^{fl/fl}$ and *Pdgfb*$^{i\Delta EC}$ retinas were labelled for activated canonical SMADs. Interestingly, the *Pdgfb*$^{i\Delta EC}$ retinas exhibited an increase in activated canonical SMAD1/5 and SMAD3, with the highest intensity in the ECs within the AVMs-like structures (**Figure 23A, C**, quantified in **23B, D**).

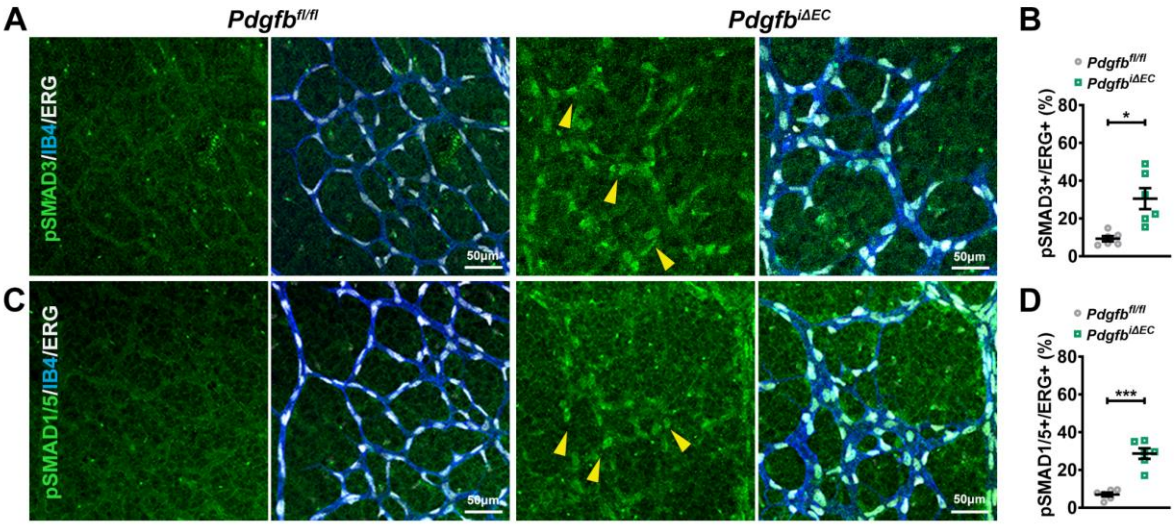

Figure 23. Loss of endothelial *Pdgfb* is associated with activation of TGFβ/BMP signaling pathways.
(A) Co-labelling of P7 *Pdgfb*$^{fl/fl}$ and *Pdgfb*$^{i\Delta EC}$ retinas with IB4 (blue), ERG (white) and pSMAD3 (green). The yellow arrowheads indicate positive pSMAD3 ECs. (B) Quantification of the percentage of pSmad3+/ERG+ ECs in P7 *Pdgfb*$^{fl/fl}$ and *Pdgfb*$^{i\Delta EC}$ retinas. (C) Co-labelling of P7 *Pdgfb*$^{fl/fl}$ and *Pdgfb*$^{i\Delta EC}$ retinas with IB4 (blue), ERG (white) and pSMAD1/5 (green). The yellow arrowheads indicate positive pSMAD1/5 ECs (D) Quantification of the percentage of pSMAD1/5+/ERG+ ECs in P7 *Pdgfb*$^{fl/fl}$ and *Pdgfb*$^{i\Delta EC}$ retinas. *P<0.05, ***P<0.001.

In addition, activation of canonical SMADs resulted in upregulation of TGFβ/BMP target genes, including ID1 (**Figure 24A**, quantified in **24C**) and ENG (**Figure 24B**, quantified in **24D**). WB analysis on mLECs isolated from P7 *Pdgfb*$^{fl/fl}$ and *Pdgfb*$^{i\Delta EC}$ mice confirmed an increase in phosphorylation of SMAD3 and SMAD1/5 upon *Pdgfb* loss (**Figure 24E**).

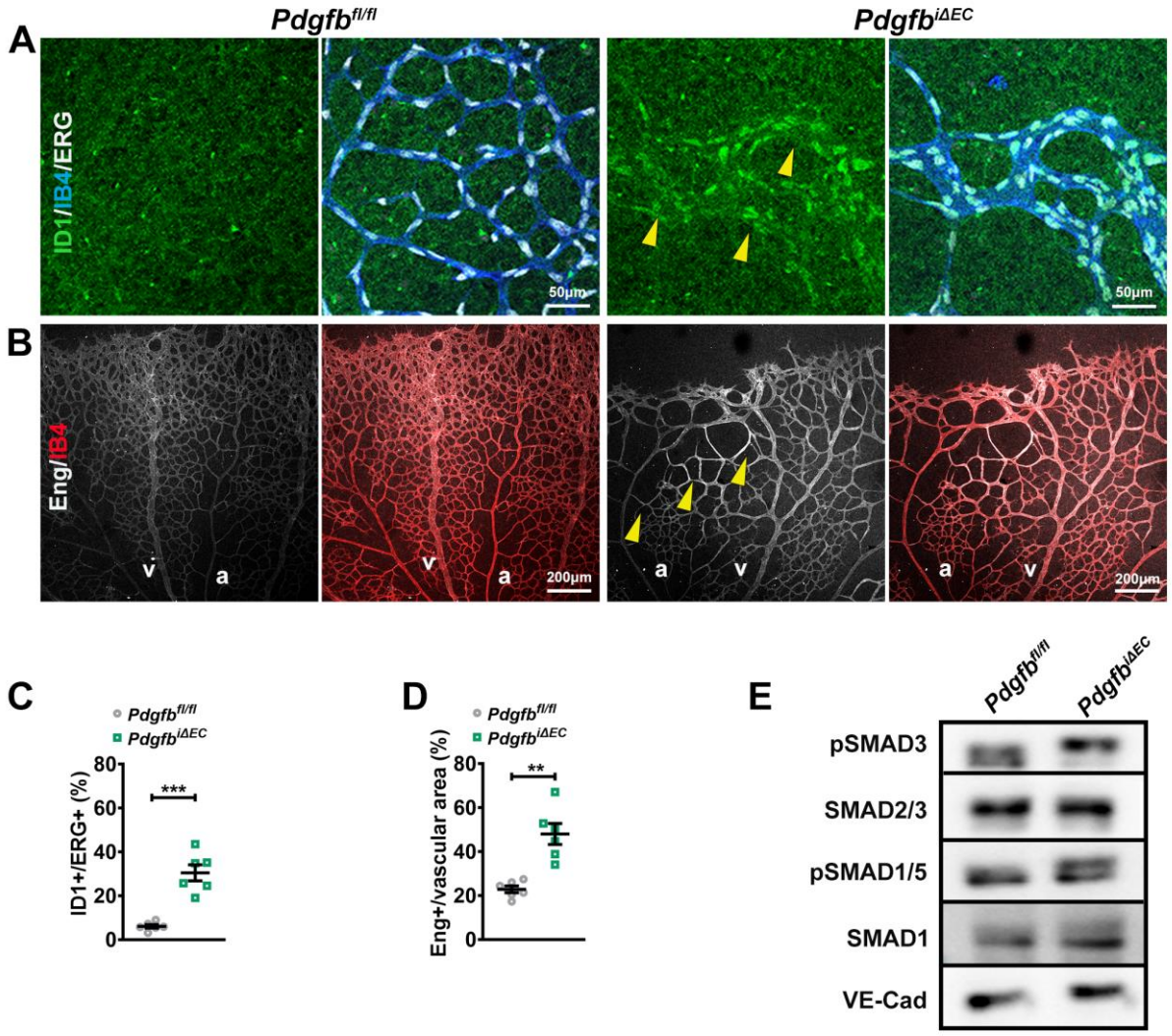

Figure 24. Loss of endothelial *Pdgfb* regulates TGFβ/BMP pathway downstream targets.
(A) Images of P7 *Pdgfb*$^{fl/fl}$ and *Pdgfb*^{iΔEC} retinas were stained with IB4 (blue), ERG (white) and ID1 (green). Yellow arrowheads indicate positive ID1 ECs. (B) Images of P7 *Pdgfb*$^{fl/fl}$ and *Pdgfb*^{iΔEC} retinas were stained with IB4 (red) and Eng (white). Yellow arrowheads indicate increased Eng expression in capillaries. (C) Quantification of the percentage of ID1+/ERG+ ECs in P7 *Pdgfb*$^{fl/fl}$ and *Pdgfb*^{iΔEC} retinas. (D) Quantification of the labelling intensity per vascular area (%) of Eng in P7 *Pdgfb*$^{fl/fl}$ and *Pdgfb*^{iΔEC} retinas. (E) WB analysis of *Pdgfb*$^{fl/fl}$ and *Pdgfb*^{iΔEC} mLECs for activated pSMAD1/5, pSMAD3, total SMAD1, SMAD2/3 and VE-Cadherin. *P<0.05, **P<0.01, ***P<0.001. a: artery, v: vein.

NOTCH signaling has been suggested as a regulator of PC function in the developing vasculature [125] and gain of function mutations in *Notch4* [126, 127] or *Notch1* [128] in ECs also result in AVM formation. To identify if increased Notch occur upon *Pdgfb* loss, *Pdgfb*$^{fl/fl}$ and *Pdgfb* ^{iΔEC} retinas were labelled for DLL4. Surprisingly, DLL4 expression was upregulated in the arteries and within the capillaries engaged in the AV shunting (**Figure 25A**, quantified in **25B**). To further validate increased NOTCH signaling upon *Pdgfb* loss, the expression of NOTCH transducers and transcriptional effectors was further analyzed. The qPCR results revealed upregulation of *Notch1* and *Notch4* receptors, as well as increased levels of the transcription

factors *Hey1*, *Hey2*, and *Hes1* (**Figure 25C**). These findings provide evidence of EC NOTCH activation upon *Pdgfb* loss. The findings here, thus emphasize that an altered AV zonation upon *Pdgfb* depletion is correlated with activation of TGFβ/BMP and NOTCH signaling pathways in ECs.

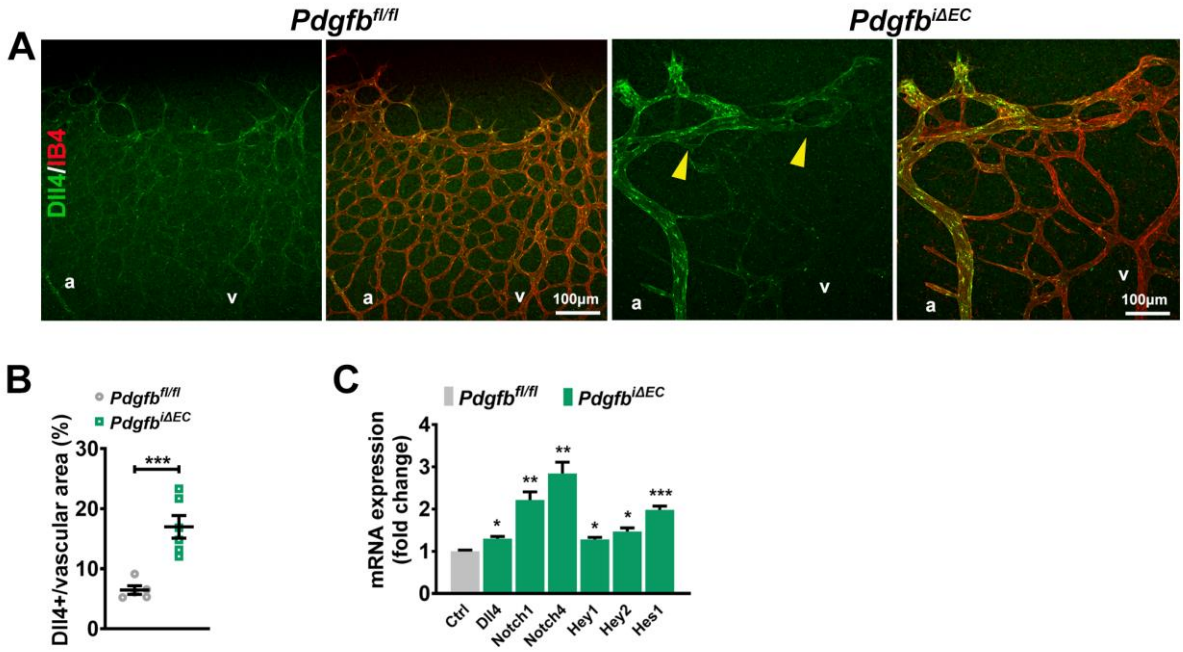

Figure 25. Loss of EC *Pdgfb* is associated with activation of NOTCH signaling pathways.
(A) Labeling for Dll4 (green) and IB4 (red) at the sprouting vascular fronts of P7 *Pdgfb*$^{fl/fl}$ and *Pdgfb*^{iΔEC} retinas. Yellow arrowheads indicate Dll4 expression in AV shunt. (B) Quantification of the labelling intensity per vascular area (%) of Dll4 in P7 *Pdgfb*$^{fl/fl}$ and *Pdgfb*^{iΔEC} retinas. (C) qPCR analysis of the expression of notch pathway-associated genes in isolated mLECs from P7 *Pdgfb*$^{fl/fl}$ and *Pdgfb*^{iΔEC} mice. *P<0.05, **P<0.01, ***P<0.001. a: artery, v: vein.

4.2.8 Capillary enlargement induces pathological flow-mediated KLF4 upregulation

Vascular homeostasis is under a permanent control by biochemical and mechanical stimuli. Mechanical stimuli such as the physiological FSS regulates MC recruitment and contributes to maintenance of arterial cell fate [45, 129]. In turn, MCs have a crucial role in the regulation of blood flow and vascular tone, as well as the directionality of blood flow at the cell-cell junctions [130].

Loss of *Pdgfb* in ECs leads to capillary enlargement and thus resulting in an altered blood flow pattern within the capillaries. To visualize alterations in flow patterns upon *Pdgfb* loss, I labelled retinas for KLF4, a robust FSS indicator in the retina vasculature [47]. In control retinas, KLF4 expression was the highest in arteries and arterioles containing the highest blood flow, followed by veins, and little expressed in low flow regions such as the vascular front and

capillary ECs. However, in *Pdgfb*^{iΔEC} retinas, KLF4 expression increased and spread throughout the dilated capillary plexus (**Figure 26A, B**), with more KLF4+ ECs in the capillaries and veins (**Figure 26C**). Interestingly, measurement of the intensity of KLF4 labeling per individual EC as an indicator of activation in response to blood flow revealed that KLF4 was more activated in capillaries and veins involved in AV shunts than in control retinas, where KLF4 was more active in arteries and arterial branch points (**Figure 26D**). The upregulation of *Klf4* mRNA expression was also confirmed by qPCR in *Pdgfb*^{iΔEC} mLECs (**Figure 26E**). These findings collectively suggest that the activation of KLF4 within the capillaries and veins upon *Pdgfb* depletion is likely a result of the combined influence of pathological flow and enhanced sensitivity of ECs to flow, as supported by the vitro data (**Figure 11A, B**).

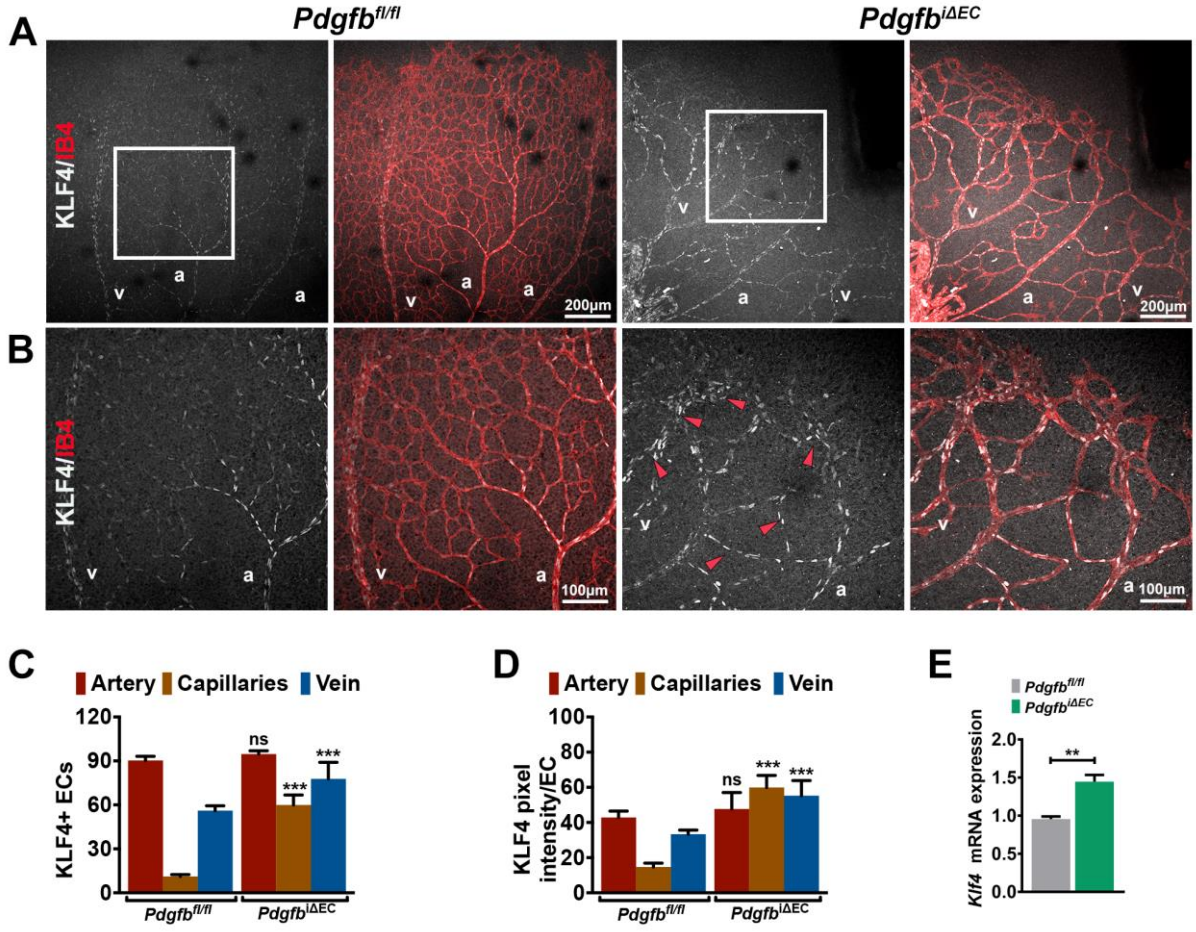

Figure 26. Capillary enlargement induces pathological flow-mediated KLF4 upregulation.
(A,B-small insets) Co-labelling of P7 *Pdgfb*$^{fl/fl}$ and *Pdgfb*^{iΔEC} retinas for KLF4 (white) and IB4 (red). KLF4+ ECs are indicated by red arrowheads that point to veins and expanded capillaries, respectively. (C,D) The number of KLF4+ ECs and the intensity of KLF4 labeling per EC in arteries, capillaries, and veins quantified in *Pdgfb*$^{fl/fl}$ and *Pdgfb*^{iΔEC} retinas. (E) mRNA expression of *Klf4* in mLECs isolated from P7 *Pdgfb*$^{fl/fl}$ and *Pdgfb*^{iΔEC} mice. ns: non-significant, **P<0.01, ***P<0.001. a: artery, v: vein.

KLF4 has been previously recognized as a direct transcriptional activator of *BMP6*, *TGF-β1*, and

DLL4 ligands [131-133]. As an increase in DLL4 ligands and activation of canonical SMADs downstream of TGF-β1 and BMP ligands were already identified, qPCR and WB was performed to identify changes in the expression levels of *Tgf-β1* and *Bmp6* in $Pdgfb^{fl/fl}$ and $Pdgfb^{i\Delta EC}$ mLECs mice. The results confirmed an increase in the expression of *Tgf-β1* and *Bmp6* at both, mRNA and protein levels (**Figure 27A, B**). To validate these findings, I labelled of retinas for BMP6 (**Figure 27C**) and TGF-β1 (**Figure 27E**). In control retinas, both ligands were expressed at very low levels. Nevertheless, in *Pdgfb* LOF retinas, the expression of BMP6 and TGF-β1 was increased at the vascular front and within the AV shunts (**Figure 27C, E** and quantified in **Figure 27D, F**). These findings were further validated by reanalysis of the previously published Betsholtz database of $Pdgfb^{ret/ret}$ mice (**Figure 27G** and **H**, https://betsholtzlab.org/Publications/RetECscRNAseq/database.html). These results suggest that hyperactive KLF4 expression in dilated capillaries of $Pdgfb^{i\Delta EC}$ retinas is associated with upregulation of TGF-β1 and BMP6.

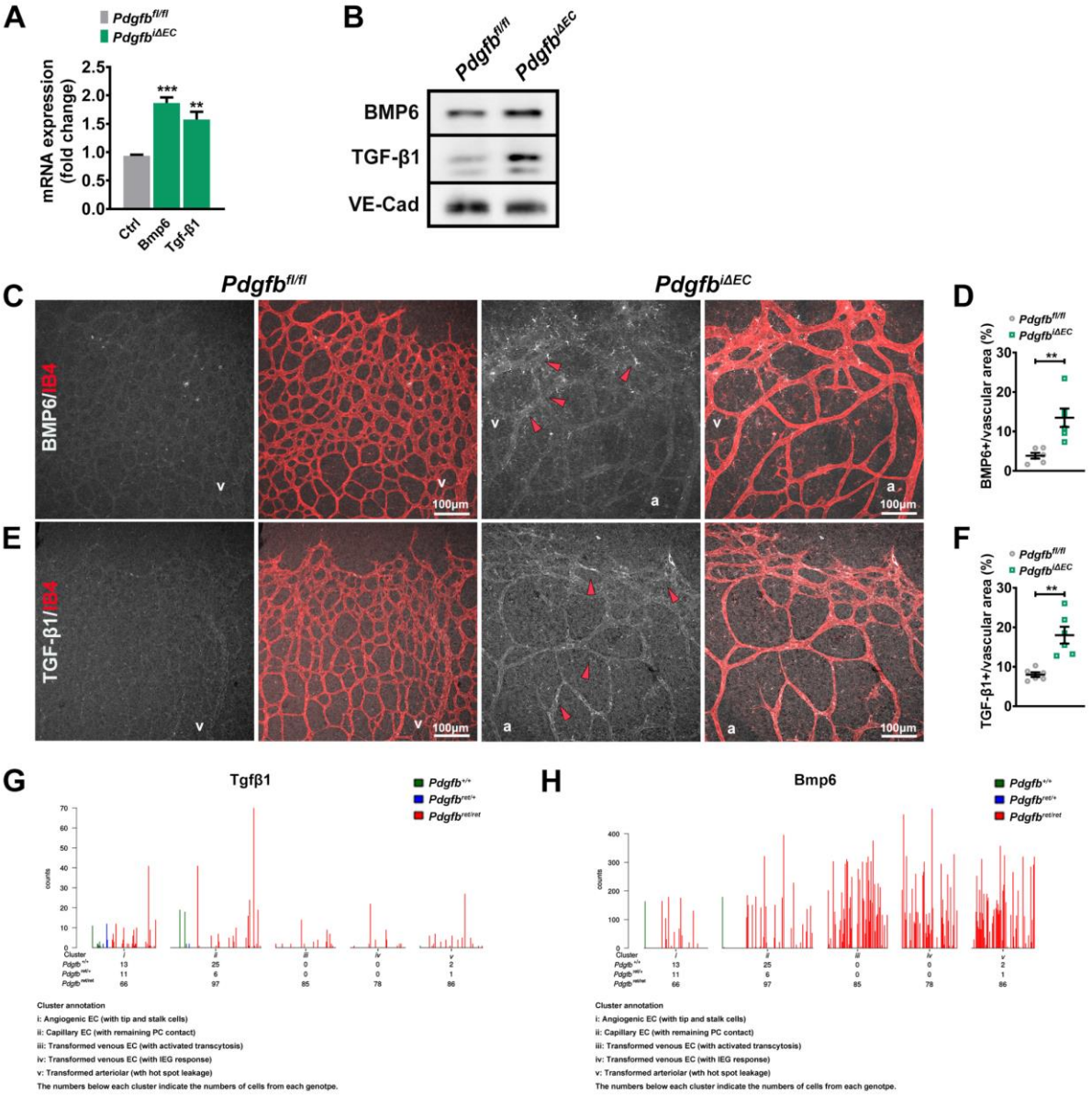

Figure 27. Flow-mediated KLF4 upregulation is associated with increased TGF-β1 and BMP6 expression.
(A) mRNA expression of *Bmp6* and *Tgf-ß1* in mLECs isolated from P7 *Pdgfb*$^{fl/fl}$ and *Pdgfb*$^{i\Delta EC}$ mice. (B) WB for TGF-β1 and BMP6 in mLECs isolated from P7 *Pdgfb*$^{fl/fl}$ and *Pdgfb*$^{i\Delta EC}$ mice. (C) Representative confocal images of BMP6 (white) and IB4 (red) staining in P7 *Pdgfb*$^{fl/fl}$ and *Pdgfb*$^{i\Delta EC}$ retinas. Red arrowheads point towards BMP6+ vessels. (D) Quantification of BMP6 immunolabelling intensity from P7 *Pdgfb*$^{fl/fl}$ and *Pdgfb*$^{i\Delta EC}$ retinas. (E) Representative confocal images of TGF-β1 (white) and IB4 (red) staining in P7 *Pdgfb*$^{fl/fl}$ and *Pdgfb*$^{i\Delta EC}$ retinas. Red arrowheads point towards TGF-β+ vessels (F) Quantification of TGF-β1 immunolabelling intensity from P7 *Pdgfb*$^{fl/fl}$ and *Pdgfb*$^{i\Delta EC}$ retinas. (G,H) Images of *Tgf-ß1* and *Bmp6* gene expression by scRNA seq in ECs from *Pdgfb*$^{ret/ret}$ brains. **P<0.01, ***P<0.001, a: artery, v: vein.

5. DISCUSSION

AVMs are direct connections between arteries and veins with a missing intervening capillary bed and are characterized by a plethora of cellular abnormalities, including an increased in EC size and number, excessive elongation and an altered orientation and EC fate. Interestingly, the same similar cellular features are under physiological FSS regulation, underlying implication of FSS-mediated EC quiescence as an additional mechanism to protect the endothelium against AVM formation. Indeed, recent advances in the field have identified loss of FSS regulation of vessel stability as a key determinant factor in AVM pathogenesis [49, 53, 62]. While in *Alk1* and *Eng* mutants, it has been proposed that disrupted EC orientation against the flow direction is the cellular event that triggers formation of AVMs, the AVMs upon *Smad4* depletion form due to loss of FSS-induced cell cycle arrest accompanied by loss of arterial identity.

Nevertheless, either inherited or sporadically occurring, PC drop accompanied by increased SMA coverage is another hallmark of AVMs. MCs and ECs act in a permanent crosstalk to maintain vascular stabilization and homeostasis. In one hand, by regulating the production of the MC recruitment genes in ECs, FSS promotes PC recruitment and its maintenance in the endothelial layer. Which of these factors regulated by FSS is crucial for protection against AVMs is still poorly understood. In turn, MCs provide dynamic control of blood perfusion within the vascular networks and, therefore, maintain an appropriate vascular tone. Yet, despite recent advances, it is still not entirely clear how dysfunction in this crosstalk contributes to the progression of many diseases and how FSS interferes with this crosstalk to protect the endothelium. Whether PC loss within the former capillaries is the primary cause of AVM formation or secondary to pathological hemodynamics-mediated AVMs remains an open question in the field. Which angiocrine-paracrine signals are implicated in maintaining functional PCs on developing endothelium to stabilize the vessels and the contribution of the FSS remains largely unknown.

Thus, the present study was set up to address the role of EC SMAD4 signaling at the convergence with physiological FSS in maintaining vascular stability with a focus on PC biology and function. Furthermore, this study examined how the FSS-SMAD4 signaling crosstalk regulates the angiocrine-paracrine PDGFB-PDGFRβ and how genetic disruption of PDGFB signaling-mediated recruitment and maintenance of PCs contribute to the pathogenesis of

AVMs.

The data obtained in the present study indicate that decreased PC coverage within the HHT-like AVMs is due to a specific loss of FSS-mediated PDGFB expression in ECs engaged in AVMs. Genetic dysregulation of angiocrine-paracrine PDGFB-PDFRβ signaling pathway by depletion of *Pdgfb* in ECs in developing vessels leads to loss of PCs accompanied by enlargement of capillaries and formation of organotypic AV shuntings. These results point on one side to an increased sensitivity of ECs depleted of PCs to FSS, due to loss of SMAD4 regulation of PDGFB expression, whereas on the other side, emphasize the origin of AVMs in the capillaries, as PC unsheathed capillary enlargement is the common feature of all AVMs irrespective of being inherited or sporadically appearing. Capillary enlargement further leads to an altered hemodynamics accompanied by an increased in KLF4 expression-mediated activation of BMP, TGF-β and NOTCH signaling pathways in ECs causing an altered capillary zonation and misdirected EC migration against the flow. Similar to the 'which came first, the egg or the chicken' conundrum, further studies with partial depletion of *Pdgfb* and *Smad4* in ECs or using Cre specific lines for ECs subtypes will allow us to discern the precise disrupted cellular and molecular mechanisms of EC-PC crosstalk that initiate AVM development versus AVM progression.

5.1 SMAD4-induced *PDGFB* expression-mediates PC recruitment

Genetic studies with depletion of *Smad4* in the ECs emphasize the crucial role for SMAD4 signaling in PC recruitment. Whereas in developing brains, *Smad4*-deficient endothelium showed ubiquitous impaired PC coverage accompanied by a decrease in the expression of NOTCH receptors and N-cadherin [43], mouse retinas from these mice show a reduction in PC coverage specifically in the AVMs [47, 134], indicating dysregulation of FSS-mediated PC recruitment or maintenance. Building on previous findings, the remaining PCs loose the expression of PDGFRβ, suggesting a specific disruption of PDGFB-PDGFRβ in AVM pathogenesis. Furthermore, BMP9 or FSS-induced *PDGFB* expression requires active SMAD4 signaling as HUVECs depleted for *SMAD4* and subject to FSS fail to upregulate *PDGFB*. Taking a step forward in identifying the cellular outcome of loss of EC *PDGFB* on PCs, in vitro experiments identified that downstream of SMAD4, PDGFB is required for mediating the orientation and migration of PCs towards the EC layer.

Yet, the implication of FSS-SMAD4 signaling crosstalk mediated PDGFB expression in controlling EC-PC communication to maintain vascular stability has never been addressed. Recently, it has been suggested that SMAD4 maintains the FSS set point and *SMAD4* depleted ECs show an exaggerated response to FSS in their elongation, size, alignment and orientation[62]. Interestingly, exogenous PDGFB treatment reversed the excessive EC elongation induced upon *SMAD4* depletion in HUVECs, suggesting that PDGFB is among the SMAD4 downstream regulators for FSS-mediated EC responses. Furthermore, HUVECs depleted for *PDGFB* showed increased sensitivity to FSS in regards to EC elongation and EC size. Yet, further studies are required to evaluate if PDGFB is also responsible for increased proliferation and/or altered EC orientation upon *Smad4* depletion and more interestingly, how PDGFB can mediate these effects in a cell autonomous manner, as the receptor is PC specific.

5.2 Key signaling components in MCs to protect ECs against AVMs formation

MCs and ECs act in a permanent crosstalk to maintain EC quiescence and vascular homeostasis. Loss of the physiological intercellular communication leads to multiple vascular abnormalities including AVM formation. In the recent years, key signaling components in MCs with a critical role in protecting the endothelium against AVM formation have been identified. One such example is the NOTCH signaling pathway, which regulates the survival and proliferation of PCs by acting upstream of PDGFRβ. Deletion of *Rbpj* in MCs results in AVM formation in 6 weeks old mice retinas [135]. Impaired migration of PCs to EC layer and loss of vascular tone upon depletion of serum response factor (*Srf*) in MCs also leads to AV shunting in developing retinas. [136]. These findings imply that MCs are required to maintain vascular quiescence and protect the endothelium against AVMs.

On the other hand, upstream of PDGFB, the activation of NOTCH [127] or inhibition of BMP9/10 signaling in ECs results in AVM development [35, 46, 47], and both signaling axis regulate *PDGFB* expression [45, 137]. Interestingly, these two pathways converge in regulating numerous shared downstream genes. One of these genes is N-cadherin [24], which plays a crucial role in facilitating EC-PC communication acting downstream of PDGFB-PDGFRβ signaling [43]. Instead, physiological FSS plays a role in regulating the activation of NOCTH and BMP9/10 in ECs [138]. Additionally, BMP9 is required for the FSS-induced expression of key regulators involved in the recruitment of MCs in ECs [45], such as *PDGFB*, *JAG1* or *TGF-β1*. These studies highlight the

multiple signaling crosstalk and the importance of upstream regulatory mechanisms for the angiocrine PDGFB production to maintain vascular homeostasis.

The impact of disrupted PDGFB/PDGFRβ signaling in EC-MC communication and the impact on vascular development has been extensively studied. Blockade of the PDGFRβ receptor by administration of an antagonistic PDGFRβ antibody (APB5) leads to partial inhibition of PC recruitment to developing retinal vessels inducing a sustained inflammation and irreversible BRB breakdown [139]. Yet, this study did not provide evidence for AVM-like structures. This might be due to either impartial depletion of PCs or rather to the experimental difficulty in identifying the AVMs. Interestingly, pathogenic mutations of *PDGFRβ* have been identified in a small fraction of patients with bAVMs [140] and its association with fusiform cerebral aneurysms [141, 142]. Elevated PDGFB expression has been found in a specific subgroup of surgically removed human sporadic bAVMs [143]. In contrast, enhancing PDGFB signaling by overexpression or administration of exogenous PDGFB leads to an increase in PC coverage promoting vessel protection against AVMs [116]. Thalidomide has also been shown to enhance the recruitment of MCs in the retinas of $Eng^{+/-}$ and $Alk1^{+/-}$ mutant mice, which is likely achieved by increasing the activity of PDGFB/PDGFRβ signaling [115, 116]. Thalidomide-induced PDGFB expression has been found to stabilize small capillaries in individuals with telangiectasias, leading to a reduction in nose bleeds in patients with HHT [144]. Furthermore, in a recent clinical study involving 18 patients with AVMs, thalidomide treatment for a course of 18 month improved the AVMs and the patient quality of life [145]. These findings represent a promising avenue for the development of targeted therapies aimed at stabilizing the vasculature to prevent AVM formation. It will be interesting to determine whether AVMs can be reversed by increasing PDGFB expression, the AVMs could be reversed also upon *Smad4* EC depletion. The molecular mechanisms underlying the effect of thalidomide on PC recruitment stimulation and maintenance is not well understood. Also, it remains unclear how thalidomide mechanistically upregulates PDGFB expression.

5.3 PDGFB-mediated PC recruitment and maintenance protects against AVMs

The present study is the first to establish a genetic connection between PDGFB signaling and the development of high flow-AVMs. Yet, further research is required to investigate the significance of PDGFB expression levels in individuals with HHT to uncover the molecular

mechanisms.

Upon EC *Pdgfb* ablation before PC recruitment occur, AV shunts develop at the vascular front characterized by low flow, while the AVMs develop close to the optic nerve in regions of high flow when *Pdgfb* is depleted at P5 when already the PCs were recruited. Yet, dilation of capillaries containing larger and more ECs was the most common aberrant cell event. These results suggest on one side that PDGFB-mediated PC recruitment and maintenance is required to maintain capillary EC size and number and on the other side that these aberrant cell responses initiate AVM development independent of flow. Nevertheless, the formation of AV shunts when PCs are already being recruited to the endothelium suggests flow implication is a secondary mechanism and resemble more the HHT-like AVMs. However, further investigation is needed to determine if other cell-disrupted features characterize these PC post-recruitment AV shunts. Furthermore, if capillary ECs are the origin of the AV shunts also in AVMs-like HHT remains to be further addressed with capillary EC specific Cre lines.

It has been proposed that the dysregulated EC migration against the direction of flow is the triggering event in AVM formation upon depletion of *Eng* or *Alk1* [49, 53, 146]. However, a recent study has demonstrated that upon *Smad4* depletion, the triggering event for AVM formation is the increase in EC proliferation-mediated loss of arterial identity [62].

Interestingly, upon *Pdgfb* depletion the enlarged capillaries contain non-proliferative, hyperplastic, and hypertrophic ECs with disorganized cell-cell junctions. Similar to previous findings in *Pdgfb*$^{ret/ret}$ brain capillaries [90], retina vasculature upon EC *Pdgfb* loss also showed capillary venous skewing, highlighting the significance of PDGFB signaling in maintaining capillary AV zonation in multiple vascular beds. Yet upon further validation, these dilated capillaries directly connected to the draining veins and arteries contained ECs positive for SOX17 and DLL4. As EC proliferation was not responsible for the increased number of ECs within the dilated capillaries, a disruption in flow-migration coupling was the most plausible cell event triggering the lesions. Indeed, an altered orientation against the direction of flow within the arteries, capillaries and venous ECs would explain the migration of arterial ECs towards the veins. As AVMs upon inactivation of *Eng*, *Alk1*, or *Smad4* have a capillary-venous origin characterized by loss of arterial identity, it will be interesting to identify if the AV shunting upon *Pdgfb* depletion originate in arteries. AVMs are characterized by venous skewing, yet upon pdgfb depletion arterial EC are specifically identified within the AV shunts.

Further investigation is required to determine whether the perturbed migration against the flow is a consequence of defective hemodynamics in the hyperplastic and hypertrophic capillaries or whether an altered attraction-repulsive mechanisms that exacerbate AV shunting. Indeed, the loss of *Pdgfb* mediated reduced PC recruitment led to the activation of the EphrinB2-EphB4 signaling pathway, which mediates the repulsive-attraction of arterial-venous ECs [147].

5.4 Altered hemodynamics mediated molecular mechanisms in AVMs

AVMs are distinguished by increased blood flow and increased sensitivity of ECs to FSS. Similar to *Smad4* depletion derived AVMs, *Pdgfb* loss led to over-activation of KLF4 within the dilated capillaries with a switch in KLF4 activation from the arteries towards the veins, accompanied by hypertensive veins (gain of α-SMA) at the expense of hypotensive arteries (loss of α-SMA). Taken together, these results suggest an altered hemodynamic pattern due to an increase in capillary size and an impaired regulation of vascular tone. At the same time, these findings are also consistent with the histology of human sporadic AVMs [113].

Yet, KLF4 activation can also be interpreted as increased sensitivity of ECs to FSS. In vitro experiments suggest that ECs become more sensitive to FSS when *PDGFB* is lost, as observed in AVMs when *Smad4* is depleted [62]. Further investigation is required to determine whether PDGFB cell autonomously limits FSS-mediated EC responses to maintain capillary EC size and AV zonation by restricting KLF4-mediated hemodynamic changes. Additionally, it is unclear whether these cellular events are a result of intrinsic and/or extrinsic signaling mediated by ensheathing PCs. Currently, it is only possible to speculate that the observed vascular malformations in these mutant mice are likely to be secondary effects of PC coverage defects. However, the possibility that autocrine mechanisms contribute to the development of AVMs cannot be completely excluded.

Our research findings suggest a model in which the loss of PCs due to EC *Pdgfb* ablation leads to the enlargement of capillaries, disrupting blood flow and increasing EC sensitivity to flow by upregulating KLF4. Excessive KLF4 induces alterations in regulatory programs that control arterial-venous identity. This leads to the simultaneous activation of arterial identity through NOTCH and TGF-β1-Smad3 pathways, as well as the activation of venous identity through BMP6-mediated Smad1/5 activation. The modified fate pattern of ECs and the disruption of

regulatory mechanisms that control their movement result in a migration confusion of ECs against the bloodstream. This confusion leads to an accumulation of ECs in capillaries, causing an increase in capillary size and ultimately their direct connections to the draining veins and arteries, causing direct AV shunting.

5.5 Limitations and future plans

The present study has several limitations, as follows:

1. Endothelial *Pdgfb* deletion results in an almost complete lack of PC coverage on the endothelium, making it challenging to determine whether the observed vascular malformations are primarily due to a cell autonomous effect of *Pdgfb* loss in the ECs or if the defect in the endothelium is secondary to complete loss of PCs. This impedes elucidation of a complete molecular mechanism, therefore the further research involving partial LOF of *Smad4* and/or *Pdgfb* is required to validate these findings and to thoroughly investigate the precise role and potential clinical applications of PDGFB in the development of AVMs.

2. AVMs upon inactivation of *Eng*, *Alk1*, or *Smad4* have a capillary-venous origin characterized by loss of arterial identity. However, the AV shunts observed in this study showed an increase in arterial characteristics, with the presence of arterial ECs in the veins. Yet, capillary dilation is characteristic of all AVMs, raising the possibility that AV shunts may have a capillary origin. Therefore, further studies are needed to address the EC subtype and the clonogenicity of lesions by developing novel genetic tools with Cre mediated depletion in different EC populations.

3. The mechanism of how SMAD4 signaling regulates FSS-induced *PDGFB* regulation as well as the molecular link between FSS induced KLF4 and PDGFB expression should also be further elucidated.

6. CONCLUSIONS

In conclusion, SMAD4 signaling is required for FSS induced PDGFB-mediated PC recruitment and maintenance in order to maintain capillary EC size and fate as well as proper axial polarity and directed migration. The main messages of the study are as follows:

1. SMAD4 is required for FSS and BMP9 induced *PDGFB* expression in ECs.

2. SMAD4 signaling is required for PDGFB-mediated PC orientation and subsequent migration towards the endothelial layer.

3. PDGFB signaling is indispensable for PC recruitment and maintenance on developing endothelium to protect against loss of PCs and vascular lesions.

4. PDGFB-mediated PC recruitment and maintenance regulates restricts capillary EC size and diameter, capillary cell fate and directed migration to maintain EC quiescence.

5. EC PDGFB preserve capillary size to restrict hemodynamics changes and upregulation of KLF4-mediated NOTCH, BMP and TGF-β activation in ECs.

7. SUMMARY

Arterial-venous malformations (AVMs) are direct connections between arteries and veins with a missing capillary bed that lacks pericytes (PCs). Recent studies have highlighted the significance of PCs and their recruitment in maintaining vascular integrity. Whether impaired PC coverage triggers AVMs or is secondary to hemodynamics changes in high-flow AVMs remains unclear. Among a plethora of regulators, PDGFB signaling has emerged as a key pathway involved in PC recruitment to the endothelial cells (ECs).

The aim of my study was to **i)** investigate the effects of the BMP9/10 - flow signaling pathway crosstalk on PDGFB-mediated PC biology and function and **ii)** elucidate the role of endothelial PDGFB-mediated PC recruitment and maintenance in the pathogenesis of AVMs.

Consistent with previous findings identifying loss of PCs on the AVM endothelium, this study identified a specific loss of PDGFRβ in the remaining PCs, indicating dysfunctional PDGFB signaling as the responsible mechanism for the PC deficit. Further *in vitro* studies confirmed this hypothesis, as *PDGFB* was synergistically upregulated by BMP9 and fluid shear stress and this effect was SMAD4 dependent. Cellularly, SMAD4 was required for PDGFB-mediated PC migration *in vitro*. Endothelial specific *Pdgfb* depleted mouse line (*Pdgfb*$^{i\Delta EC}$) was generated for *in vivo* experiments to determine whether disrupted EC-PC crosstalk contributes to AVM formation. Interestingly, disruption of EC *Pdgfb*-mediated PC loss and maintenance leads to AVM-like structures. In addition, endothelial PDGFB signaling-mediated PC recruitment is required to maintain capillary EC size and diameter, cell fate, arterial-venous identity and EC migration against the bloodstream to promote appropriate vascular tone and stability of vessels and protect against AVM formation. Mechanistically, I identified that PDGFB protects the developing endothelium against hemodynamics changes by restricting KLF4-mediated NOTCH, BMP and TGF-β activation in ECs. Taken together, these results suggest that SMAD4-flow synergy modulate the PDGFB signaling mediated PC recruitment and maintenance to maintain EC quiescence. Targeting SMAD4-PDGFB signaling may be a potential therapeutic approach to prevent AVM formation by restoring and enhancing PC recruitment and maintenance.

8. REFERENCES

1. Bideau, A, Plauchu, H, Brunet, G, Robert, J: Epidemiological investigation of Rendu-Osler disease in France: its geographical distribution and prevalence. *Popul,* 44**:** 3-22, 1989.
2. Kjeldsen, AD, Vase, P, Green, A: Hereditary haemorrhagic telangiectasia: a population-based study of prevalence and mortality in Danish patients. *J Intern Med,* 245**:** 31-39, 1999. https://doi.org/10.1046/j.1365-2796.1999.00398.x
3. McDonald, J, Wooderchak-Donahue, W, VanSant Webb, C, Whitehead, K, Stevenson, DA, Bayrak-Toydemir, P: Hereditary hemorrhagic telangiectasia: genetics and molecular diagnostics in a new era. *Front Genet,* 6**:** 1, 2015. https://doi.org/10.3389/fgene.2015.00001
4. Duerig, I, Pylaeva, E, Ozel, I, Weinwright, S, Thiel, I, Bordbari, S, Domnich, M, Siakaeva, E, Lakomek, A, Toppe, F, Schleupner, C, Geisthoff, U, Lang, S, Droege, F, Jablonska, J: Non-functional TGF-beta/ALK1/ENG Signaling Pathway supports neutrophil pro-angiogenic activity in Hereditary Hemorrhagic Telangiectasia. *J Leukoc Biol*, 2023. https://doi.org/10.1093/jleuko/qiad090
5. Fernandez, LA, Sanz-Rodriguez, F, Blanco, FJ, Bernabeu, C, Botella, LM: Hereditary hemorrhagic telangiectasia, a vascular dysplasia affecting the TGF-beta signaling pathway. *Clin Med Res,* 4**:** 66-78, 2006. https://doi.org/10.3121/cmr.4.1.66
6. Cunha, SI, Magnusson, PU, Dejana, E, Lampugnani, MG: Deregulated TGF-beta/BMP Signaling in Vascular Malformations. *Circ Res,* 121**:** 981-999, 2017. https://doi.org/10.1161/CIRCRESAHA.117.309930
7. Johnson, DW, Berg, JN, Baldwin, MA, Gallione, CJ, Marondel, I, Yoon, SJ, Stenzel, TT, Speer, M, Pericak-Vance, MA, Diamond, A, Guttmacher, AE, Jackson, CE, Attisano, L, Kucherlapati, R, Porteous, ME, Marchuk, DA: Mutations in the activin receptor-like kinase 1 gene in hereditary haemorrhagic telangiectasia type 2. *Nat Genet,* 13**:** 189-195, 1996. https://doi.org/10.1038/ng0696-189
8. McAllister, KA, Grogg, KM, Johnson, DW, Gallione, CJ, Baldwin, MA, Jackson, CE, Helmbold, EA, Markel, DS, McKinnon, WC, Murrell, J, et al.: Endoglin, a TGF-beta binding protein of endothelial cells, is the gene for hereditary haemorrhagic telangiectasia type 1. *Nat Genet,* 8**:** 345-351, 1994. https://doi.org/10.1038/ng1294-345
9. Howe, JR, Roth, S, Ringold, JC, Summers, RW, Jarvinen, HJ, Sistonen, P, Tomlinson, IP, Houlston, RS, Bevan, S, Mitros, FA, Stone, EM, Aaltonen, LA: Mutations in the SMAD4/DPC4 gene in juvenile polyposis. *Science,* 280**:** 1086-1088, 1998. https://doi.org/10.1126/science.280.5366.1086
10. Wooderchak-Donahue, WL, McDonald, J, O'Fallon, B, Upton, PD, Li, W, Roman, BL, Young, S, Plant, P, Fulop, GT, Langa, C, Morrell, NW, Botella, LM, Bernabeu, C, Stevenson, DA, Runo, JR, Bayrak-Toydemir, P: BMP9 mutations cause a vascular-anomaly syndrome with phenotypic overlap with hereditary hemorrhagic telangiectasia. *Am J Hum Genet,* 93**:** 530-537, 2013. https://doi.org/10.1016/j.ajhg.2013.07.004
11. Faughnan, ME, Palda, VA, Garcia-Tsao, G, Geisthoff, UW, McDonald, J, Proctor, DD, Spears, J, Brown, DH, Buscarini, E, Chesnutt, MS, Cottin, V, Ganguly, A, Gossage, JR, Guttmacher, AE, Hyland, RH, Kennedy, SJ, Korzenik, J, Mager, JJ, Ozanne, AP, Piccirillo, JF, Picus, D, Plauchu, H, Porteous, ME, Pyeritz, RE, Ross, DA, Sabba, C, Swanson, K, Terry, P, Wallace, MC, Westermann, CJ, White, RI, Young, LH, Zarrabeitia, R, Group, HHTFI-GW: International guidelines for the diagnosis and management of hereditary haemorrhagic telangiectasia. *J Med Genet,* 48**:** 73-87, 2011. https://doi.org/10.1136/jmg.2009.069013
12. Haitjema, T, Disch, F, Overtoom, TT, Westermann, CJ, Lammers, JW: Screening family members of patients with hereditary hemorrhagic telangiectasia. *Am J Med,* 99**:** 519-524, 1995. https://doi.org/10.1016/s0002-9343(99)80229-0
13. Fleetwood, IG, Steinberg, GK: Arteriovenous malformations. *Lancet,* 359**:** 863-873, 2002. https://doi.org/10.1016/S0140-6736(02)07946-1
14. Halim, AX, Johnston, SC, Singh, V, McCulloch, CE, Bennett, JP, Achrol, AS, Sidney, S, Young, WL: Longitudinal risk of intracranial hemorrhage in patients with arteriovenous malformation of the brain within a defined population. *Stroke,* 35**:** 1697-1702, 2004. https://doi.org/10.1161/01.STR.0000130988.44824.29
15. Faughnan, ME, Mager, JJ, Hetts, SW, Palda, VA, Ratjen, F: Second International Guidelines for the Diagnosis and Management of Hereditary Hemorrhagic Telangiectasia. *Ann Intern Med,* 174**:** 1035-1036, 2021. https://doi.org/10.7326/L21-0067
16. Dabus, G, Linfante, I, Benenati, J, Perlyn, CA, Martinez-Galdamez, M: Interventional management of high-flow craniofacial vascular malformations: a database analysis and review of the literature. *J Neurointerv Surg,* 9**:** 92-96, 2017. https://doi.org/10.1136/neurintsurg-2016-012315

17. Milic, A, Chan, RP, Cohen, JH, Faughnan, ME: Reperfusion of pulmonary arteriovenous malformations after embolotherapy. *J Vasc Interv Radiol,* 16**:** 1675-1683, 2005. https://doi.org/10.1097/01.RVI.0000182163.25493.BB
18. Liu, AS, Mulliken, JB, Zurakowski, D, Fishman, SJ, Greene, AK: Extracranial arteriovenous malformations: natural progression and recurrence after treatment. *Plast Reconstr Surg,* 125**:** 1185-1194, 2010. https://doi.org/10.1097/PRS.0b013e3181d18070
19. Massague, J: TGFbeta signalling in context. *Nat Rev Mol Cell Biol,* 13**:** 616-630, 2012. https://doi.org/10.1038/nrm3434
20. Morikawa, M, Derynck, R, Miyazono, K: TGF-beta and the TGF-beta Family: Context-Dependent Roles in Cell and Tissue Physiology. *Cold Spring Harb Perspect Biol,* 8, 2016. https://doi.org/10.1101/cshperspect.a021873
21. Lee, HW, Chong, DC, Ola, R, Dunworth, WP, Meadows, S, Ka, J, Kaartinen, VM, Qyang, Y, Cleaver, O, Bautch, VL, Eichmann, A, Jin, SW: Alk2/ACVR1 and Alk3/BMPR1A Provide Essential Function for Bone Morphogenetic Protein-Induced Retinal Angiogenesis. *Arterioscler Thromb Vasc Biol,* 37**:** 657-663, 2017. https://doi.org/10.1161/ATVBAHA.116.308422
22. David, L, Mallet, C, Mazerbourg, S, Feige, JJ, Bailly, S: Identification of BMP9 and BMP10 as functional activators of the orphan activin receptor-like kinase 1 (ALK1) in endothelial cells. *Blood,* 109**:** 1953-1961, 2007. https://doi.org/10.1182/blood-2006-07-034124
23. Alt, A, Miguel-Romero, L, Donderis, J, Aristorena, M, Blanco, FJ, Round, A, Rubio, V, Bernabeu, C, Marina, A: Structural and functional insights into endoglin ligand recognition and binding. *PLoS One,* 7**:** e29948, 2012. https://doi.org/10.1371/journal.pone.0029948
24. Larrivee, B, Prahst, C, Gordon, E, del Toro, R, Mathivet, T, Duarte, A, Simons, M, Eichmann, A: ALK1 signaling inhibits angiogenesis by cooperating with the Notch pathway. *Dev Cell,* 22**:** 489-500, 2012. https://doi.org/10.1016/j.devcel.2012.02.005
25. Cunha, SI, Bocci, M, Lovrot, J, Eleftheriou, N, Roswall, P, Cordero, E, Lindstrom, L, Bartoschek, M, Haller, BK, Pearsall, RS, Mulivor, AW, Kumar, R, Larsson, C, Bergh, J, Pietras, K: Endothelial ALK1 Is a Therapeutic Target to Block Metastatic Dissemination of Breast Cancer. *Cancer Res,* 75**:** 2445-2456, 2015. https://doi.org/10.1158/0008-5472.CAN-14-3706
26. Ntumba, K, Akla, N, Oh, SP, Eichmann, A, Larrivee, B: BMP9/ALK1 inhibits neovascularization in mouse models of age-related macular degeneration. *Oncotarget,* 7**:** 55957-55969, 2016. https://doi.org/10.18632/oncotarget.11182
27. Bourdeau, A, Dumont, DJ, Letarte, M: A murine model of hereditary hemorrhagic telangiectasia. *J Clin Invest,* 104**:** 1343-1351, 1999. https://doi.org/10.1172/JCI8088
28. Li, DY, Sorensen, LK, Brooke, BS, Urness, LD, Davis, EC, Taylor, DG, Boak, BB, Wendel, DP: Defective angiogenesis in mice lacking endoglin. *Science,* 284**:** 1534-1537, 1999. https://doi.org/10.1126/science.284.5419.1534
29. Arthur, HM, Ure, J, Smith, AJ, Renforth, G, Wilson, DI, Torsney, E, Charlton, R, Parums, DV, Jowett, T, Marchuk, DA, Burn, J, Diamond, AG: Endoglin, an ancillary TGFbeta receptor, is required for extraembryonic angiogenesis and plays a key role in heart development. *Dev Biol,* 217**:** 42-53, 2000. https://doi.org/10.1006/dbio.1999.9534
30. Oh, SP, Seki, T, Goss, KA, Imamura, T, Yi, Y, Donahoe, PK, Li, L, Miyazono, K, ten Dijke, P, Kim, S, Li, E: Activin receptor-like kinase 1 modulates transforming growth factor-beta 1 signaling in the regulation of angiogenesis. *Proc Natl Acad Sci U S A,* 97**:** 2626-2631, 2000. https://doi.org/10.1073/pnas.97.6.2626
31. Srinivasan, S, Hanes, MA, Dickens, T, Porteous, ME, Oh, SP, Hale, LP, Marchuk, DA: A mouse model for hereditary hemorrhagic telangiectasia (HHT) type 2. *Hum Mol Genet,* 12**:** 473-482, 2003. https://doi.org/10.1093/hmg/ddg050
32. Torsney, E, Charlton, R, Diamond, AG, Burn, J, Soames, JV, Arthur, HM: Mouse model for hereditary hemorrhagic telangiectasia has a generalized vascular abnormality. *Circulation,* 107**:** 1653-1657, 2003. https://doi.org/10.1161/01.CIR.0000058170.92267.00
33. Choi, EJ, Walker, EJ, Shen, F, Oh, SP, Arthur, HM, Young, WL, Su, H: Minimal homozygous endothelial deletion of Eng with VEGF stimulation is sufficient to cause cerebrovascular dysplasia in the adult mouse. *Cerebrovasc Dis,* 33**:** 540-547, 2012. https://doi.org/10.1159/000337762
34. Garrido-Martin, EM, Nguyen, HL, Cunningham, TA, Choe, SW, Jiang, Z, Arthur, HM, Lee, YJ, Oh, SP: Common and distinctive pathogenetic features of arteriovenous malformations in hereditary hemorrhagic telangiectasia 1 and hereditary hemorrhagic telangiectasia 2 animal models--brief report. *Arterioscler Thromb Vasc Biol,* 34**:** 2232-2236, 2014. https://doi.org/10.1161/ATVBAHA.114.303984

35. Mahmoud, M, Allinson, KR, Zhai, Z, Oakenfull, R, Ghandi, P, Adams, RH, Fruttiger, M, Arthur, HM: Pathogenesis of arteriovenous malformations in the absence of endoglin. *Circ Res,* 106**:** 1425-1433, 2010. https://doi.org/10.1161/CIRCRESAHA.109.211037
36. Park, SO, Wankhede, M, Lee, YJ, Choi, EJ, Fliess, N, Choe, SW, Oh, SH, Walter, G, Raizada, MK, Sorg, BS, Oh, SP: Real-time imaging of de novo arteriovenous malformation in a mouse model of hereditary hemorrhagic telangiectasia. *J Clin Invest,* 119**:** 3487-3496, 2009. https://doi.org/10.1172/JCI39482
37. Walker, EJ, Su, H, Shen, F, Choi, EJ, Oh, SP, Chen, G, Lawton, MT, Kim, H, Chen, Y, Chen, W, Young, WL: Arteriovenous malformation in the adult mouse brain resembling the human disease. *Ann Neurol,* 69**:** 954-962, 2011. https://doi.org/10.1002/ana.22348
38. Tual-Chalot, S, Garcia-Collado, M, Redgrave, RE, Singh, E, Davison, B, Park, C, Lin, H, Luli, S, Jin, Y, Wang, Y, Lawrie, A, Jakobsson, L, Arthur, HM: Loss of Endothelial Endoglin Promotes High-Output Heart Failure Through Peripheral Arteriovenous Shunting Driven by VEGF Signaling. *Circ Res,* 126**:** 243-257, 2020. https://doi.org/10.1161/CIRCRESAHA.119.315974
39. Trotter, JF, Suhocki, PV, Lina, JR, Martin, LW, Parrish, JL, Swantkowski, T: Hereditary hemorrhagic telangiectasia causing high output cardiac failure: treatment with transcatheter embolization. *Am J Gastroenterol,* 93**:** 1569-1571, 1998. https://doi.org/10.1111/j.1572-0241.1998.00486.x
40. Ergun, T, Lakadamyali, H, Lakadamyali, H, Eldem, O: A case of high-output heart failure secondary to bilateral multiple pulmonary arterio-venous malformations treated with Amplatzer vascular plug. *Anadolu Kardiyol Derg,* 9**:** E17-18, 2009.
41. Ginon, I, Decullier, E, Finet, G, Cordier, JF, Marion, D, Saurin, JC, Dupuis-Girod, S: Hereditary hemorrhagic telangiectasia, liver vascular malformations and cardiac consequences. *Eur J Intern Med,* 24**:** e35-39, 2013. https://doi.org/10.1016/j.ejim.2012.12.013
42. Lan, Y, Liu, B, Yao, H, Li, F, Weng, T, Yang, G, Li, W, Cheng, X, Mao, N, Yang, X: Essential role of endothelial Smad4 in vascular remodeling and integrity. *Mol Cell Biol,* 27**:** 7683-7692, 2007. https://doi.org/10.1128/MCB.00577-07
43. Li, F, Lan, Y, Wang, Y, Wang, J, Yang, G, Meng, F, Han, H, Meng, A, Wang, Y, Yang, X: Endothelial Smad4 maintains cerebrovascular integrity by activating N-cadherin through cooperation with Notch. *Dev Cell,* 20**:** 291-302, 2011. https://doi.org/10.1016/j.devcel.2011.01.011
44. Gariano, RF, Gardner, TW: Retinal angiogenesis in development and disease. *Nature,* 438**:** 960-966, 2005. https://doi.org/10.1038/nature04482
45. Baeyens, N, Larrivee, B, Ola, R, Hayward-Piatkowskyi, B, Dubrac, A, Huang, B, Ross, TD, Coon, BG, Min, E, Tsarfati, M, Tong, H, Eichmann, A, Schwartz, MA: Defective fluid shear stress mechanotransduction mediates hereditary hemorrhagic telangiectasia. *J Cell Biol,* 214**:** 807-816, 2016. https://doi.org/10.1083/jcb.201603106
46. Ola, R, Dubrac, A, Han, J, Zhang, F, Fang, JS, Larrivee, B, Lee, M, Urarte, AA, Kraehling, JR, Genet, G, Hirschi, KK, Sessa, WC, Canals, FV, Graupera, M, Yan, M, Young, LH, Oh, PS, Eichmann, A: PI3 kinase inhibition improves vascular malformations in mouse models of hereditary haemorrhagic telangiectasia. *Nat Commun,* 7**:** 13650, 2016. https://doi.org/10.1038/ncomms13650
47. Ola, R, Kunzel, SH, Zhang, F, Genet, G, Chakraborty, R, Pibouin-Fragner, L, Martin, K, Sessa, W, Dubrac, A, Eichmann, A: SMAD4 Prevents Flow Induced Arteriovenous Malformations by Inhibiting Casein Kinase 2. *Circulation,* 138**:** 2379-2394, 2018. https://doi.org/10.1161/CIRCULATIONAHA.118.033842
48. Choi, H, Kim, BG, Kim, YH, Lee, SJ, Lee, YJ, Oh, SP: BMP10 functions independently from BMP9 for the development of a proper arteriovenous network. *Angiogenesis,* 26**:** 167-186, 2023. https://doi.org/10.1007/s10456-022-09859-0
49. Jin, Y, Muhl, L, Burmakin, M, Wang, Y, Duchez, AC, Betsholtz, C, Arthur, HM, Jakobsson, L: Endoglin prevents vascular malformation by regulating flow-induced cell migration and specification through VEGFR2 signalling. *Nat Cell Biol,* 19**:** 639-652, 2017. https://doi.org/10.1038/ncb3534
50. Benn, A, Alonso, F, Mangelschots, J, Genot, E, Lox, M, Zwijsen, A: BMP-SMAD1/5 Signaling Regulates Retinal Vascular Development. *Biomolecules,* 10, 2020. https://doi.org/10.3390/biom10030488
51. Singh, E, Redgrave, RE, Phillips, HM, Arthur, HM: Arterial endoglin does not protect against arteriovenous malformations. *Angiogenesis,* 23**:** 559-566, 2020. https://doi.org/10.1007/s10456-020-09731-z
52. Lee, HW, Xu, Y, He, L, Choi, W, Gonzalez, D, Jin, SW, Simons, M: Role of Venous Endothelial Cells in Developmental and Pathologic Angiogenesis. *Circulation,* 144**:** 1308-1322, 2021. https://doi.org/10.1161/CIRCULATIONAHA.121.054071
53. Park, H, Furtado, J, Poulet, M, Chung, M, Yun, S, Lee, S, Sessa, WC, Franco, CA, Schwartz, MA, Eichmann, A: Defective Flow-Migration Coupling Causes Arteriovenous Malformations in Hereditary Hemorrhagic Telangiectasia. *Circulation,* 144**:** 805-822, 2021. https://doi.org/10.1161/CIRCULATIONAHA.120.053047

54. Pu, W, He, L, Han, X, Tian, X, Li, Y, Zhang, H, Liu, Q, Huang, X, Zhang, L, Wang, QD, Yu, Z, Yang, X, Smart, N, Zhou, B: Genetic Targeting of Organ-Specific Blood Vessels. *Circ Res,* 123**:** 86-99, 2018. https://doi.org/10.1161/CIRCRESAHA.118.312981
55. Bayrak-Toydemir, P, McDonald, J, Markewitz, B, Lewin, S, Miller, F, Chou, LS, Gedge, F, Tang, W, Coon, H, Mao, R: Genotype-phenotype correlation in hereditary hemorrhagic telangiectasia: mutations and manifestations. *Am J Med Genet A,* 140**:** 463-470, 2006. https://doi.org/10.1002/ajmg.a.31101
56. Snodgrass, RO, Chico, TJA, Arthur, HM: Hereditary Haemorrhagic Telangiectasia, an Inherited Vascular Disorder in Need of Improved Evidence-Based Pharmaceutical Interventions. *Genes (Basel),* 12, 2021. https://doi.org/10.3390/genes12020174
57. Al-Samkari, H, Kasthuri, RS, Parambil, JG, Albitar, HA, Almodallal, YA, Vazquez, C, Serra, MM, Dupuis-Girod, S, Wilsen, CB, McWilliams, JP, Fountain, EH, Gossage, JR, Weiss, CR, Latif, MA, Issachar, A, Mei-Zahav, M, Meek, ME, Conrad, M, Rodriguez-Lopez, J, Kuter, DJ, Iyer, VN: An international, multicenter study of intravenous bevacizumab for bleeding in hereditary hemorrhagic telangiectasia: the InHIBIT-Bleed study. *Haematologica,* 106**:** 2161-2169, 2021. https://doi.org/10.3324/haematol.2020.261859
58. Al-Samkari, H, Albitar, HA, Olitsky, SE, Clancy, MS, Iyer, VN: Systemic bevacizumab for high-output cardiac failure in hereditary hemorrhagic telangiectasia: an international survey of HHT centers. *Orphanet J Rare Dis,* 14**:** 256, 2019. https://doi.org/10.1186/s13023-019-1239-6
59. Buscarini, E, Botella, LM, Geisthoff, U, Kjeldsen, AD, Mager, HJ, Pagella, F, Suppressa, P, Zarrabeitia, R, Dupuis-Girod, S, Shovlin, CL, Vascern, HHT: Safety of thalidomide and bevacizumab in patients with hereditary hemorrhagic telangiectasia. *Orphanet J Rare Dis,* 14**:** 28, 2019. https://doi.org/10.1186/s13023-018-0982-4
60. Crist, AM, Zhou, X, Garai, J, Lee, AR, Thoele, J, Ullmer, C, Klein, C, Zabaleta, J, Meadows, SM: Angiopoietin-2 Inhibition Rescues Arteriovenous Malformation in a Smad4 Hereditary Hemorrhagic Telangiectasia Mouse Model. *Circulation,* 139**:** 2049-2063, 2019. https://doi.org/10.1161/CIRCULATIONAHA.118.036952
61. Zhou, X, Pucel, JC, Nomura-Kitabayashi, A, Chandakkar, P, Guidroz, AP, Jhangiani, NL, Bao, D, Fan, J, Arthur, HM, Ullmer, C, Klein, C, Marambaud, P, Meadows, SM: ANG2 Blockade Diminishes Proangiogenic Cerebrovascular Defects Associated With Models of Hereditary Hemorrhagic Telangiectasia. *Arterioscler Thromb Vasc Biol,* 43**:** 1384-1403, 2023. https://doi.org/10.1161/ATVBAHA.123.319385
62. Banerjee, K, Lin, Y, Gahn, J, Cordero, J, Gupta, P, Mohamed, I, Graupera, M, Dobreva, G, Schwartz, MA, Ola, R: SMAD4 maintains the fluid shear stress set point to protect against arterial-venous malformations. *J Clin Invest,* 133, 2023. https://doi.org/10.1172/JCI168352
63. Young, K, Conley, B, Romero, D, Tweedie, E, O'Neill, C, Pinz, I, Brogan, L, Lindner, V, Liaw, L, Vary, CP: BMP9 regulates endoglin-dependent chemokine responses in endothelial cells. *Blood,* 120**:** 4263-4273, 2012. https://doi.org/10.1182/blood-2012-07-440784
64. Iriarte, A, Figueras, A, Cerda, P, Mora, JM, Jucgla, A, Penin, R, Vinals, F, Riera-Mestre, A: PI3K (Phosphatidylinositol 3-Kinase) Activation and Endothelial Cell Proliferation in Patients with Hemorrhagic Hereditary Telangiectasia Type 1. *Cells,* 8, 2019. https://doi.org/10.3390/cells8090971
65. Ruiz, S, Zhao, H, Chandakkar, P, Papoin, J, Choi, H, Nomura-Kitabayashi, A, Patel, R, Gillen, M, Diao, L, Chatterjee, PK, He, M, Al-Abed, Y, Wang, P, Metz, CN, Oh, SP, Blanc, L, Campagne, F, Marambaud, P: Correcting Smad1/5/8, mTOR, and VEGFR2 treats pathology in hereditary hemorrhagic telangiectasia models. *J Clin Invest,* 130**:** 942-957, 2020. https://doi.org/10.1172/JCI127425
66. Drape, E, Anquetil, T, Larrivee, B, Dubrac, A: Brain arteriovenous malformation in hereditary hemorrhagic telangiectasia: Recent advances in cellular and molecular mechanisms. *Front Hum Neurosci,* 16**:** 1006115, 2022. https://doi.org/10.3389/fnhum.2022.1006115
67. Bastide, B, Neyses, L, Ganten, D, Paul, M, Willecke, K, Traub, O: Gap junction protein connexin40 is preferentially expressed in vascular endothelium and conductive bundles of rat myocardium and is increased under hypertensive conditions. *Circ Res,* 73**:** 1138-1149, 1993. https://doi.org/10.1161/01.res.73.6.1138
68. Reed, KE, Westphale, EM, Larson, DM, Wang, HZ, Veenstra, RD, Beyer, EC: Molecular cloning and functional expression of human connexin37, an endothelial cell gap junction protein. *J Clin Invest,* 91**:** 997-1004, 1993. https://doi.org/10.1172/JCI116321
69. Bruzzone, R, Haefliger, JA, Gimlich, RL, Paul, DL: Connexin40, a component of gap junctions in vascular endothelium, is restricted in its ability to interact with other connexins. *Mol Biol Cell,* 4**:** 7-20, 1993. https://doi.org/10.1091/mbc.4.1.7

70. Herzog, Y, Kalcheim, C, Kahane, N, Reshef, R, Neufeld, G: Differential expression of neuropilin-1 and neuropilin-2 in arteries and veins. *Mech Dev,* 109**:** 115-119, 2001. https://doi.org/10.1016/s0925-4773(01)00518-4
71. Lawson, ND, Scheer, N, Pham, VN, Kim, CH, Chitnis, AB, Campos-Ortega, JA, Weinstein, BM: Notch signaling is required for arterial-venous differentiation during embryonic vascular development. *Development,* 128**:** 3675-3683, 2001. https://doi.org/10.1242/dev.128.19.3675
72. Shutter, JR, Scully, S, Fan, W, Richards, WG, Kitajewski, J, Deblandre, GA, Kintner, CR, Stark, KL: Dll4, a novel Notch ligand expressed in arterial endothelium. *Genes Dev,* 14**:** 1313-1318, 2000.
73. You, LR, Lin, FJ, Lee, CT, DeMayo, FJ, Tsai, MJ, Tsai, SY: Suppression of Notch signalling by the COUP-TFII transcription factor regulates vein identity. *Nature,* 435**:** 98-104, 2005. https://doi.org/10.1038/nature03511
74. Saint-Geniez, M, Argence, CB, Knibiehler, B, Audigier, Y: The msr/apj gene encoding the apelin receptor is an early and specific marker of the venous phenotype in the retinal vasculature. *Gene Expr Patterns,* 3**:** 467-472, 2003. https://doi.org/10.1016/s1567-133x(03)00062-0
75. Yamamizu, K, Yamashita, JK: Roles of cyclic adenosine monophosphate signaling in endothelial cell differentiation and arterial-venous specification during vascular development. *Circ J,* 75**:** 253-260, 2011. https://doi.org/10.1253/circj.cj-10-0915
76. Tzima, E, Kiosses, WB, del Pozo, MA, Schwartz, MA: Localized cdc42 activation, detected using a novel assay, mediates microtubule organizing center positioning in endothelial cells in response to fluid shear stress. *J Biol Chem,* 278**:** 31020-31023, 2003. https://doi.org/10.1074/jbc.M301179200
77. Coon, BG, Baeyens, N, Han, J, Budatha, M, Ross, TD, Fang, JS, Yun, S, Thomas, JL, Schwartz, MA: Intramembrane binding of VE-cadherin to VEGFR2 and VEGFR3 assembles the endothelial mechanosensory complex. *J Cell Biol,* 208**:** 975-986, 2015. https://doi.org/10.1083/jcb.201408103
78. Rochon, ER, Menon, PG, Roman, BL: Alk1 controls arterial endothelial cell migration in lumenized vessels. *Development,* 143**:** 2593-2602, 2016. https://doi.org/10.1242/dev.135392
79. Edelman, DA, Jiang, Y, Tyburski, J, Wilson, RF, Steffes, C: Pericytes and their role in microvasculature homeostasis. *J Surg Res,* 135**:** 305-311, 2006. https://doi.org/10.1016/j.jss.2006.06.010
80. Villiers, A: C ompt. Rend. Acad. S ci. *Paris,* 112**:** 536, 1891.
81. Zimmermann, KW: Der feinere Bau der Blutcapillaren. *Zeitschrift für Anatomie und Entwicklungsgeschichte,* 68**:** 29-109, 1923. https://doi.org/10.1007/BF02593544
82. Dias Moura Prazeres, PH, Sena, IFG, Borges, IDT, de Azevedo, PO, Andreotti, JP, de Paiva, AE, de Almeida, VM, de Paula Guerra, DA, Pinheiro Dos Santos, GS, Mintz, A, Delbono, O, Birbrair, A: Pericytes are heterogeneous in their origin within the same tissue. *Dev Biol,* 427**:** 6-11, 2017. https://doi.org/10.1016/j.ydbio.2017.05.001
83. Hellstrom, M, Gerhardt, H, Kalen, M, Li, X, Eriksson, U, Wolburg, H, Betsholtz, C: Lack of pericytes leads to endothelial hyperplasia and abnormal vascular morphogenesis. *J Cell Biol,* 153**:** 543-553, 2001. https://doi.org/10.1083/jcb.153.3.543
84. Armulik, A, Genove, G, Betsholtz, C: Pericytes: developmental, physiological, and pathological perspectives, problems, and promises. *Dev Cell,* 21**:** 193-215, 2011. https://doi.org/10.1016/j.devcel.2011.07.001
85. Nehls, V, Drenckhahn, D: Heterogeneity of microvascular pericytes for smooth muscle type alpha-actin. *J Cell Biol,* 113**:** 147-154, 1991. https://doi.org/10.1083/jcb.113.1.147
86. Hill, RA, Tong, L, Yuan, P, Murikinati, S, Gupta, S, Grutzendler, J: Regional Blood Flow in the Normal and Ischemic Brain Is Controlled by Arteriolar Smooth Muscle Cell Contractility and Not by Capillary Pericytes. *Neuron,* 87**:** 95-110, 2015. https://doi.org/10.1016/j.neuron.2015.06.001
87. Mills, SJ, Cowin, AJ, Kaur, P: Pericytes, mesenchymal stem cells and the wound healing process. *Cells,* 2**:** 621-634, 2013. https://doi.org/10.3390/cells2030621
88. Shepro, D, Morel, NM: Pericyte physiology. *FASEB J,* 7**:** 1031-1038, 1993. https://doi.org/10.1096/fasebj.7.11.8370472
89. Smyth, LCD, Rustenhoven, J, Scotter, EL, Schweder, P, Faull, RLM, Park, TIH, Dragunow, M: Markers for human brain pericytes and smooth muscle cells. *J Chem Neuroanat,* 92**:** 48-60, 2018. https://doi.org/10.1016/j.jchemneu.2018.06.001
90. Mae, MA, He, L, Nordling, S, Vazquez-Liebanas, E, Nahar, K, Jung, B, Li, X, Tan, BC, Chin Foo, J, Cazenave-Gassiot, A, Wenk, MR, Zarb, Y, Lavina, B, Quaggin, SE, Jeansson, M, Gu, C, Silver, DL, Vanlandewijck, M, Butcher, EC, Keller, A, Betsholtz, C: Single-Cell Analysis of Blood-Brain Barrier Response to Pericyte Loss. *Circ Res,* 128**:** e46-e62, 2021. https://doi.org/10.1161/CIRCRESAHA.120.317473
91. Tilton, RG, Kilo, C, Williamson, JR: Pericyte-endothelial relationships in cardiac and skeletal muscle capillaries. *Microvasc Res,* 18**:** 325-335, 1979. https://doi.org/10.1016/0026-2862(79)90041-4

92. van Splunder, H, Villacampa, P, Martinez-Romero, A, Graupera, M: Pericytes in the disease spotlight. *Trends Cell Biol*, 2023. https://doi.org/10.1016/j.tcb.2023.06.001
93. Cucu, I, Nicolescu, MI: A Synopsis of Signaling Crosstalk of Pericytes and Endothelial Cells in Salivary Gland. *Dent J (Basel),* 9, 2021. https://doi.org/10.3390/dj9120144
94. Sanchez-Palencia, DM, Bigger-Allen, A, Saint-Geniez, M, Arboleda-Velasquez, JF, D'Amore, PA: Coculture Assays for Endothelial Cells-Mural Cells Interactions. *Methods Mol Biol,* 1464**:** 35-47, 2016. https://doi.org/10.1007/978-1-4939-3999-2_4
95. Antonelli-Orlidge, A, Saunders, KB, Smith, SR, D'Amore, PA: An activated form of transforming growth factor beta is produced by cocultures of endothelial cells and pericytes. *Proc Natl Acad Sci U S A,* 86**:** 4544-4548, 1989. https://doi.org/10.1073/pnas.86.12.4544
96. Trost, A, Bruckner, D, Rivera, FJ, Reitsamer, HA: Pericytes in the Retina. *Adv Exp Med Biol,* 1122**:** 1-26, 2019. https://doi.org/10.1007/978-3-030-11093-2_1
97. Ando, K, Fukuhara, S, Izumi, N, Nakajima, H, Fukui, H, Kelsh, RN, Mochizuki, N: Clarification of mural cell coverage of vascular endothelial cells by live imaging of zebrafish. *Development,* 143**:** 1328-1339, 2016. https://doi.org/10.1242/dev.132654
98. Kemp, SS, Aguera, KN, Cha, B, Davis, GE: Defining Endothelial Cell-Derived Factors That Promote Pericyte Recruitment and Capillary Network Assembly. *Arterioscler Thromb Vasc Biol,* 40**:** 2632-2648, 2020. https://doi.org/10.1161/ATVBAHA.120.314948
99. Lindahl, P, Johansson, BR, Leveen, P, Betsholtz, C: Pericyte loss and microaneurysm formation in PDGF-B-deficient mice. *Science,* 277**:** 242-245, 1997. https://doi.org/10.1126/science.277.5323.242
100. Andrae, J, Gallini, R, Betsholtz, C: Role of platelet-derived growth factors in physiology and medicine. *Genes Dev,* 22**:** 1276-1312, 2008. https://doi.org/10.1101/gad.1653708
101. Eilken, HM, Dieguez-Hurtado, R, Schmidt, I, Nakayama, M, Jeong, HW, Arf, H, Adams, S, Ferrara, N, Adams, RH: Pericytes regulate VEGF-induced endothelial sprouting through VEGFR1. *Nat Commun,* 8**:** 1574, 2017. https://doi.org/10.1038/s41467-017-01738-3
102. Milam, KE, Parikh, SM: The angiopoietin-Tie2 signaling axis in the vascular leakage of systemic inflammation. *Tissue Barriers,* 3**:** e957508, 2015. https://doi.org/10.4161/21688362.2014.957508
103. Teichert, M, Milde, L, Holm, A, Stanicek, L, Gengenbacher, N, Savant, S, Ruckdeschel, T, Hasanov, Z, Srivastava, K, Hu, J, Hertel, S, Bartol, A, Schlereth, K, Augustin, HG: Pericyte-expressed Tie2 controls angiogenesis and vessel maturation. *Nat Commun,* 8**:** 16106, 2017. https://doi.org/10.1038/ncomms16106
104. Leveen, P, Pekny, M, Gebre-Medhin, S, Swolin, B, Larsson, E, Betsholtz, C: Mice deficient for PDGF B show renal, cardiovascular, and hematological abnormalities. *Genes Dev,* 8**:** 1875-1887, 1994. https://doi.org/10.1101/gad.8.16.1875
105. Soriano, P: Abnormal kidney development and hematological disorders in PDGF beta-receptor mutant mice. *Genes Dev,* 8**:** 1888-1896, 1994. https://doi.org/10.1101/gad.8.16.1888
106. Hellstrom, M, Kalen, M, Lindahl, P, Abramsson, A, Betsholtz, C: Role of PDGF-B and PDGFR-beta in recruitment of vascular smooth muscle cells and pericytes during embryonic blood vessel formation in the mouse. *Development,* 126**:** 3047-3055, 1999. https://doi.org/10.1242/dev.126.14.3047
107. Park, DY, Lee, J, Kim, J, Kim, K, Hong, S, Han, S, Kubota, Y, Augustin, HG, Ding, L, Kim, JW, Kim, H, He, Y, Adams, RH, Koh, GY: Plastic roles of pericytes in the blood-retinal barrier. *Nat Commun,* 8**:** 15296, 2017. https://doi.org/10.1038/ncomms15296
108. Keller, A, Westenberger, A, Sobrido, MJ, Garcia-Murias, M, Domingo, A, Sears, RL, Lemos, RR, Ordonez-Ugalde, A, Nicolas, G, da Cunha, JE, Rushing, EJ, Hugelshofer, M, Wurnig, MC, Kaech, A, Reimann, R, Lohmann, K, Dobricic, V, Carracedo, A, Petrovic, I, Miyasaki, JM, Abakumova, I, Mae, MA, Raschperger, E, Zatz, M, Zschiedrich, K, Klepper, J, Spiteri, E, Prieto, JM, Navas, I, Preuss, M, Dering, C, Jankovic, M, Paucar, M, Svenningsson, P, Saliminejad, K, Khorshid, HR, Novakovic, I, Aguzzi, A, Boss, A, Le Ber, I, Defer, G, Hannequin, D, Kostic, VS, Campion, D, Geschwind, DH, Coppola, G, Betsholtz, C, Klein, C, Oliveira, JR: Mutations in the gene encoding PDGF-B cause brain calcifications in humans and mice. *Nat Genet,* 45**:** 1077-1082, 2013. https://doi.org/10.1038/ng.2723
109. Lindblom, P, Gerhardt, H, Liebner, S, Abramsson, A, Enge, M, Hellstrom, M, Backstrom, G, Fredriksson, S, Landegren, U, Nystrom, HC, Bergstrom, G, Dejana, E, Ostman, A, Lindahl, P, Betsholtz, C: Endothelial PDGF-B retention is required for proper investment of pericytes in the microvessel wall. *Genes Dev,* 17**:** 1835-1840, 2003. https://doi.org/10.1101/gad.266803
110. Torok, O, Schreiner, B, Schaffenrath, J, Tsai, HC, Maheshwari, U, Stifter, SA, Welsh, C, Amorim, A, Sridhar, S, Utz, SG, Mildenberger, W, Nassiri, S, Delorenzi, M, Aguzzi, A, Han, MH, Greter, M, Becher, B, Keller, A: Pericytes regulate vascular immune homeostasis in the CNS. *Proc Natl Acad Sci U S A,* 118, 2021. https://doi.org/10.1073/pnas.2016587118

111. Vazquez-Liebanas, E, Nahar, K, Bertuzzi, G, Keller, A, Betsholtz, C, Mae, MA: Adult-induced genetic ablation distinguishes PDGFB roles in blood-brain barrier maintenance and development. *J Cereb Blood Flow Metab,* 42**:** 264-279, 2022. https://doi.org/10.1177/0271678X211056395
112. Armulik, A, Genove, G, Mae, M, Nisancioglu, MH, Wallgard, E, Niaudet, C, He, L, Norlin, J, Lindblom, P, Strittmatter, K, Johansson, BR, Betsholtz, C: Pericytes regulate the blood-brain barrier. *Nature,* 468**:** 557-561, 2010. https://doi.org/10.1038/nature09522
113. Winkler, EA, Birk, H, Burkhardt, JK, Chen, X, Yue, JK, Guo, D, Rutledge, WC, Lasker, GF, Partow, C, Tihan, T, Chang, EF, Su, H, Kim, H, Walcott, BP, Lawton, MT: Reductions in brain pericytes are associated with arteriovenous malformation vascular instability. *J Neurosurg,* 129**:** 1464-1474, 2018. https://doi.org/10.3171/2017.6.JNS17860
114. Chen, W, Guo, Y, Walker, EJ, Shen, F, Jun, K, Oh, SP, Degos, V, Lawton, MT, Tihan, T, Davalos, D, Akassoglou, K, Nelson, J, Pile-Spellman, J, Su, H, Young, WL: Reduced mural cell coverage and impaired vessel integrity after angiogenic stimulation in the Alk1-deficient brain. *Arterioscler Thromb Vasc Biol,* 33**:** 305-310, 2013. https://doi.org/10.1161/ATVBAHA.112.300485
115. Lebrin, F, Srun, S, Raymond, K, Martin, S, van den Brink, S, Freitas, C, Breant, C, Mathivet, T, Larrivee, B, Thomas, JL, Arthur, HM, Westermann, CJ, Disch, F, Mager, JJ, Snijder, RJ, Eichmann, A, Mummery, CL: Thalidomide stimulates vessel maturation and reduces epistaxis in individuals with hereditary hemorrhagic telangiectasia. *Nat Med,* 16**:** 420-428, 2010. https://doi.org/10.1038/nm.2131
116. Zhu, W, Chen, W, Zou, D, Wang, L, Bao, C, Zhan, L, Saw, D, Wang, S, Winkler, E, Li, Z, Zhang, M, Shen, F, Shaligram, S, Lawton, M, Su, H: Thalidomide Reduces Hemorrhage of Brain Arteriovenous Malformations in a Mouse Model. *Stroke,* 49**:** 1232-1240, 2018. https://doi.org/10.1161/STROKEAHA.117.020356
117. Dubrac, A, Kunzel, SE, Kunzel, SH, Li, J, Chandran, RR, Martin, K, Greif, DM, Adams, RH, Eichmann, A: NCK-dependent pericyte migration promotes pathological neovascularization in ischemic retinopathy. *Nat Commun,* 9**:** 3463, 2018. https://doi.org/10.1038/s41467-018-05926-7
118. Birdsey, GM, Dryden, NH, Amsellem, V, Gebhardt, F, Sahnan, K, Haskard, DO, Dejana, E, Mason, JC, Randi, AM: Transcription factor Erg regulates angiogenesis and endothelial apoptosis through VE-cadherin. *Blood,* 111**:** 3498-3506, 2008. https://doi.org/10.1182/blood-2007-08-105346
119. Pontes-Quero, S, Fernandez-Chacon, M, Luo, W, Lunella, FF, Casquero-Garcia, V, Garcia-Gonzalez, I, Hermoso, A, Rocha, SF, Bansal, M, Benedito, R: High mitogenic stimulation arrests angiogenesis. *Nat Commun,* 10**:** 2016, 2019. https://doi.org/10.1038/s41467-019-09875-7
120. Pitulescu, ME, Schmidt, I, Giaimo, BD, Antoine, T, Berkenfeld, F, Ferrante, F, Park, H, Ehling, M, Biljes, D, Rocha, SF, Langen, UH, Stehling, M, Nagasawa, T, Ferrara, N, Borggrefe, T, Adams, RH: Dll4 and Notch signalling couples sprouting angiogenesis and artery formation. *Nat Cell Biol,* 19**:** 915-927, 2017. https://doi.org/10.1038/ncb3555
121. Samulowitz, U, Kuhn, A, Brachtendorf, G, Nawroth, R, Braun, A, Bankfalvi, A, Bocker, W, Vestweber, D: Human endomucin: distribution pattern, expression on high endothelial venules, and decoration with the MECA-79 epitope. *Am J Pathol,* 160**:** 1669-1681, 2002. https://doi.org/10.1016/S0002-9440(10)61114-5
122. Corada, M, Orsenigo, F, Morini, MF, Pitulescu, ME, Bhat, G, Nyqvist, D, Breviario, F, Conti, V, Briot, A, Iruela-Arispe, ML, Adams, RH, Dejana, E: Sox17 is indispensable for acquisition and maintenance of arterial identity. *Nat Commun,* 4**:** 2609, 2013. https://doi.org/10.1038/ncomms3609
123. Fang, JS, Coon, BG, Gillis, N, Chen, Z, Qiu, J, Chittenden, TW, Burt, JM, Schwartz, MA, Hirschi, KK: Shear-induced Notch-Cx37-p27 axis arrests endothelial cell cycle to enable arterial specification. *Nat Commun,* 8**:** 2149, 2017. https://doi.org/10.1038/s41467-017-01742-7
124. Chavkin, NW, Genet, G, Poulet, M, Jeffery, ED, Marziano, C, Genet, N, Vasavada, H, Nelson, EA, Acharya, BR, Kour, A, Aragon, J, McDonnell, SP, Huba, M, Sheynkman, GM, Walsh, K, Hirschi, KK: Endothelial cell cycle state determines propensity for arterial-venous fate. *Nat Commun,* 13**:** 5891, 2022. https://doi.org/10.1038/s41467-022-33324-7
125. Arboleda-Velasquez, JF, Primo, V, Graham, M, James, A, Manent, J, D'Amore, PA: Notch signaling functions in retinal pericyte survival. *Invest Ophthalmol Vis Sci,* 55**:** 5191-5199, 2014. https://doi.org/10.1167/iovs.14-14046
126. Uyttendaele, H, Ho, J, Rossant, J, Kitajewski, J: Vascular patterning defects associated with expression of activated Notch4 in embryonic endothelium. *Proc Natl Acad Sci U S A,* 98**:** 5643-5648, 2001. https://doi.org/10.1073/pnas.091584598
127. Carlson, TR, Yan, Y, Wu, X, Lam, MT, Tang, GL, Beverly, LJ, Messina, LM, Capobianco, AJ, Werb, Z, Wang, R: Endothelial expression of constitutively active Notch4 elicits reversible arteriovenous malformations in adult mice. *Proc Natl Acad Sci U S A,* 102**:** 9884-9889, 2005. https://doi.org/10.1073/pnas.0504391102

128. Krebs, LT, Starling, C, Chervonsky, AV, Gridley, T: Notch1 activation in mice causes arteriovenous malformations phenocopied by ephrinB2 and EphB4 mutants. *Genesis,* 48**:** 146-150, 2010. https://doi.org/10.1002/dvg.20599
129. Van Gieson, EJ, Murfee, WL, Skalak, TC, Price, RJ: Enhanced smooth muscle cell coverage of microvessels exposed to increased hemodynamic stresses in vivo. *Circ Res,* 92**:** 929-936, 2003. https://doi.org/10.1161/01.RES.0000068377.01063.79
130. Gonzales, AL, Klug, NR, Moshkforoush, A, Lee, JC, Lee, FK, Shui, B, Tsoukias, NM, Kotlikoff, MI, Hill-Eubanks, D, Nelson, MT: Contractile pericytes determine the direction of blood flow at capillary junctions. *Proc Natl Acad Sci U S A,* 117**:** 27022-27033, 2020. https://doi.org/10.1073/pnas.1922755117
131. Cuttano, R, Rudini, N, Bravi, L, Corada, M, Giampietro, C, Papa, E, Morini, MF, Maddaluno, L, Baeyens, N, Adams, RH, Jain, MK, Owens, GK, Schwartz, M, Lampugnani, MG, Dejana, E: KLF4 is a key determinant in the development and progression of cerebral cavernous malformations. *EMBO Mol Med,* 8**:** 6-24, 2016. https://doi.org/10.15252/emmm.201505433
132. He, M, Zheng, B, Zhang, Y, Zhang, XH, Wang, C, Yang, Z, Sun, Y, Wu, XL, Wen, JK: KLF4 mediates the link between TGF-beta1-induced gene transcription and H3 acetylation in vascular smooth muscle cells. *FASEB J,* 29**:** 4059-4070, 2015. https://doi.org/10.1096/fj.15-272658
133. Boriushkin, E, Zhang, H, Becker, M, Peachey, J, Shatat, MA, Adams, RH, Hamik, A: Kruppel-like factor 4 regulates developmental angiogenesis through disruption of the RBP-J-NICD-MAML complex in intron 3 of Dll4. *Angiogenesis,* 22**:** 295-309, 2019. https://doi.org/10.1007/s10456-018-9657-y
134. Crist, AM, Lee, AR, Patel, NR, Westhoff, DE, Meadows, SM: Vascular deficiency of Smad4 causes arteriovenous malformations: a mouse model of Hereditary Hemorrhagic Telangiectasia. *Angiogenesis,* 21**:** 363-380, 2018. https://doi.org/10.1007/s10456-018-9602-0
135. Nadeem, T, Bogue, W, Bigit, B, Cuervo, H: Deficiency of Notch signaling in pericytes results in arteriovenous malformations. *JCI Insight,* 5, 2020. https://doi.org/10.1172/jci.insight.125940
136. Orlich, MM, Dieguez-Hurtado, R, Muehlfriedel, R, Sothilingam, V, Wolburg, H, Oender, CE, Woelffing, P, Betsholtz, C, Gaengel, K, Seeliger, M, Adams, RH, Nordheim, A: Mural Cell SRF Controls Pericyte Migration, Vessel Patterning and Blood Flow. *Circ Res,* 131**:** 308-327, 2022. https://doi.org/10.1161/CIRCRESAHA.122.321109
137. Hellstrom, M, Phng, LK, Hofmann, JJ, Wallgard, E, Coultas, L, Lindblom, P, Alva, J, Nilsson, AK, Karlsson, L, Gaiano, N, Yoon, K, Rossant, J, Iruela-Arispe, ML, Kalen, M, Gerhardt, H, Betsholtz, C: Dll4 signalling through Notch1 regulates formation of tip cells during angiogenesis. *Nature,* 445**:** 776-780, 2007. https://doi.org/10.1038/nature05571
138. Jahnsen, ED, Trindade, A, Zaun, HC, Lehoux, S, Duarte, A, Jones, EA: Notch1 is pan-endothelial at the onset of flow and regulated by flow. *PLoS One,* 10**:** e0122622, 2015. https://doi.org/10.1371/journal.pone.0122622
139. Ogura, S, Kurata, K, Hattori, Y, Takase, H, Ishiguro-Oonuma, T, Hwang, Y, Ahn, S, Park, I, Ikeda, W, Kusuhara, S, Fukushima, Y, Nara, H, Sakai, H, Fujiwara, T, Matsushita, J, Ema, M, Hirashima, M, Minami, T, Shibuya, M, Takakura, N, Kim, P, Miyata, T, Ogura, Y, Uemura, A: Sustained inflammation after pericyte depletion induces irreversible blood-retina barrier breakdown. *JCI Insight,* 2**:** e90905, 2017. https://doi.org/10.1172/jci.insight.90905
140. Gao, S, Nelson, J, Weinsheimer, S, Winkler, EA, Rutledge, C, Abla, AA, Gupta, N, Shieh, JT, Cooke, DL, Hetts, SW, Tihan, T, Hess, CP, Ko, N, Walcott, BP, McCulloch, CE, Lawton, MT, Su, H, Pawlikowska, L, Kim, H: Somatic mosaicism in the MAPK pathway in sporadic brain arteriovenous malformation and association with phenotype. *J Neurosurg,* 136**:** 148-155, 2022. https://doi.org/10.3171/2020.11.JNS202031
141. Parada, CA, El-Ghazali, FM, Toglia, D, Ruzevick, J, McAvoy, M, Emerson, S, Karasozen, Y, Busald, T, Nazem, AA, Suranowitz, SM, Shalhub, S, Marshall, DA, Gonzalez-Cuyar, LF, Dorschner, MO, Ferreira, M, Jr.: Somatic Mosaicism of a PDGFRB Activating Variant in Aneurysms of the Intracranial, Coronary, Aortic, and Radial Artery Vascular Beds. *J Am Heart Assoc,* 11**:** e024289, 2022. https://doi.org/10.1161/JAHA.121.024289
142. Chenbhanich, J, Hu, Y, Hetts, S, Cooke, D, Dowd, C, Devine, P, Center, UCG, Russell, B, Kang, SHL, Chang, VY, Abla, AA, Cornett, P, Yeh, I, Lee, H, Martinez-Agosto, JA, Frieden, IJ, Shieh, JT: Segmental overgrowth and aneurysms due to mosaic PDGFRB p.(Tyr562Cys). *Am J Med Genet A,* 185**:** 1430-1436, 2021. https://doi.org/10.1002/ajmg.a.62126
143. Yildirim, O, Bicer, A, Ozkan, A, Kurtkaya, O, Cirakoglu, B, Kilic, T: Expression of platelet-derived growth factor ligand and receptor in cerebral arteriovenous and cavernous malformations. *J Clin Neurosci,* 17**:** 1557-1562, 2010. https://doi.org/10.1016/j.jocn.2010.04.028
144. Invernizzi, R, Quaglia, F, Klersy, C, Pagella, F, Ornati, F, Chu, F, Matti, E, Spinozzi, G, Plumitallo, S, Grignani, P, Olivieri, C, Bastia, R, Bellistri, F, Danesino, C, Benazzo, M, Balduini, CL: Efficacy and safety of thalidomide

for the treatment of severe recurrent epistaxis in hereditary haemorrhagic telangiectasia: results of a non-randomised, single-centre, phase 2 study. *Lancet Haematol,* 2**:** e465-473, 2015. https://doi.org/10.1016/S2352-3026(15)00195-7

145. Boon, LM, Dekeuleneer, V, Coulie, J, Marot, L, Bataille, A-C, Hammer, F, Clapuyt, P, Jeanjean, A, Dompmartin, A, Vikkula, M: Case report study of thalidomide therapy in 18 patients with severe arteriovenous malformations. *Nature Cardiovascular Research,* 1**:** 562-567, 2022. https://doi.org/10.1038/s44161-022-00080-2
146. Sugden, WW, Meissner, R, Aegerter-Wilmsen, T, Tsaryk, R, Leonard, EV, Bussmann, J, Hamm, MJ, Herzog, W, Jin, Y, Jakobsson, L, Denz, C, Siekmann, AF: Endoglin controls blood vessel diameter through endothelial cell shape changes in response to haemodynamic cues. *Nat Cell Biol,* 19**:** 653-665, 2017. https://doi.org/10.1038/ncb3528
147. Herbert, SP, Huisken, J, Kim, TN, Feldman, ME, Houseman, BT, Wang, RA, Shokat, KM, Stainier, DY: Arterial-venous segregation by selective cell sprouting: an alternative mode of blood vessel formation. *Science,* 326**:** 294-298, 2009. https://doi.org/10.1126/science.1178577

9. PUBLICATIONS

1. Yanzhu Lin, Johannes Gahn, Kuheli Banerjee, Gergana Dobreva, Mahak Singhal, Alexandre Dubrac, Roxana Ola, *Role of endothelial PDGFB in arterio-venous malformations pathogenesis*. Under revision in **Angiogenesis**.

2. Kuheli Banerjee*, Yanzhu Lin*, Johannes Gahn*, Julio Cordero, Purnima Gupta, Islam Mohamed, Mariona Graupera, Gergana Dobreva, Martin A. Schwartz, Roxana Ola, *SMAD4 maintains the fluid shear stress set point to protect against arterial-venous malformations.* **Journal of Clinical Investigation**, 2023. 133(18) (*equally contributing authors).

10. CURRICULUM VITAE

Personnel

Family name and first name	Lin, Yanzhu
Birthday:	12.01.1993
Place of birth:	Guangdong, China

School education

09.2008-06.2011	Xixiang Middle School High school diploma

University education

09.2008-06.2011	Jinan University Bachelor of Clinical Medicine
09.2017-06.2020	Sun Yat-Sen University Master of Oncology
10.2020-Present	Heidelberg University MD student

11. ACKNOWLEDGEMENTS

I would like to take a moment to sincerely thank everyone for their support and encouragement over the past three years.

First and foremost, I would like to extend my deepest appreciation to my supervisor, Roxana Ola, for her unwavering support throughout the entire thesis process. Under the guidance of my supervisor, I dived into my thesis research and successfully completed it after three years of diligent effort. Roxana provided me with invaluable support in both life and academic work during my time studying in Germany, which helped me greatly in completing this thesis. From designing my dissertation to conducting the experiments and interpreting the experimental results, she consistently and patiently addressed all of my inquiries. Her wisdom and deep insights were present in every step. I was thoroughly impressed by her vast knowledge, extensive experience, abundance of innovative ideas, and her laid-back personality. This thesis would not have been feasible without her invaluable assistance.

I would like to thank Prof. Gergana Dobreva, Dr. Alexandre Dubrac and Dr. Mahak Singhal, for their invaluable recommendations and important contribution on this research. Their expertise and critical evaluation greatly improved the quality of this work.

I would like to acknowledge the contributions of Prof. Thomas Wieland for providing reagents and resources that were essential to the completion of this work. I would like to thank all the technicians, Tina, Sabina, Doris, and Heinz for their constant willingness to order reagents and support in the daily lab work and for the really great atmosphere in the lab.

I would like to sincerely thank our department secretary, Irene, for her invaluable help during my time in Germany. I am especially grateful for her active support in my visa application and registration process.

I would like to express my gratitude to the China Scholarship Council (CSC) for providing me with a full scholarship during my studies in Germany. This generous support enabled me to seamlessly continue my studies abroad.

I am deeply grateful to my colleagues Kuheli, Johannes, Tanmaya, Zohrah, Nabil, and Santosh who have provided a stimulating intellectual environment and have been a source of inspiration and encouragement. Their discussions, feedback, and support have contributed

significantly to the development of this study. The time I spent with them was both enjoyable and fulfilling and left a lasting impression of my time in Germany. They will forever be etched in my memories as the most beautiful landscape.

I am grateful to Nan, Yohanes, and Xin for their help with my experiments, for their unwavering support and constant encouragement when I was anxious, and for their listening ear when I felt down during my years of study. Thank you for their kind care and concern. I would like to thank Yonggang, Yinuo, Yongqin, and Nalan from the Prof. Gergana Dobreva' lab for their invaluable support and encouragement on my personal and academic journey. Their research directions and experiences have greatly broadened my academic horizons.

Finally, I am grateful to my family for their unwavering support, understanding, and encouragement throughout this journey. Their love, belief in me, and patience have been my constant motivation.

Once again, I would like to express my sincere gratitude to everyone involved in the completion of this thesis. Their contributions have been invaluable and I am truly grateful for their support.